

**LOG POROSITY AND LITHOLOGY PREDICTION FROM
SEISMIC DATA: FRONTIER AND TENSLEEP
FORMATION, WYOMING**

BY

ABUZAR MAMUN ALI FUAD

A Thesis Presented to the
DEANSHIP OF GRADUATE STUDIES

KING FAHD UNIVERSITY OF PETROLEUM & MINERALS
DHRAHAN, SAUDI ARABIA

In Partial Fulfillment of the
Requirements for the Degree of

MASTER OF SCIENCE
In
GEOPHYSICS

May 2015

KING FAHD UNIVERSITY OF PETROLEUM & MINERALS

DHAHRAN- 31261, SAUDI ARABIA

DEANSHIP OF GRADUATE STUDIES

This thesis, written by **ABUZAR MAMUN ALI FUAD** under the direction his thesis advisor and approved by his thesis committee, has been presented and accepted by the Dean of Graduate Studies, in partial fulfillment of the requirements for the degree **MASTER OF SCIENCE IN GEOPHYSICS.**

Gabor Korvin 21/4/2015

Prof. Gabor Korvin
(Advisor)

Abdulazeez Abdulraheem

Dr. Abdulazeez Abdulraheem
(Member)

Osman Mahmoud Abdullatif

Dr. Osman Mahmoud Abdullatif
(Member)



Dr. Salam A. Zummo
Dean of Graduate Studies

21/4/2015

Date

© ABUZAR MAMUN ALI FUAD

2015

Dedication

I dedicate my thesis work to my family and many friends. A special feeling of gratitude to my dear parents, Khadija and Mamun whose words of moral support and determination still ring in my ears.

ACKNOWLEDGMENTS

All my praises and thanks to God Almighty the giver of bountiful blessings and gifts for helping and guiding me to accomplish this work. Prayers and peace of Allah be upon the noble Prophet and upon his family and companions, the honorable followers.

First and foremost I would like to express my great and sincere gratitude to my thesis chairman, **Prof. Gabor Korvin**. He has been supportive and encouraging since the days I began looking for thesis topic, helped me not only by providing a research assistantship and topic during my thesis period, but also academically and emotionally through the rough route to accomplish this master program. He helped and guided me over more than two years of study and development. And during the harshest times when writing this research, he provided me the moral support and the liberty I needed to carry on. I am particularly grateful for all the assistance given by him.

My special thanks are extended to my committee members who guided me through all roads to accomplish this work. Thank you Dr. **Abdulazeez Abdulraheem**, and Dr. **Osman Mahmoud Abdullatif** for scientific support, and being part of my Committee, as thesis readers, and an inspiration in many ways. Your tremendous excitement and willingness to give feedback made the accomplishment of this thesis an unforgettable experience.

Many people have supported and taught me immensely at the KFUPM, I praise the enormous amount of support and teaching by them. Special acknowledgement goes to the ESD faculty and staffs for their unyielding support.

I would like to acknowledge KFUPM for giving me the opportunity to carry out my master degree and availing any support needed. Last but not least I will never forget who have made this data available to anyone, special thank goes to SEG and RMOTC for providing this precious data set for public use.

Finally, I would like to thank my colleagues in graduate program, the administrators in our school department and the local Sudanese community for helping me during my study.

TABLE OF CONTENTS

ACKNOWLEDGMENTS	III
TABLE OF CONTENTS.....	V
LIST OF TABLES	VIII
LIST OF FIGURES	IX
LIST OF ABBREVIATIONS.....	XVI
ABSTRACT.....	XVII
ملخص الرسالة.....	XVIII
CHAPTER 1 INTRODUCTION	1
1.1 Introduction.....	1
1.2 Problem Statement.....	1
1.3 Study Objective.....	2
1.4 Geological setting of Target Formations	3
1.4.1 Frontier Formation	3
1.4.2 Tensleep Formation	4
1.5 Available Data	6
1.6 Scientific Importance	7
1.7 Thesis Organization	7
2 CHAPTER 2 LITERATURE REVIEW	9
3 CHAPTER 3 METHODOLOGY	15
3.1 POROSITY CORRECTION AND LITHOLOGY IDENTIFICATION.....	15
3.1.1 Finding the True Porosity	15

3.1.2 Finding the Fractional Composition	16
3.1.3 Shale Effect Correction.....	18
3.2 Well Log Pre-Processing	19
3.2.1 Well log Smoothing and Normalizing	19
3.3 Seismic Attributes Derivation.....	20
3.4 Post Stack Seismic Inversion.....	24
3.4.1 Colored Inversion Approach.....	24
3.5 Well to Seismic Tie.....	24
3.6 Multi-attribute Linear Regression.....	26
3.6.1 Conventional crossplotting	26
3.6.2 Generalizing of crossplotting to include multiple attributes.....	26
3.6.3 Determining the Number of Attributes by Stepwise Regression.....	30
3.7 Theoretical Background of the Neural Networks	32
3.7.1 Feed Forward Back Propagation ANN's	32
3.7.2 Radial Basis Function (RBF) ANN's	39
CHAPTER 4 RESULTS AND DISCUSSION.....	43
4.1 Wavelet Estimation.....	43
4.2 Post-stack inversion	47
4.3 Results of Lithology and Porosity Estimation	50
4.3.1 Lithology Identification of Second Wall Creek and Tensleep.....	50
4.3.2 Application of Neural Networks.....	61
4.3.3 Corrected Neutron Porosity Result	68
CHAPTER 5 CONCLUSION AND RECOMMENDATION.....	90
APPENDIX.....	98

VITAE.....	102
------------	-----

LIST OF TABLES

Table 3.1: Finding the fractional composition lithology of composite rocks (after Gabor Korvin, 2011. Unpublished manuscript).....	17
Table 3.2: List of some seismic attributes and their significance.....	23
Table 3.3: List of inverted seismic attributes and the employed method of inversion.....	23
Table 4.1: The correlation coefficients and corresponding estimation errors of inversion result.....	49
Table 4.2: Lithology results of a single seismic attributes estimation, the last two columns contain the estimation and coefficients of correlation (Second Wall Creek).....	55
Table 4.3: Single seismic attribute Table with corresponding estimation errors and coefficients of correlation for Tensleep reservoir... ..	56
Table 4.4: Performance of stepwise regression, implemented for the lithology prediction problem in Second Creek reservoir. Every line illustrates a different attribute transform with increasing number of seismic attributes involved. The set of multi-attributes for each row involves all previous attributes. The error of validation for each transform is illustrated in the final column in the same units as the target log.....	58
Table 4.5: Result of stepwise regression, implemented to the lithology prediction problem in Tensleep reservoirs. Each row reveals a different set of multi-attributes with increasing numbers of attributes. The set of	

attributes in each row contain all previous attributes. The last column gives the validation error of that transform.....	58
Table 4.6: Results of porosity prediction employing a single seismic attribute, with estimation errors and coefficients of correlation (Second Wall Creek).....	71
Table 4.7: Results of porosity prediction employing a single seismic attribute, with estimation errors and coefficients of correlation (Tensleep reservoir).....	72
Table 4.8: Performance of stepwise regression, implemented for the porosity prediction problem in Second Creek reservoir. Each row shows a different attribute transform. The multi attribute transform for every row involves all previous attributes. The final column illustrated corresponding validations.....	73
Table 4.9: Stepwise regression Performance, implemented for porosity prediction problem in Tensleep reservoirs. Each row reveals a different attribute transform. The attribute transform for every row involves all previous ones above it. The final column illustrated error of estimation for that conversion.....	73
Table 5.1: Processing workflow (Courtesy of EXCEL Geophysical Services Inc).....	100

LIST OF FIGURES

Figure 1.1: A gamma ray/ resistivity log, Frontier Formation, northern Moxa Arch(from Dutton et al 1992)sandstones are shaded; B1 _ B5 are sandstone in A second frontier.....	5
Figure 1.2: A stratigraphic column of reservoir (Tensleep) and the caprock (Goose Egg Fm.) (After P. Yin et al., 2005).....	6
Figure 3.1: Differences between the frequency content of the trace of seismic attribute (right) against that of the target log (left). After (Hampson et al., 2001)	19
Figure 3.2: Architecture of a simple ANN's with hidden layer. In this scenario, the O1, O2 and O3 are input, hidden, and the output layer respectively. Every circle represents a node.....	34
Figure 3.3: Hyperbolic tangent sigmoid transfer function. Note how quickly the function saturates for absolute values greater than three. To make full use of the shape of this transfer function, the inputs are normalized to the range -1 to 1.....	35
Figure 3.4: Log sigmoid transfer function. Note how quickly the function saturates for absolute values greater than five. To make full use of the shape of this transfer function, the inputs are normalized to the range -1 to 1.....	35
Figure 4.1: Amplitude of extracted wavelet by statistical approach in time domain from the seismic data alone. The extracted wavelet	

parameters are: wavelet length 200ms, sample rate 2ms, taper length 25, and Phase type is constant with zero phase rotation..... .44

Figure 4.2: Phase spectra and amplitude of the extracted wavelet in (figure 4.1).

Note that the maximum frequency, and spectral amplitude are around 100, and 40 Hz respectively. It is a zero phase wavelet.44

Figure 4.3: Wavelet extracted by statistical approach from the well logs alone.

The parameters of extracted wavelet are: wavelet length 200 ms, sample rate 2ms, length of taper 25, and Phase type is constant with zero phase rotation. Note that this wavelet is slightly shifted compared with (Figure 4.1) which indicates there is phase shift between synthetic seismogram and seismic data that has to be corrected.....45

Figure 4.4: Phase spectra and Amplitude in frequency domain of the extracted wavelet in (figure 4.3). The maximum frequency and amplitude of this wavelet are around 100 Hz, and 0.02 (occurring at around 35Hz) respectively, however it is not a zero phase wavelet because the phase is rotated around -33 degrees. This phase information is used to solve phase mismatch problem.....46

Figure 4.5: Cross plot between original acoustic impedance calculated from log data (x axis) and inverted acoustic impedance calculated from seismic data being constrained by well logs (y axis), the red is the regression line.48

Figure 4.6: Crossplot of actual lithology and Filter 5/10-15/20 attribute (Second Wall Creek).....	57
Figure 4.7: Crossplot of original lithology and Dominant Frequency attribute	57
Figure 4.8: Plot of validation error of wells showing the optimal combination of attributes to estimate lithology is four. The black dots show the error using all wells, whereas the red dots illustrate the error once one well is removed. (Second Wall Creek).	59
Figure 4.9: Plot of Validation error for all wells showing that the optimal number of attributes to estimate lithology is five. The black dots illustrate the error when we utilizing all wells, whereas the red dot illustrate the error when one well is removed, (Tensleep).....	59
Figure 4.10: Cross validation between original lithology log calculated from density and neutron porosity logs and predicted lithology log estimated by using combinations of 4 different attributes. (Second Wall Creek).....	60
Figure 4.11: Cross plot between original lithology log calculated from density and neutron porosity logs and predicted lithology log estimated from combinations of five attributes. (Tensleep).....	60
Figure 4.12: Result of using RBF neural networks with the same attributes as in the figure (4-10). Note the improvement in correlation and error between predicted and calculated logs compared with the case of multi linear regression (Second Wall Creek).....	64

Figure 4.13: Result of using RBF neural networks with the same attributes as in the (figure 4.11). Note the improvement in correlation and error between predicted and calculated logs compared with the case of multi linear regression. (Tensleep).....64

Figure 4.14: Result of using RBF neural networks with the same configuration parameters as in (Figure 4.13). However, one well has been excluded. Note the improvement in correlation and error between predicted and calculated logs compared with the case of six attributes. (Tensleep).....65

Figure 4.15: Result of using RBFNN's, with the same combination of attributes and parameters as (Figure 4.13), after excluding two wells with high error contribution. Note the improvement in correlation and error between predicted and calculated logs. (Tensleep).....65

Figure 4.16: The estimation errors for each of the 9 wells (Second Wall Creek). The black line illustrates the estimation error when a particular well is utilized in the prediction. The red line illustrates the validation error when the specified well is not employed in the prediction.66

Figure 4.17: The estimation for each of the 8 wells (Tensleep reservoir). The black line illustrates the error of estimation when a particular well is employed in prediction. The red line illustrates the error of validation that well when is not employed in the prediction.66

Figure 4.18: Applying the RBFNN's utilizing set of four attributes (Second Wall Creek). The original lithology and the predicted log is shown in black and red respectively.....67

Figure 4.19: Applying the RBFNN's utilizing set of six attributes (Tensleep). The original lithology and the predicted log is shown in black and red respectively.....	67
Figure 4.20: Cross plot of a single attribute (Amplitude Weighted Cosine Phase) against square root of porosity (Second Wall Creek)	74
Figure 4.21: Crossplot of single attribute Instantaneous Frequency against actual porosity (Tensleep).	74
Figure 4.22: Validation for all wells showing that the optimal set of attributes to estimate porosity is five. The red and black dots illustrate the error when one well is removed and error using all wells (Second Wall Creek).....	75
Figure 4.23: Validation for all wells showing that the optimal set of attributes to estimate porosity is five. The red and black dots illustrate the error when one well is removed and error using all wells (Tensleep).....	75
Figure 4.24: Crossplot of original porosity logs against estimated porosity logs in Second Wall Creek.	76
Figure 4.25: Crossplot of original porosity logs against estimated porosity logs in Tensleep reservoir.....	76
Figure 4.26: Crossplot of estimated porosity versus original porosity. (Second Wall Creek reservoir).....	79
Figure 4.27: Crossplot of estimated porosity against original porosity (Tensleep reservoir).....	79

Figure 4.28: Errors of the RBF Neural Network results (Second Wall Creek) using four attributes. The black and red line are Error of the actual and the estimated porosity log.	80
Figure 4.29: Errors of the RBF Neural Network results (Tensleep) using four attributes. The black and red line are Error of the actual and the estimated porosity log.	81
Figure 4.30: RBF results using 4 attributes (Second Wall Creek reservoir). The actual porosity log in black; the estimated log in red.	81
Figure 4.31: RBF results using 5 attributes (Tensleep). The actual porosity log in black; the estimated log in red.	82
Figure 4.32: Inline 147 from the 3D volume, with well 62-11 superimposed at crossline 172, showing (a) inverted impedance, (b) porosity predicted by the RBF algorithm, and (c) the lithology derived by the RBF algorithm.	87
Figure (4.33) Inline 46 from the 3D seismic survey, illustrating (a) inverted impedance, (b) RBF prediction of lithology.....	89
Figure 5.1: Fractional lithology log of 11 wells form Tensleep reservoir, the horizontal scale of 1, 2 and 3 is corresponding to sand, lime and dolo stone numerical codes, respectively. Note that the all three types of rocks actually occur in the graph.....	98
Figure 5.2: Fractional lithology log of 10 wells form Second Wall Creek reservoir, the horizontal scale of 1, 2 and 3 is corresponding to sand, lime and dolomite numerical codes, respectively. Note that the dominate rock types in all wells is sandstone.....	99

LIST OF ABBREVIATIONS

3C	: Three Components
3D seismic	: Three Dimensional Seismic
ANN	: Artificial Neural Networks
AVO	: Amplitude Variation with Offset
DFA	: Discriminant Factor Analysis
GMDH	: Group Method of Data Handling
GRNN	: Generalized Regression Neural Network
PCA	: Principle Component Analysis
RBFN	: Radial Basis Function Neural Network
V_p	: P-wave Velocity
V_s	: Shear Wave Velocity

ABSTRACT

Full Name : Abuzar Mamun Ali Fuad

Thesis Title : Log Porosity and Lithology Prediction From Seismic Data: Frontier And Tensleep Formations, Wyoming

Major Field : Geophysics

Date of Degree : May, 2015

In this study, I addressed the problem of converting seismic amplitudes into rock characterization, through integration of petrophysical measurements and 3D seismic data. Particularly, I present an application that allows interpreters to obtain porosity and fractional lithology constituent 2D maps from post-stack 3D seismic data. I used 3D seismic cube, density and neutron logs of two target reservoirs in Teapot basin as input data. In this technique, seismic amplitudes were transformed to attribute combinations by stepwise regression analysis, then attributes transformed into fractional lithology constituent and porosity by training Radial Basis Function Neural Network with available well log. To evaluate the credibility of the attributes to log properties transformation, cross-well validation was performed. In this procedure one well is omitted from the training set and the transformation is re-calculated. The accuracy of the transformation in estimating properties from the omitted well is then evaluated, this is applied to each well in the training set. The comparison between actual and predicted log reveals good matching, which is indicated by small differences between estimation and validation errors. The overall results of two approaches reveal a better illumination of the two reservoir targets. The fractional lithology constituent approach can be used for automated interpretations and can work as an extension of conventional interpretation techniques.

ملخص الرسالة

الاسم الكامل : ابوذر مأمون علي فواد

عنوان الرسالة : تتبؤ بالخصائص المسامية و الليثولوجية من معلومات الاهتزازية: مكون فورنتير و تينسليب , وايؤمن

التخصص : الجيوفيزاء

تاريخ الدرجة العلمية : مايو 2015

في هذه الاطروحة تمت مناقشة إمكانية تحويل المعلومات الاهتزازية الى خصائص صخرية. قدمت هذه الاطروحة على وجه خاص, تطبيق يسمح بتحويل البيانات الاهتزازية ثلاثة الابعاد الى خصائص المسامية و نسب المعادن المكونه لصخر.

تم استخدام البيانات الاهتزازية ثلاثة الابعاد بالإضافة الى تسجيلات الآبار لكل من المسامية و الكثافة لمكمنين في حوض تبيوت لتحقيق الغرض من الدراسة. في هذا التطبيق, البيانات الاهتزازية تم تحويلها الى سمات الاهتزازية, و من ثم تم تحويل تلك سمات الاهتزازية الى خصائص المساميه و نسب المعادن المكونه للصخر باستخدام نموذج الذكاء الاصطناعي. لتحقق من مصداقية نموذج الذكاء الاصطناعي في عملية تحويل البيانات الاهتزازية الى خصائص صخرية. تم استخدام تسجيلات الآبار المتوفرة في عملية التحقق . آلية التحقق في كل مرة تتم بحذف بئر واحدة من تدريب نموذج الذكاء الاصطناعي ثم يتم قياس قدرة النموذج في التنبؤ بمعلومات البئر المحذوفة, تم تكرار عملية التتحقق على كل تسجيلات الآبار المتوفرة للتدريب . و من ثم تم عمل مقارنة بين التسجيلات الحقيقية للآبار و التسجيلات التي تم استنتاجها من البيانات الاهتزازية بواسطة نموذج الذكاء الاصطناعي. اظهرت هذه المقارنة تشابه كبير بين التسجيلين. هذا التشابه يظهر جلياً في قياس الخطأ الناتج عن التدريب و الخطأ الناتج عن التتحقق.

في محمل النتائج كانت نسبة الخطأ الناتج عن التدريب و التحقق صغيرة نسبياً . أظهر تطبيق المساميه و نسب المعادن المكونة للصخور إمكانية و دقة عالية في إيجاد و التنبؤ بالتغييرات الجانبية للمكامن البترولية في منطقة الدراسة. تطبيق نسبة المكون المعدني للصخر الذي تم استحداثه في هذه الدراسة يمكن استخدامه في عملية التقسيير الآلي وكأداة إضافية لآدوات التقسيير الموجودة حالياً.

CHAPTER 1

INTRODUCTION

1.1 Introduction

Estimation of log properties from seismic volume by integrating well log and multi seismic attributes data has become the cornerstone in reservoir characterization studies. Nonlinear and inhomogeneous behaviors of reservoir properties associated with petroleum systems are considered the major concerns during understanding and integrating seismic and well log data. It is also similarly difficult to spatially characterize the relationship between reservoir variables obtained from both data sources. Statistical approaches, such as multi-linear regression analysis and neural networks, are widely employed to estimate reservoir properties from well logs and seismic amplitude (Nikravesh et al, 1998). In the last decade, artificial intelligence algorithms such as Self-Organizing Maps, NeuroFuzzy, Radial Basis Function, Discriminative Analysis and Learning Vector Quantization have gained attention as promising and powerful tools to solve nonlinear and complex problems, particularly in the prediction of reservoir characteristics (Nikravesh and Aminzadeh, 1998; Hampson et al., 2001; Nikravesh and Hassibi, 2003; Bosch et al, 2005; Hamada and Elshafei, 2010; Bosch et al., 2010).

1.2 Problem Statement

Prediction of subsurface properties, such as fractional lithology composition and porosity variations, from seismic volume has always been a fundamental problem in the earth

sciences. The traditional approach that employs seismic data to estimate reservoir properties consisted of searching for a physical relationship between the properties to be identified and seismic attributes, then employing that attribute over the entire seismic data in order to estimate the target properties. Even in cases when the functional relationships between target properties and attributes can be obtained, the physical basis is not often solid or clear. From the other hand, inferring such properties from well log data is considered more reliable, however costly, time-consuming and difficult. Properties such as porosity, and lithology variations (fractional composition) are among the most essential properties of reservoir systems that are typically distributed spatially in a non-uniform and non-linear manner. Although integration of multi attributes and available log is considered more reliable and efficient in estimating reservoir properties. However, the integration of this type of data set is not straightforward, and could produce false results. Therefore, special knowledge of accurate well to seismic integration is required to achieve proper estimation of reservoir properties. Moreover the presence of shale affects the amount of effective porosity. Therefore a special correction has to be made in order to correctly estimate such variables.

1.3 Study Objective

The main objective of this research is to predict well log measured properties, namely porosity and fractional lithology (fractional composition) variations via integrating multi seismic attributes and well logs by using ANN to predict spatial reservoir property changes. As far as I know the approach (fractional lithology) I proposed is new and nobody has done it before. The work can be divided into subcomponents as follows:

1. To correct the neutron porosity fractional values in order to compute the correct porosity values.
2. To correlate between multi-attributes transforms with available porosity logs to predict pseudo log porosity over the entire zone of interest (*Frontier Second Wall Creek* and *Tensleep reservoirs*) from full stack seismic volume.
3. To use the proposed new log (fractional lithology log) guided with seismic attributes to estimate the lithological fraction over the *Frontier Second Wall Creek* and *Tensleep reservoirs*.

1.4 Geological setting of Target Formations

This study makes use of data over the Frontier Second Wall Creek and Tensleep Formation, Wyoming. Several studies of the formation have been published by USGS and other geoscientists addressing stratigraphic, geological, geochemistry and geophysical aspects (Anna, 2009; Dennen et al., 2005; Kirschbaum and Roberts, 2005).

1.4.1 Frontier Formation

The Upper Cretaceous Frontier Formation was deposited as an eastward-prograding clastic wedge into a foreland basin as result of the Sevier orogenic disturbance in Late Cretaceous Cenomanian to Turonian period. Distal lithologies consist of marine nearshore strata, whereas proximal lithologies of the clastic wedge consist of coarse-grained non-marine fluvial strata intersecting into marine strata. The Frontier is confining between the Mowry Shale and Cody Shale as upper and lower strata respectively; the

upper and lower boarder of the Frontier are marked by the Clay Spur Bentonite Bed and an unnamed bentonite, respectively. Ammonite zones that bracket the Frontier include *Calycoceras gilberti* at the base and *Scaphites nigricollensis* at the top (Merewether et al., 1976, 1979).

Frontier Formation consists of three members namely the lower Belle Fourche Member, the middle Emigrant Gap Member (unnamed member by Merewether et al., 1976), and the upper Wall Creek Sandstone Member. About half of the total interval is composed of fine-grained rocks and includes laminated to variably bioturbated shales and siltstones with different bentonite beds. Facies and geometry of sandstones infer probable deposition as delta lobes (Bhattacharya and Willis, 2001). The deltas were perhaps truncated at the top during transgression, as evidenced by truncated inclined beds, a lack of subaerial exposure, and presence of topset lags.

The porosity of this formation varies from near zero to 20 percent, with hydrocarbon-producing sandstones having porosities between 10 to 20 percent. The Wall Creek Sandstone Member thicknesses are around 400 ft in western Converse County and eastern Natrona County, Wyoming (Anna, 2009). In this study I will focus on one single member of Frontier Formation (the second Wall Creek Sands reservoir) figure (1.1).

1.4.2 Tensleep Formation

Tensleep formation is equivalent to Minnelusa Formation C, D, and E cycles (Anna, 2009). The Tensleep has similar depositional and reservoir properties as the Minnelusa Formation; which is, it includes multiple boundaries as a result to frequent and high-amplitude sea-level variations. A generalized upward succession of Tensleep strata

consists of thick marine carbonate beds, thin low porosity interdune sandstone layers, generally porous and permeable eolian crossbedded dune sandstones, and thin discontinuous carbonates. The siliciclastic units form the dominant reservoir, whereas dolomites, although vuggy, rarely produce because of their low bulk permeability and porosity. Tensleep production in the Basin Margin is from large anticlines such as those found at Teapot Dome and Salt Creek fields and from stratigraphic traps such as those at North Fork field and parts of Sussex field (Anna, 2009). The porosity values of this formation vary from near zero to 10 percent, with hydrocarbon-producing sandstones having porosities around 10 percent. The Tensleep formation thickness is as much as 320 ft, it is underlain by Permian Goose Egg formation and is overlying the Madison formation (Anna, 2009) figure (1.1).

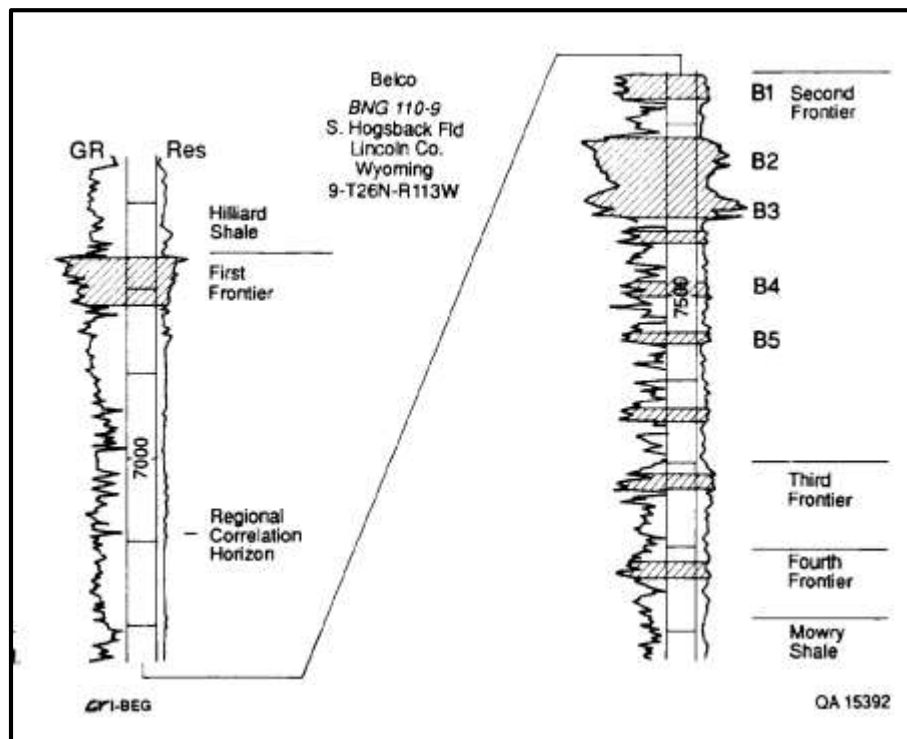


Figure1.1: A gamma ray/ resistivity log, Frontier Formation, northern Moxa Arch(from Dutton et al 1992)sandstones are shaded; B1 _ B5 are sandstone in second frontier.

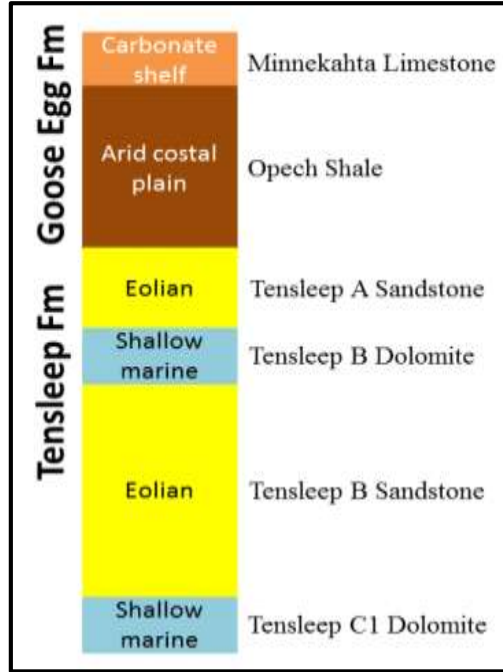


Figure 1.2: A stratigraphic column of reservoir (Tensleep) and the caprock (Goose Egg Fm.) (After P. Yin et al., 2005).

1.5 Available Data

There is a comprehensive database available for this study, it is one among the open dataset put by SEG in their website for the benefit of students, teachers and researchers. The validity, credibility and high quality of the data is guaranteed by SEG, the link to data is http://wiki.seg.org/wiki/Open_data. My selected data include well-log material from 12 wells, well-log curves consisting of:

- gamma ray and Caliper
- Bulk density
- Neutron porosity

- P-wave sonic log

In addition to the log data, there is a 3-D seismic cube covering the fields of interest. The processing steps applied to the raw seismic data are shown in the Appendix (Table 5.1). The survey area has inlines (ILN) 1-345 (increment = 1) and crosslines (XLN) 1-188 (increment = 1). Other survey parameters are: inline spacing, 110 ft; crossline spacing, 110 ft; sample rate, 2 ms, and record length of 3 seconds.

1.6 Scientific Importance

From one hand, this study addresses the problem of estimating porosity by integrating sparse well logs data with multi seismic attributes, form other hand it provides a detailed information about porosity distribution in the two target reservoirs. The lithological fractions (fractional composition) on the basis of neutron and density logs along with seismic attributes will be investigated. The use of the above described approach along with lithological fraction estimation allows a better understanding of lateral lithological (fractional composition) changes within these reservoirs. The lateral lithology changes associated with these reservoirs will be obtained using neural networks.

1.7 Thesis Organization

The thesis is composed of 5 chapters. The first chapter introduces an overview and the motivation of this study. A brief of the geological setting of the two target reservoirs is presented and the available petrophysical and geophysical characterization datasets are described. The second chapter summarizes the literature and previous work in the area of lithology identification and porosity estimation from seismic data, with special emphasis

to recent advancement. The third chapter focuses on data preparation and well-log pre-processing, identifies the lithology log codes and describes the porosity calculation. The procedures of establishing seismic-to-well ties will be also explained.

I employed the *Elog* and *STRATA* modules of the Hampson-Russell for the well-log analysis and seismic-to-well tie, and inverting seismic data to acoustic impedance and density properties by means of a model-based (acoustic impedance) inversion algorithm using P-wave sonic, density curves, picked horizons, and extracted wavelets. *EMERGE* was used to calculate some attributes and to optimize the functional correlation between the seismic attributes and well log (well log normalizing and smoothing). At the end of Chapter 3, the two types of algorithms, namely multi-linear regression and ANN's utilized to correlate between log and seismic attribute will be discussed mathematically.

In Chapter 4, Uncertainty Analysis is carried out and discussed, using results of estimated acoustic impedance. The uncertainty analysis of predicted porosity and lithology of the target zones is evaluated according to the principles of the *Design of Experiments* by (Hampson et al. 2001). Graphs and different section slices of the target zone are presented.

Chapter 5 serves for conclusions and recommendations. There is also an Appendix

CHAPTER 2

LITERATURE REVIEW

Seismic attributes were introduced as interpretation technique in seismic exploration in the early 1970's. Since then attribute analysis has become the corner stone of seismic interpretation. First, attributes were considered and analyzed in a qualitative manner. Later, since the late 1990's, the quantitative analysis and description of attributes have become commonly accepted and applied via integration with log data. Integration of seismic attributes with well log data to predict pseudo log properties is widely used especially in prediction of litho-facies and porosity. Litho-facies illumination is crucial in reservoir exploration and development for facies always controls petrophysical variations. Illumination of litho-facies generally relies on core data and outcrop description. However availability of the core and outcrop data is always big concern, therefore establishing correlations between litho-facies and available data, such as well logs and seismic, is highly desirable. Many approaches have been proposed, based on statistical techniques to estimate litho-facies from well logs (Sakurai and Melvin, 1988; Avseth et al., 2001; Tang et al., 2004). The previous decades have also witnessed successful implementations of Artificial Neural Networks (Derek et al., 1990; Wong et al., 1995; Siripitayananon et al., 2001; Helle et al., 2002) and fuzzy logic algorithms (Cuddy, 2000; Saggaf and Nebrija, 2003) in reservoir properties estimation.

The breakthrough of ANN's for reservoir properties identification has encouraged geoscientists, leading to claims that the technique has the high potential to overcome

other statistical tools employed in the reservoir characterization. However, the proper application of ANN's needs experimentation with changing the layers structure of ANN's and a time consuming training, particularly in case of a huge amount of input data (Wong et al., 1995; Avseth et al., 2001; and Illoghalu, 2003). All approaches employ a training data set consisting of observed cases with full knowledge about both predictors, in our case (seismic attributes) and groups (litho-facies and porosity).

Taner et al., (1979) applied complex trace analysis to seismic data and demonstrated its usefulness in geologic interpretation especially when displayed in color as a guidance in conveying seismic information to the interpreter.

Wolff and Pelissier (1982) employed principal component analysis (PCA) to separate and cluster the measured log value into different domains which could be considered as indicators for lithology. PCA maps the actual input space into another output space of lesser dimensions such that the distances between the projected points are closest to the distances in the original space. In other words, the emphasis is to minimize the distortion inflicted by the projection.

Busch et al., (1987) utilized discriminant factor analysis (DFA) to map the well log to litho-facies. DFA maps the original input space (log) into an output space of lesser dimensions so that the projected cluster centers are as far apart as possible while the projected points from same cluster are as near as possible to each other.

Rogers et al., (1992) developed a computer program to automatically determine lithologies from well logs using a back-propagation NN. The neural network was very efficient to determine the lithologies (limestone, dolomite, sandstone, shale, sandy and

dolomitic limestones, sandy dolomite, and shale sandstone) from selected well logs and did it much faster than an experienced human log analyst.

Schultz et al., (1994) were the first to employ multiple seismic attributes to estimate log properties away from well control, their results were presented in three articles.

Santoso et al., (1995) predicted the porosity of a limestone reservoir by employing post-stack seismic attributes and AVO analysis.

Smith and Maret (1995) estimated the sand-shale ratio of the target reservoirs in Myanmar by employing both statistical and deterministic approaches with attributes derived from pre and post-stack seismic volume. Models were calibrated at two wells in order to predict the lithologies and target reservoir parameters into places far from the wells. Their results show that, the two models provide same sands and shales distribution in the target reservoir, which is better than in the existing regional model.

Todorov et al., (1998) utilized multiple attributes from a 3C (3-component) 3D seismic survey to predict well logs using a nonlinear statistical approach. Stepwise regression was employed to determine the optimal set of seismic attributes to be used as input in a neural network for sonic velocity estimation.

Walls et al., (1999) characterized reservoir lithology employing neural networks, post-stack seismic data, well log and core.

Saggaf and Nebrija (2000) identified litho-facies from well logs by employing NN's that perform vector quantization on the input data. Their approach could be used in different

modes (supervised, semi-supervised, unsupervised) and it produced similar results to those obtained manually by an experienced geologist.

David et al., (2001) quantified and mapped the abundance and distribution of the dolomite across the Arab-D reservoir in Ghawar field, using density and neutron porosity as input data. Analysis of the presence and distribution of the dolomite in the field showed that dolomite occurs as a series of linear trends, which was attributed to structural events.

Hampson et al., (2001) described approach for estimating pseudo-log from seismic. The data consisted of a number of target logs from wells tied to a 3-D seismic cube, the aim had been to calculate a multi-attribute transform, which is a nonlinear or linear transform between the target log values and an optimally selected subset of the seismic attributes.

Hampson et al., (2003) presented the application of the radial basis function neural network (RBFN) to estimate pseudo-log from seismic attributes. The outputs of the new technique were compared with the generalized regression neural network (GRNN) outputs, discussed by Hampson et al. (2001). The error between the estimated and actual the log samples has shown the improvement of the results of RBFN over GRNN when the three are small number of samples.

Iturrarán and Spurlin (2005) used the gamma test as guidance for selecting the appropriate combinations of the seismic attributes in porosity prediction from 3D seismic data. They also addressed the problem of the minimum number of data required to estimate the desired log properties and maximal number of attributes to be combined.

Yumei and Sprecher (2006) evaluated the predictability performance of a naïve Bayes classifier by comparing it with a sophisticated statistical algorithm (the linear discriminant analysis). They considered log and core data from marine sediments of the Tensleep reservoir. The result of the both approaches seem reasonable, and the predictions of the Gaussian naïve Bayes classifier are same as those relying on the linear discriminant analysis.

Phan and Sen (2010) integrate well log and multi seismic attributes to quantitatively estimate porosity and permeability from pre-stack seismic volume.

AlBinHassan and Wang (2011) introduced a new nonlinear regression approach, named the group method of data handling (GMDH). The new approach performed better than the conventional statistical approaches in terms of selecting the best network structure, and the nodes number, which resulted in better prediction of porosity distribution than that obtained using ANN.

Adekanle and Enikanselu (2013) estimated porosity of ‘XLD’ Field, in Niger Delta via integrating sparse well log measurements with properties obtained from 3D seismic simultaneous inversion. The estimated porosity from inversion properties was found suitable for making reservoir management decisions. Besides, the result gave a geologically realistic porosity distribution which aids to understand the variations of the subsurface reservoirs in the study area.

Chaki et al., (2013) designed a modular neural network to predict sand fraction between the well tops taking three seismic attributes as input. Their result showed that, the

modular based neural networks can be applied to characterize reservoir parameters if the input values are seismic attributes.

Kumar et al., (2014) used relative seismic impedance to predict porosity in the Eagle Ford shale. This study proved that if the seismic data have well-preserved low-frequency content, the relative acoustic impedance alone can be sufficient to estimate porosity due to its sensitivity to the low-frequency components of the model.

Na’imi et al., (2014) employed non-linear support vector regression algorithm with some selected seismic attributes, to find quantitative relationship between porosity and water saturation. Support vector regression was found to be a powerful tool to estimate reservoir properties from seismic data and the results show improvement over conventional neural network.

|

CHAPTER 3

METHODOLOGY

I applied different pre-processing, correction and calculations steps to the well log data before correlating them with multi seismic attributes and inverted volume. These steps include

3.1 Porosity correction and lithology identification

The neutron-density-sonic master charts permit the determination of porosity and provide insight into lithology. Chart selection depends on the anticipated mineralogy. Neutron-density can be utilized to distinguish between the common reservoir rocks [quartz sandstone, calcite (limestone) and dolomite] and shale and some evaporites.

3.1.1 Finding the True Porosity

From the apparent limestone neutron porosity fractional value ϕ_N one computes the corrected neutron porosity value for sandstone, limestone and dolo-stone respectively as follows:

$$\phi_{N,SST,CORR} = 0.222 \phi_N^2 + 1.021 \phi_N + 0.39 \quad [1]$$

$$\phi_{N,Lst,CORR} = \phi_N \quad [2]$$

$$\phi_{N,SST,CORR} = 1.40 \phi_N^2 + 0.389 \phi_N + 0.01259 \quad [3]$$

3.1.2 Finding the Fractional Composition

Here the aim is to find the unknown lithology from measured $\phi_{N,m}$ and ρ_M values (i.e. from the measured neutron porosity and density). There are the following seven cases possible, listed in (table 3.1). Suppose that for the measured $\phi_{N,M}$ the measured density ρ_M is between two successive pure lithology curves (cases 3 and 5 in the (Table 3.1)). Let

$$\rho_{M,lith1} < \rho_M < \rho_{M,lith2} \quad [4]$$

then the percentage content of lith1 is

$$\rho_{lith1} [\%] = 100X \frac{\rho_M - \rho_{M,lith1}}{\rho_{M,lith2} - \rho_{M,lith1}} \quad [5]$$

and the percentage content of lith2 is

$$\rho_{lith2} [\%] = 100X \frac{\rho_{M,lith2} - \rho_M}{\rho_{M,lith2} - \rho_{M,lith1}} \quad [6]$$

Using Eqs [5, and 6] one can calculate the fractions of the lithology by following steps explained for different cases in (Table 3.1). The result is a new log named lithology fraction log, which gives percentages fraction of each composite rocks based on the Schlumberger master chart. For example we can code the composite rocks in the scale of this new log starting from one up to three. The value "1" indicates - pure sand, "2" and "3" are for pure lime and dolomite respectively. Fractional values between the numbers indicate the rock is not pure lithologically. For example "1.2" means a lithology consisting of 80% sand and 20% lime, or "2.6" means a lithology with 40% limestone and 60% dolomite, and so on. This way we can identify and quantify the lithology fraction of the entire well log based on the neutron porosity and density logs.

Table 3.1: Finding the fractional composition lithology of composite rocks (after Gabor Korvin, 2011. Unpublished manuscript).

Case number	If	then the lithology is	Percent composition
1	$\rho_m \leq \rho_{m,sst}$	Not clean (shaly), shale correction is necessary, see <i>Section 3</i>	Eliminate shale, and try again! See <i>Section 3</i>
2	$\rho_m = \rho_{m,sst}$	Pure sandstone	100% sst
3	$\rho_{m,sst} < \rho_m < \rho_{m,lst}$	Sandstone/limestone mixture	See Eqs.[5 and 6] with <i>lith1=sst</i> , <i>lith2=lst</i>
4	$\rho_m = \rho_{m,lst}$	Pure limestone	100% lst
5	$\rho_{m,lst} < \rho_m < \rho_{m,dst}$	Limestone/dolostone mixture	See Eqs.[5 and 6] with <i>lith1=lst</i> , <i>lith2=dst</i>
6	$\rho_m = \rho_{m,dst}$	Pure dolostone	100% dst
7	$\rho_{m,dst} < \rho_m$	Not clean (shaly), shale correction is necessary, see <i>Section 3</i>	Eliminate shale, and try again! See <i>Section 3</i>

3.1.3 Shale Effect Correction

Whenever crossplot of neutron and density data lie outside the boundaries of the three different rock curves, is indicating present of shale effects, which can be computed from the *Natural Gamma Ray Log* as follows in (Eq.7) we use conventional Well Logging notations

$$Vsh = \frac{(Gr - Grcs)}{(Grsh - Grcs)} \quad [7]$$

Abbreviations mean Vsh = (fractional) shale volume, Gr = Gamma Ray reading, $Grcs$ = Gamma Ray reading in clean sand, sh = shale, $Grsh$ = Gamma Ray reading in shale.

After computing Vsh , the measured $\Phi_{N,m}$ and the measured density ρ_m is corrected for shale as follows:

By the mixture rule of densities, we have for any shaly lithology (including for the unknown measured one)

$$\rho_{M,rock} = V_{shale}\rho_{shale} + (1 - V_{shale})\rho_{cleanrock} \quad [8]$$

wherfrom

$$\rho_{shalecorr} = \rho_{cleanrock} = \frac{\rho_{M,rock} - V_{shale}\rho_{shale}}{(1 - V_{shale})} \quad [9]$$

For the shale-correction of the neutron porosity we use the formula:

$$\phi_{N,shalecorr} = \phi_N - V_{shale} \phi_{N,shale} \quad [10]$$

3.2 Well Log Pre-Processing

To make the well logs directly comparable to the seismic data, a significant amount of pre-processing is necessary.

3.2.1 Well log Smoothing and Normalizing

The first processing steps is despiking. The despiking of the well logs is achieved through applying filtering to logs with a running mean filter of specified length. The running mean filter has significant impact on the results that are visually evident in the log character.

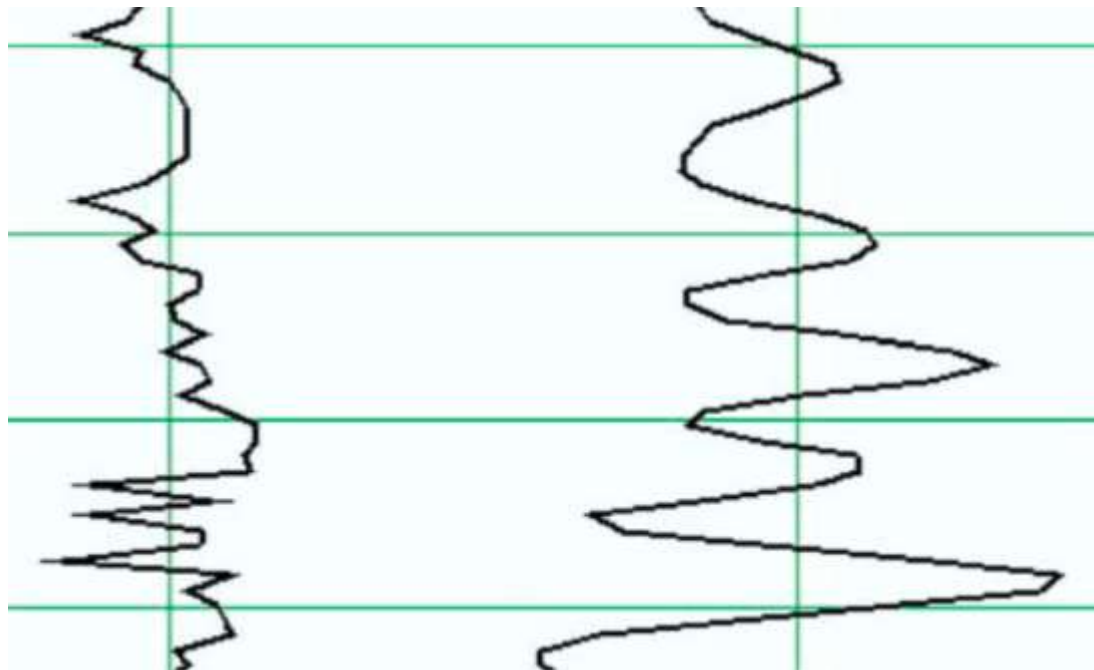


Figure 3.1: Differences between the frequency content of the trace of seismic attribute (right) against that of the target log (left). After (Hampson et al., 2001)

3.3 Seismic Attributes Derivation

Seismic attributes are measures of kinematic and statistical features of seismic data. A seismic trace is the product of complicated interrelationships between bed properties such as thickness, porosity, water saturation, and lithological properties. A seismic trace can be transformed into an attribute through amplifying one, or more, of above mentioned properties.

So far hundreds of seismic attributes have been derived and published, however only a few of these are of real significance and well enough understood to be quantitative, actually many seem to be redundant. We have chosen to use *Instantaneous Attributes*, so called because they are calculated at every time sample of the seismic trace. A detailed list of the attributes used, and their potential geologic significance is shown in (Table 3.2). The instantaneous phase, frequency, and envelope of the seismic traces is computed through complex trace analysis. In the theory of complex trace analysis, a seismic trace, $S(t)$, can be expressed as the real part of an *analytical signal* $s(t)$ that consists of an imaginary and a real part (Taner et al., 1979).

$$S(t) = s(t) + js^*(t) \quad [11]$$

where $j = \sqrt{-1}$, $s^*(t)$ is the trace's so-called *quadrature component* which can be uniquely obtained by Hilbert transform from the observed signal $s(t)$ if the theoretical assumptions about the *physical realizability* of the trace are met.

Eq. [11] may be re-written in polar form to produce two other instantaneous attributes Eqs. [12and 13]:

$$A(t) = [s(t)^2 + js^*(t)^2]^{1/2} \quad [12]$$

$$\Phi(t) = \arctan\left[\frac{js^*(t)}{S(t)}\right] \quad [13]$$

where $A(t)$ is the amplitude envelope and $\Phi(t)$ is the instantaneous phase. The seismic trace and its Hilbert transform may be reconstructed via combining amplitude of the instantaneous phase and envelope such that

$$S(t) = A(t)\cos(\Phi(t)) \quad [14]$$

$$js^*(t) = A(t)\sin(\Phi(t)) \quad [15]$$

Another instantaneous attribute may be derived by differentiating the instantaneous phase (the rate of change of phase with respect to time). This yields the instantaneous frequency attribute $\omega(t)$:

$$\omega(t) = \frac{d\Phi(t)}{dt} \quad [16]$$

The above three instantaneous attributes (amplitude, phase, and frequency) are the basic seismic attributes. More attributes are calculated from the basic three as listed above in Eqs. [11 to 15] (Taner et al., 1994), this is implemented in the multi-attribute program EMERGE. These main attributes are generally used in the statistical derivation of reservoir properties. Some of these attributes derived from the primary ones are:

Amplitude-weighted Cosine Phase: This is the product of the cosine of the instantaneous phase and amplitude envelope. In equation form,

$$Ac(t) = A(t)\cos(\Phi(t)) \quad [17]$$

Amplitude-weighted instantaneous frequency: This attribute is defined as the product of the instantaneous frequency and the amplitude envelop:

$$AF(t) = A(t)\omega(t) \quad [18]$$

Amplitude-weighted phase: It is the product of the instantaneous phase, and amplitude envelope.

$$AP(t) = A(t)\Phi(t) \quad [29]$$

Derivative: The (numerical) derivative of the input trace is found via simply taking the difference between adjacent seismic trace sample points:

$$D(t) = s(t) - s(t - 1) \quad [20]$$

Integrate: This seismic attribute is constructed by computing first the running sum of the input trace. Then, the smoothed seismic trace is subtracted from the running sum. The default smoother length is 50 samples. In equation form, the integrate attribute is represented by

$$I(t) = \sum_{i=1}^N [S(t)] - s^\wedge(t) \quad [21]$$

where $s^\wedge(t)$ is the smoothed trace

Integrated Absolute Amplitude: it is defined as the running sum of the absolute amplitude of the seismic trace input, minus the smoothed amplitude envelope. In equation form:

$$I(t) = \sum_{i=1}^N [A(t)] - A^\wedge(t) \quad [22]$$

where $A^\wedge(t)$ = the smoothed envelope

Table 3.2: List of some seismic attributes and their significance.

Attribute	Significance in interpretation
Amplitude	Acoustic Impedance Contrast
Instantaneous Phase	Indicative of Lateral Continuity
Instantaneous Frequency	Bed Thickness Indicator
Amplitude Envelope	Reflection Strength
First Derivative of the Amplitude	Absorption Effects
Second Derivative of the Amplitude	Bed Thickness; Reflection Strength
Integrated Absolute Amplitude	Low Frequency Trends

Table 3.3: List of inverted seismic attributes and the employed method of inversion.

External Attribute	Method
Acoustic Impedance Contrast	Colored inversion approach
Acoustic Impedance Contrast	Sparse spike approach

3.4 Post Stack Seismic Inversion

There are several different approaches currently well established to invert seismic data spanning from very naïve to sophisticated methods. In this study I employed a Parametric Inversion method, namely Colored Inversion.

3.4.1 Colored Inversion Approach

Colored Inversion (Lancaster and Whitcombe, 2000) utilizes a method whose philosophy is borrowed from seismic processing, which simultaneously analyze the power spectra of a seismic trace and the well log to find an operator that would transform the spectrum of the average seismic trace to that of a fitted smooth curve which is representing the average reflectivity log spectrum. This gives the spectrum of the operator in question. Theory shows us that a phase rotation of 90 degree is also needed. This rotation is integrated into the operator. The theory behind this approach is that we consider the input seismic being zero phase. The Colored Inversion operator is simply an inverse-Fourier-transformed back to time domain then applied to seismic volume using a convolution algorithm.

3.5 Well to Seismic Tie

The second pre-processing step is the depth to time conversion. The seismic traces are sampled in units of time, the well logs are sampled in units of depth. Since the objective is to create synthetic seismic data, it is recommended to reference the well logs in time rather than depth.

Well log to Seismic tie is fundamental step in seismic interpretation (White and Simm, 2003). The main difficulty is that seismic amplitudes are usually interpreted in time domain, whereas well logs are measured in depth domain. Seismic-well-tie provides a functional relationship of time and depth which allows comparison of log properties recorded on wells with seismic attributes.

Tying wells to seismic data usually consists of forward modeling that is calculating a synthetic seismogram from p-wave and density logs, then comparing the synthetic data to the measured seismic. Problems arise for all kind of reasons: the accuracy of the logs, the quality of seismic data, uncertainty about handling the shallow section, uncertainty about integrating checkshots, and uncertainty about wavelets. Tying wells can be performed in the following steps:

1. calculate time-depth functional relationship from the sonic log
2. calculate reflection coefficients from the density and sonic logs
3. construct a synthetic seismogram utilizing the reflection coefficients
4. match the synthetic seismogram with the nearest seismic trace
5. update the time-depth functional relationship (if needed)

The results of each of these steps should be separately checked to assure correct well-seismic-ties. Every step can be modeled for credibility enhancing of the well-seismic-ties.

For example, check shots enhance the credibility of the function relationship of initial time to depth conversion. Error-free well logs enhance the quality of well-seismic-ties, as shown by White and Hu (1998). Credible modeling approaches for synthetic seismograms improve the correlation with seismic traces (White and Hu, 1998; White and Simm, 2003). A step of particular importance is an accurate wavelet estimation to be

used for synthetic seismogram modeling, and of course the seismic data must be of very high-quality for a good tie.

3.6 Multi-attribute Linear Regression

3.6.1 Conventional crossplotting

Assuming we have a particular seismic attribute, the easiest way for checking if there is an acceptable correlation between this seismic attribute and the target log properties is to crossplot the two variables. Assuming a linear functional correlation between the two parameters, a straight line fit of the form:

$$y = a + bx \quad [23]$$

can be found by regression analysis, that is by minimizing the mean-squared prediction error of coefficients a and b in Eq. [23] should minimize the expression

$$E^2 = \frac{1}{N} \sum_{i=1}^N (y_i - a - bx_i)^2 \quad [24]$$

The computed estimated error E is a measure of the how goodness-of-fit for the line of the regression, where the sum is over all samples in the plot.

3.6.2 Generalizing of crossplotting to include multiple attributes

The generalization of the traditional linear analysis to multi-variate linear regression can be done as follows, in the simplest case of only three attributes at every time sample. The target log can be modeled as a linear combination:

$$L(t) = w_0 + w_1 A_1(t) + w_2 A_2(t) + w_3 A_3(t) \quad [25]$$

After minimization of the mean-squared prediction error, the weights may be derived as values minimizing the expression

$$E^2 = \frac{1}{N} \sum_{i=1}^N (L_i - w_0 + w_1 A_{1i}(t) + w_2 A_{2i}(t) + w_3 A_{3i}(t))^2 \quad [26]$$

Let us consider the case when we have three attributes and four log samples, in matrix form the problem is formulated as

$$L1 = w_0 + w_1 A_{11} + w_2 A_{21} + w_3 A_{31} \quad [27]$$

$$L2 = w_0 + w_1 A_{12} + w_2 A_{22} + w_3 A_{32}$$

$$LN = w_0 + w_1 A_{1N} + w_2 A_{2N} + w_3 A_{3N}$$

Where the subscripts in A_{ij} are indicating the j -th sample point of the i -th attribute. In matrix form:

$$\begin{bmatrix} L1 \\ L2 \\ L3 \\ L4 \end{bmatrix} = \begin{bmatrix} 1 & A11 & A21 & A31 \\ 1 & A12 & A22 & A32 \\ : & : & : & : \\ 1 & A1N & A2N & A3N \end{bmatrix} \begin{bmatrix} w0 \\ w1 \\ w2 \\ w3 \end{bmatrix} \quad [28]$$

or

$$\mathbf{L} = \mathbf{AW} \quad [29]$$

where \mathbf{L} is a vector representing the known target values (log), \mathbf{W} is a 4×1 matrix with the unknown weights and \mathbf{A} is an $N \times 4$ matrix representing the attribute. Least-squares minimization gives the solution as

$$W = [A^T A]^{-1} A^T L \quad [30]$$

Based on (Hampson et al., 2001) a more detailed form of this equation is

$$\begin{bmatrix} w_0 \\ w_1 \\ w_2 \\ w_3 \end{bmatrix} = \begin{bmatrix} N & \sum A_{1i} & \sum A_{2i} & \sum A_{3i} \\ \sum A_{1i} & \sum A_{1i}^2 & \sum A_{1i} A_{2i} & \sum A_{1i} A_{3i} \\ \sum A_{2i} & \sum A_{1i} A_{2i} & \sum A_{2i}^2 & \sum A_{2i} A_{3i} \\ \sum A_{3i} & \sum A_{1i} A_{3i} & \sum A_{2i} A_{3i} & \sum A_{3i}^2 \end{bmatrix}^{-1} \begin{bmatrix} L_i \\ A_{1i} L_i \\ A_{2i} L_i \\ A_{3i} L_i \end{bmatrix} \quad [31]$$

This approach assumes an individual weight for every attribute. However the resolution of the target well log is much higher than that of the corresponding attributes of seismic trace (figure 3.1). So it is not possible to compare the seismic attributes trace with the well log in a sample point-by- sample point manner. A better way is to consider that every sample point on well log is represented by a number of neighboring sample points in a trace of the attribute. Generally, for any kind of well log property we can assume a special short filter operator which smears out the influences of each well log value over a range of contiguous traces of seismic sample points (Hampson et al., 2001). When we include such an operator into the Eq. [25], the equation becomes

$$L(t) = w_0 + w_1 * A_1(t) + w_2 * A_2(t) + w_3 * A_3(t) \quad [32]$$

where w_i are operators of some prescribed length and $*$ is indicating convolution. Note that the number of unknowns (weights and filter coefficients) to be estimated has increased to (operator length times number of attributes) +1. By minimizing the mean-squared prediction error we can easily find both the weights and the operator coefficients.

$$E^2 = \frac{1}{N} \sum_{i=1}^N (L_i - w_0 + w_1 * A_{1i}(t) + w_2 * A_{2i}(t) + w_3 * A_{3i}(t))^2 \quad [33]$$

As a simplest example, consider Eq. [32] for the case of four sample values and two attributes. With a convolution filter of 3-point length,

$$w_i = [w_i(-1), w_i(0), w_i(+1)] \quad [34]$$

Eq. [32] can be arranged in matrix form as:

$$\begin{bmatrix} L_1 \\ L_2 \\ L_3 \\ L_4 \end{bmatrix} = w_0 + \begin{bmatrix} w_1(0) & w_1(-1) & 0 & 0 \\ w_1(+1) & w_1(0) & w_1(-1) & 0 \\ 0 & w_1(+1) & w_1(0) & w_1(-1) \\ 0 & 0 & w_1(+1) & w_1(0) \end{bmatrix} \begin{bmatrix} A_{11} \\ A_{12} \\ A_{13} \\ A_{14} \end{bmatrix} \quad [35]$$

$$+ \begin{bmatrix} w_2(0) & w_2(-1) & 0 & 0 \\ w_2(+1) & w_2(0) & w_2(-1) & 0 \\ 0 & w_2(+1) & w_2(0) & w_2(-1) \\ 0 & 0 & w_2(+1) & w_2(0) \end{bmatrix} \begin{bmatrix} A_{21} \\ A_{22} \\ A_{23} \\ A_{24} \end{bmatrix}$$

By rearranging Eq. [35] we obtain

$$\begin{bmatrix} L_1 \\ L_2 \\ L_3 \\ L_4 \end{bmatrix} = w_0 + w_1(-1) \begin{bmatrix} A_{12} \\ A_{13} \\ A_{14} \\ 0 \end{bmatrix} + w_1(0) \begin{bmatrix} A_{11} \\ A_{12} \\ A_{13} \\ A_{14} \end{bmatrix} + w_1(+1) \begin{bmatrix} 0 \\ A_{11} \\ A_{12} \\ A_{13} \end{bmatrix} \quad [36]$$

$$+ w_2(-1) \begin{bmatrix} A_{22} \\ A_{23} \\ A_{24} \\ 0 \end{bmatrix} + w_2(0) \begin{bmatrix} A_{21} \\ A_{22} \\ A_{23} \\ A_{24} \end{bmatrix} + w_2(+1) \begin{bmatrix} 0 \\ A_{21} \\ A_{22} \\ A_{23} \end{bmatrix}$$

Eq. [36] shows that the inclusion of the convolutional operator of length N has multiplied the number of attributes by a factor of N , by shifting the attributes by -1 and +1 sample point the additional attributes can be obtained. By employing the same least-squares solution technique illustrated in the multi linear regression above, the final result derivation is

$$\begin{bmatrix} w_1(-1) \\ w_1 0 \\ w_1(-1) \end{bmatrix} = \begin{bmatrix} A_{12} & A_{13} & A_{14} & 0 \\ A_{11} & A_{12} & A_{13} & A_{14} \\ 0 & A_{11} & A_{12} & A_{13} \end{bmatrix}^{-1} \begin{bmatrix} A_{11} & A_{12} & 0 \\ A_{13} & A_{12} & A_{11} \\ A_{14} & A_{13} & A_{12} \\ 0 & A_{14} & A_{13} \end{bmatrix} \begin{bmatrix} L_1 \\ L_2 \\ L_3 \\ L_4 \end{bmatrix} \quad [37]$$

or

$$\begin{bmatrix} w_1(-1) \\ w_1 0 \\ w_1(-1) \end{bmatrix} = \begin{bmatrix} \sum_{i=2}^4 A_{1i}^2 & \sum_{i=2}^4 A_{1i} A_{1i-1} & \sum_{i=2}^3 A_{1i} A_{1i-2} \\ \sum_{i=2}^3 A_{1i} A_{1i+1} & \sum_{i=1}^4 A_{1i}^2 & \sum_{i=2}^4 A_{1i} A_{1i-1} \\ \sum_{i=2}^2 A_{1i} A_{1i+1} & \sum_{i=1}^3 A_{1i} A_{1i+1} & \sum_{i=1}^3 A_{1i}^2 \end{bmatrix}^{-1} \begin{bmatrix} \sum_{i=2}^4 A_{1i} L_{i-1} \\ \sum_{i=2}^4 A_{1i} \\ \sum_{i=2}^4 A_{1i} L_{i+1} \end{bmatrix} \quad [38]$$

3.6.3 Determining the Number of Attributes by Stepwise Regression

A stepwise regression algorithm was proposed by (Draper and Smith, 1966) as a fast, although not optimal approach. The idea behind this approach is the observation that if a linear combination of N seismic attributes is known to optimize some objective function,

then the best linear combination of $N + 1$ seismic attributes including the former N seismic attributes could only perform equally or better. (To prove this observe that the combination of N attributes can be considered as a special combination of $N+1$ attributes, by taking the $N+1^{\text{st}}$ with zero weight). During stepwise regression, the previously computed coefficients must be re-calculated. The procedure is implemented in the following steps. First, obtain the first, optimal single seismic attribute by exhaustive search. For every meaningful seismic attribute in the list, for example acoustic impedance, instantaneous phase, and so on, solve for the optimal coefficients and estimate the error of the prediction. The optimal one is the attribute with the minimum estimation error, let us call it optimal single attribute1. Second, search for the best combination of two attributes considering the optimal single attribute 1 to be one of them. From the other available and meaningful seismic attributes, form the best combination of two attributes, for example, (optimal single attribute1, instantaneous phase), (optimal single attribute1, second derivative), and so on. For each such pair of attributes, solve for the optimal weights and find the prediction error. The optimal two attributes is the pair for which this error is the smallest. Call the second attribute from the optimal combination as attribute 2, etc. Continue this procedure as long as needed. At each step of adding new attribute we also measure validation error, (which is the average error for all hidden wells, is employed as an estimation of the likely prediction error when the weight design is applied to the volume) we stop adding more new attribute when the validation error is starting not improving or even starts increasing.

Observe that the required computation time to implement this approach is much less than for an exhaustive normal search that would use all possible combinations. The main

theoretical difficulty with this approach is that we cannot be certain of really arriving at the optimal selection. However, the approach has the positive feature that we do not have to check whether the seismic attributes in the list are independent or not, because the stepwise regression spontaneously picks another seismic attribute whose contribution in a direction perpendicular to the subspace spanned by linear combinations of the former attributes is greatest. Consider, for instance, that we have a pair of seismic attributes, say, S_i and S_j , which depend on each other as : $S_j = a + b * S_i$. If during the stepwise regression – process one will be selected, say, S_i , then S_j will not be selected, because including S_j would not improve the estimation.

3.7 Theoretical Background of the Neural Networks

An artificial neural network (ANN) generates a nonlinear mapping between a set of input data and target outputs data. The properties of such nonlinear mapping depend not only upon the type and adjustable parameters of the ANN employed, but in a certain manner also on the input and output data used. This study aims to use *feed forward* (also called *back propagation*) ANN's, and Radial Basis Function implemented in the EMERGE software.

3.7.1 Feed Forward Back Propagation ANN's

This type of neural network is consisting of an input layer, one or more hidden layers, and an output layer (Figure 3.2) (Martin et al. 1996). Every layer has a number of neurons, every neurons of the previous and next layers is connected simultaneously. The input layer neurons are performing no computation, because they are simply input gates.

The hidden and output layers neurons have weights and biases connecting them to the neurons in the previous layer (Martin et al., 1996). Every neuron sums the weighted and biased inputs from each neuron in the previous layer and then computes a nonlinear function of the sum. This way, the output data and target input relationship is nonlinear. In the neurons one can utilize the commonly employed sigmoid-shaped nonlinear transfer function, the hyperbolic tangent sigmoid (Figure 3.2) and Eq. [39] or the log sigmoid (Figure 3.3) and Eq. [40]. The hyperbolic tangent sigmoid transfer and the log-sigmoid transfer functions respectively are

$$\tanh(n) = \frac{e^n - e^{-n}}{e^n + e^{-n}} \quad [39]$$

$$\log(n) = \frac{1}{1 + e^{-n}} \quad [40]$$

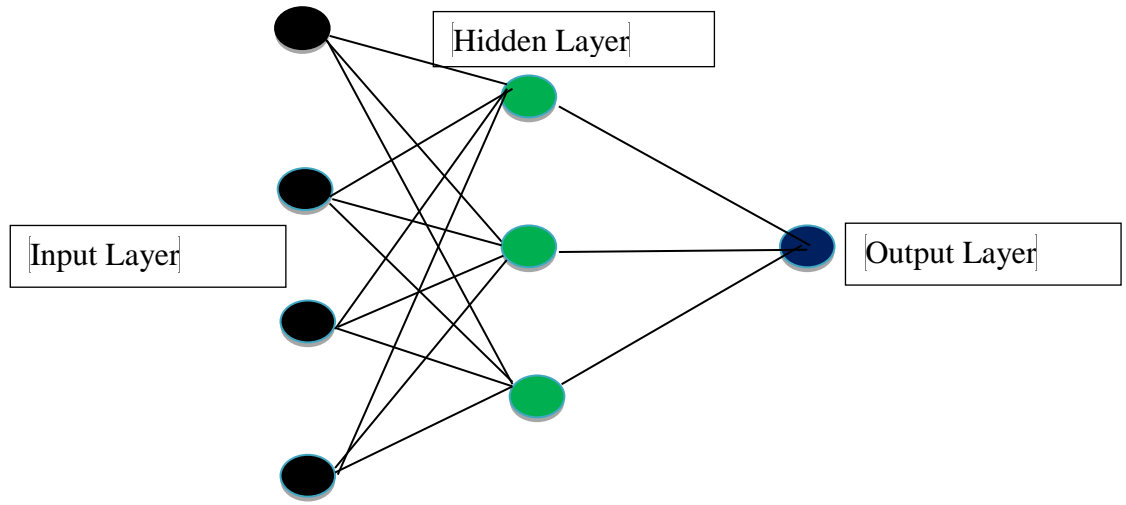


Figure 3.2: Architecture of a simple ANN's with hidden layer. In this scenario, the O1, O2 and O3 are input, hidden, and the output layer respectively. Every circle represents a node.

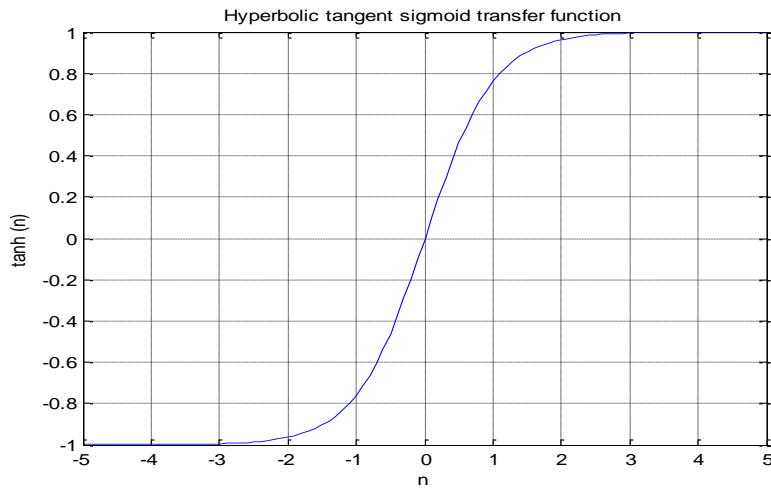


Figure 3. 3: Hyperbolic tangent sigmoid transfer function. Note how quickly the function saturates for absolute values greater than three. To make full use of the shape of this transfer function, the inputs are normalized to the range -1 to 1.

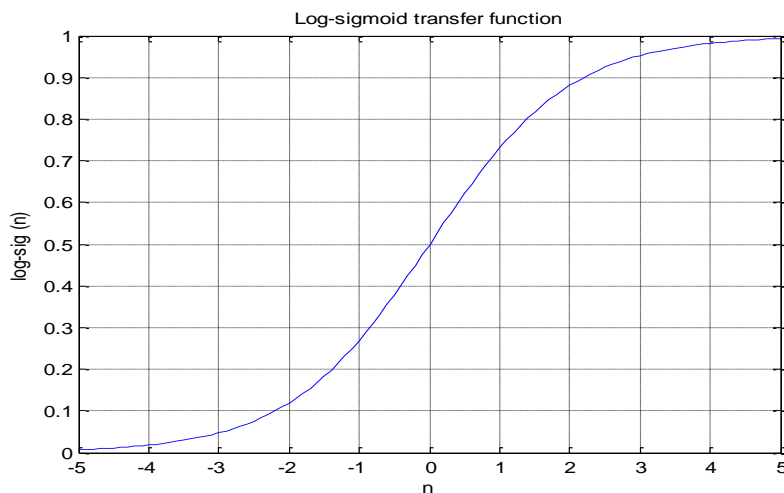


Figure 3. 4: Log sigmoid transfer function. Note how quickly the function saturates for absolute values greater than five. To make full use of the shape of this transfer function, the inputs are normalized to the range -1 to 1.

The output layer is the weighted and biased sum from the output of the neurons in the last hidden layer. This sum is not transformed in a nonlinear manner. Let the input vector, \mathbf{I} , be of length k . (Bias is a constant input given to neurons, the introduction of BIAS neurons permits us to move the transfer function curve horizontally along the input axis while keeping the curvature/ shape unchanged. This will make the network to produce arbitrary outputs different from the defaults and hence we can shift the input-to-output mapping to suit our particular needs).

For simplicity, suppose the case of single hidden layer. The output of the j -th neuron in such case, with transfer function f_2 is:

$$O_{2j} = f_2 \left(\sum_{i=1}^k I_i W_{ij} + b_{ij} \right) \quad [41]$$

$$O_3 = (\sum_{j=1}^n O_{2j} W_{ij} + b_{ij}) \quad [42]$$

where W_{ij} and b_{ij} are the weights and biases respectively, corresponding to the edge connecting the j th neuron in the hidden layer to the i th neuron in the input layer. The final output has single neuron, in case a single predicted property.

In order to correctly map the inputs to the output, the network will continuously update the weights and biases along the edges connecting each pair of neurons from successive layers till some performance criterion is achieved. This process is called *training*. Many different training algorithms exist, but error *backpropagation* is the most common for multi-layered neural networks (Martin et al., 1996; Taji et al., 1999). The ANN minimizes the difference between the predicted and target values using some specified error criterion. In backpropagation it is the square of mean error between the network

target and the input values that is used as the objective function to be minimized. Actually, in this case, as has been demonstrated, using the mean absolute error as the performance criterion would yield better results (Taji et all., 1999). I describe below backpropagation using mean absolute error, and the method when gradient descent method with momentum and a variable learning rate are utilized to train the ANN's.

For estimation-target pairs, $(p_1, L_1), (p_2, L_2) \dots (p_N, L_N)$, we want to minimize the mean

$$E = \frac{1}{N} \sum_{j=1}^N |L_j - p_j| \quad [43]$$

absolute error:

As the objective function is non-differentiable, this minimization can be accomplished by gradient descent. The name comes from the idea that in order to descend towards the local minimum of a function, one can take steps always in the direction of the negative gradient of the function at that value. For example, if γ is sufficiently small, then x^{n+1} will be closer to the local minimum of F than was x^n . (Superscripts are iteration numbers and F is the objective function to be minimized).

$$x^{n+1} = x^n - \gamma \Delta F(x^n) \quad [44]$$

This is an iterative process, which in many circumstances will converge towards some local minimum. Our aim is, therefore, to move towards the minimum in the mean absolute error surface, E . Weights and biases, w and b , are iteratively updated until this minimum is reached or reasonably well approximated. This is done for all weights and

biases in the network for a number of iterations until some stopping criterion is reached.

The gradient descent algorithm in this case becomes:

$$w_{ij}^{n+1} = w_{ij}^n - \gamma \Delta \partial \frac{E(w_{ij}^n)}{(w_{ij}^n)} \quad [45]$$

$$b_{ij}^{n+1} = b_{ij}^n - \gamma \Delta \partial \frac{E(b_{ij}^n)}{(b_{ij}^n)} \quad [46]$$

The value of γ can change between successive iterations, in this case it is called an adaptive learning rate. Convergence can be sped up if the learning rate is increased on flat parts of the error surface, and decreased where the slope is steep. To implement this in a simple way, the learning rate is increased if the error decreases, and decreased if the error increases.

A momentum operator may also be employed to stabilize the trajectory of the convergence. This will act as a low pass filter to smooth any oscillations in the convergence trajectory. To clarify momentum learning, let us recall that at the n -th iteration the weight update is:

$$\Delta w_{ij}^n = -\gamma \frac{\partial E(w_{ij}^n)}{\partial (w_{ij}^n)} \quad [47]$$

Momentum is the additional learning rate used at the beginning of learning to make learning faster. e.g. learning error is usually initially very large, so one starts with high momentum and adjust weights more aggressively. Later on during learning as the error decreases, momentum should also decrease so learning goes more slowly but it will be less likely to overshoot the target.

With momentum learning, updating becomes:

$$\Delta w_{ij}^n = \alpha \Delta w_{ij}^{n-1} - (1 - \alpha)\gamma \frac{\partial E(w_{ij}^n)}{\partial (w_{ij}^n)} \quad [48]$$

for some α that satisfies

$$0 < \alpha < 1 \quad [49]$$

Weights and biases will now converge quickly and stably towards the minimum on the mean absolute error surface (Martin et al., 1996). In this way, Neural Networks can create a transformation that minimizes the error between the output and the desired target.

3.7.2 Radial Basis Function (RBF) ANN's

Radial basis function (RBF) networks are feed-forward ANN's learned by a supervised learning algorithm (activation function in form of RBF). Such type of ANN's are typically built up of a single hidden layer where the functions of activation are selected from a set of functions named basis functions. Although this RBF NN is seem like back propagation one in various procedure, but RBF networks learns quicker, and less sensitive to non-stationary of the inputs.

Moody and Darken (1989), Popularized RBFNN and have proved to be a powerful neural network configuration. The RBF networks is different than the other networks by having one hidden layer that employ Gaussians as basis functions. Every unit in the hidden layer measures the degree of similarity between the weights or centers of the input vector and input vector itself. The basis unit is specialized pattern recognition. The basis units and outputs are connected through weights which employed to take linear combinations of the hidden layer's units to produce the final output.

3.7.2.1 Structure of the RBF Networks

Broomhead and Lowe (1988) were the pioneers to introduce RBF in the configuration of NN's. The configuration of an RBFNN's in its simple model has three level of layers. The input level consists of neurons whose dimension is similar to M of the input Z .

3.7.2.2 Hidden layer

This layer consists of nonlinear parts that are liked to all of the neurons in the input. Every hidden part has its input from all the nodes in the input layer. The hidden units contains a basis function, which has the two parameters: center and width. The mean of the basis function for a node i at the hidden layer is a vector c_i whose size is the same as of the input u , and there are generally various centers associated with every unit in the network. The radial distance d_i , between the input vector Z and the center of the basis function c_i is calculated for each unit i in the hidden layer as

$$d_i = ||Z - c_i|| \quad [50]$$

where $\|\cdot\|$ denotes the Euclidean norm.

The output h_i of each hidden unit i is then calculated by applying the basis function G to this distance.

$$h_i = G(d_i, \sigma_i) \quad [51]$$

where σ_i is a smoothness parameter and can also be interpreted as the variance of a Gaussian distribution centered on d_i .

3.7.2.3 Output layer

The mapping from the input space to the hidden unit space is nonlinear, however the mapping from the hidden unit space to the output space is linear. The j -th output is calculated as

$$x_j = F_j(Z) = w_{0j} + \sum_{i=1}^l w_{ij} h_i \quad j = 1, 2, \dots, M \quad [52]$$

In summary, the mathematical model of the RBF network can be formulated as:

$$X = F(Z), F: \mathbb{R}^N \rightarrow \mathbb{R}^M \quad [53]$$

$$x_j = F_j(Z) = w_{0j} + \sum_{i=1}^l w_{ij} G(||Z - c_i||) \quad j = 1, \quad [54]$$

The weight is calculated as in the following simple case (considering three attributes only):

$$\begin{aligned} x_1 &= w_1 A_{11} + w_2 A_{12} + w_N A_{1N} \\ x_2 &= w_1 A_{12} + w_2 A_{22} + w_N A_{2N} \\ &\vdots \quad : \quad : \quad : \quad : \\ x_N &= w_1 A_{N1} + w_2 A_{N2} + w_N A_{NN} \end{aligned} \quad [55]$$

the subscript A_{ij} is indicating the j th sample of the i th attribute. The equations above can be arranged in matrix form as

$$\begin{bmatrix} x_1 \\ \vdots \\ x_N \end{bmatrix} = \begin{bmatrix} A_{11} & \cdots & A_{1N} \\ \vdots & \ddots & \vdots \\ A_{N1} & \cdots & A_{NN} \end{bmatrix} \begin{bmatrix} w_1 \\ \vdots \\ w_N \end{bmatrix} \quad [56]$$

Or

$$X = AW \quad [57]$$

The solution to Eq.57 is simply the matrix inverse.

$$W = [A + \lambda I]^{-1} X \quad [58]$$

where λ is a pre-whitening factor and I is the identity matrix. When the weights are calculated, they are applied to the application dataset using the equation (54)

CHAPTER 4

RESULTS AND DISCUSSION

4.1 Wavelet Estimation

Wavelet estimation is a sensitive part in my study especially in the stage of seismic-to-well tie, and inversion of acoustic impedance. I estimated the wavelet by two different methods: (1) statistical approach by estimating wavelet using seismic data (2) deterministic approach by estimating wavelet from well-log data, then I accounted for the phase shift between the two results to optimize the correlation between seismic data and synthetics seismogram. In case 1 I extracted 200-ms long wavelets, constrained by the cosine taper with 25% wavelet length at both start and end of the wavelets to limit side-lobe amplitudes (figure 4.1). I extracted the wavelet from the average of nine traces centered at the well location. The estimated wavelets in frequency domain were zero phase (figure 4.2), due to the fact that the seismic data had been processed for zero phase.

In case 2, to improve the correlation and matching between synthetics and seismic section, I also extracted a wavelet, by utilizing information of the well logs to determine the correct phase. I extracted 150-ms long wavelets, constrained by the cosine taper with 20% wavelet length at both start and end to limit side-lobe amplitudes and to get constant phase (figure 4.3). In frequency domain I found the average phase to be -33 degrees (figure 4.4). Then the two results were combined to yield better correlation and well-to-seismic-tie.

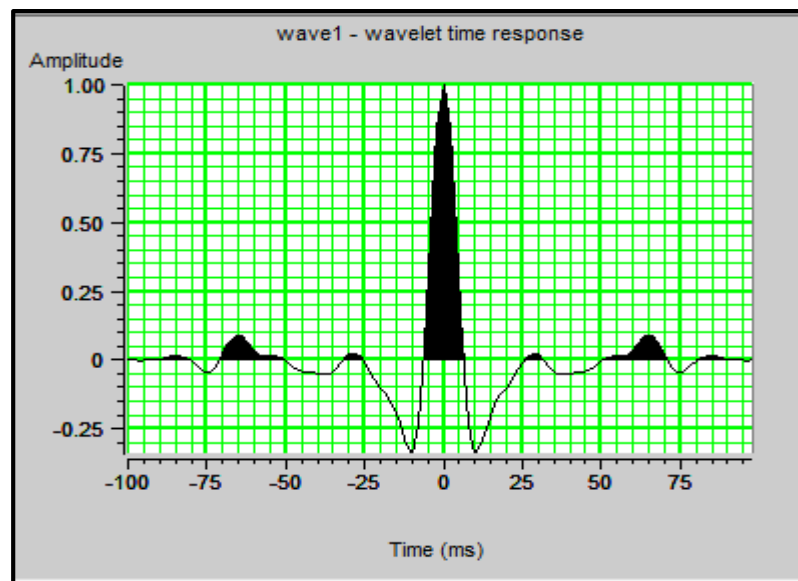


Figure 4.1: Amplitude of extracted wavelet by statistical approach in time domain from the seismic data alone. The extracted wavelet parameters are: wavelet length 200ms, sample rate 2ms, taper length 25, and Phase type is constant with zero phase rotation

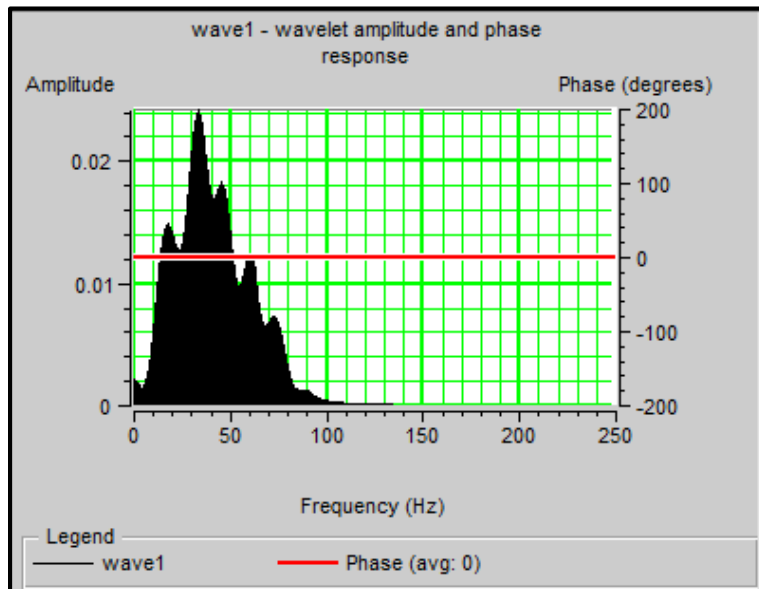


Figure 4.2: Phase spectra and amplitude of the extracted wavelet in (figure 4.1). Note that the maximum frequency, and spectral amplitude are around 100, and 40 Hz respectively. It is a zero phase wavelet.

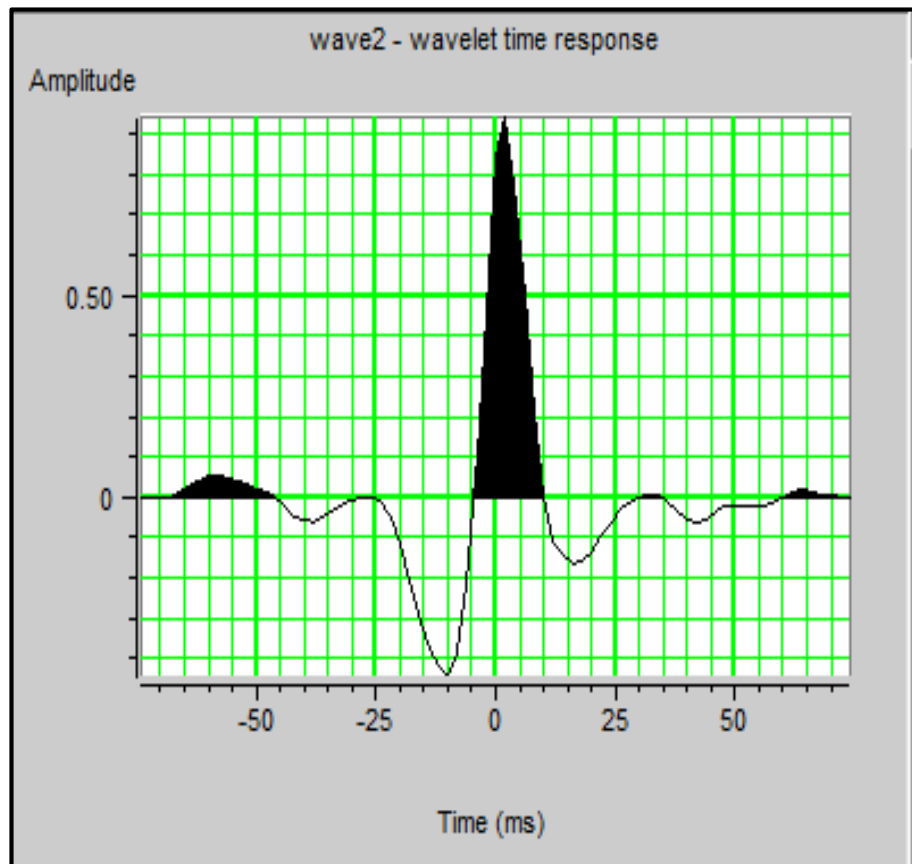


Figure 4.3: Wavelet extracted by statistical approach from the well logs alone. The parameters of extracted wavelet are: wavelet length 200 ms, sample rate 2ms, length of taper 25, and Phase type is constant with zero phase rotation. Note that this wavelet is slightly shifted compared with (Figure 4.1) which indicates there is phase shift between synthetic seismogram and seismic data that has to be corrected.

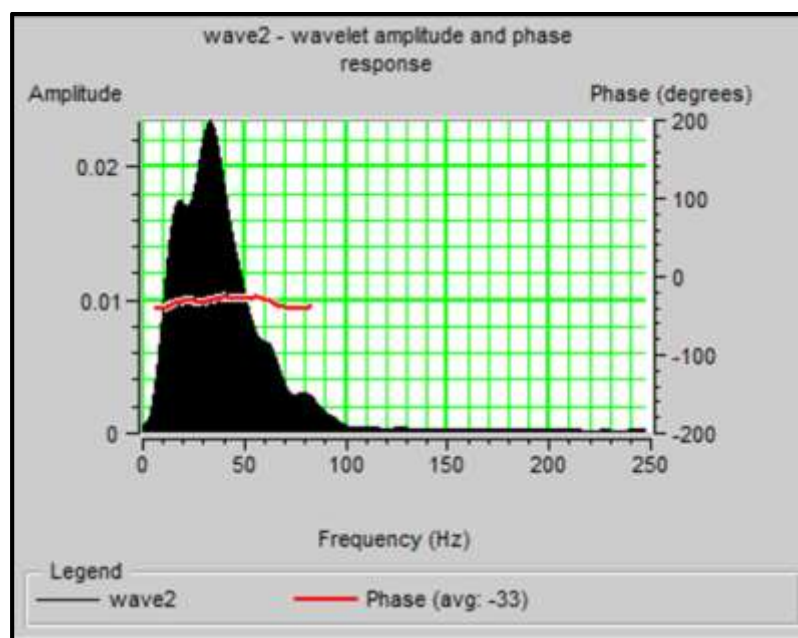


Figure 4.4: Phase spectra and Amplitude in frequency domain of the extracted wavelet in (figure 4.3). The maximum frequency and amplitude of this wavelet are around 100 Hz, and 0.02 (occurring at around 35Hz) respectively, however it is not a zero phase wavelet because the phase is rotated around -33 degrees. This phase information is used to solve phase mismatch problem.

4.2 Post-stack inversion

For performing post-stack seismic inversion, a primary velocity model of the earth's subsurface is constructed from two data streams consisting of picked horizons and velocity/density information in the form of well logs. The main role of this model is to add a consistent low frequency component missing from the seismic, and using it in a full inversion of the seismic data. Different post-stack inversion algorithms are available however only one "colored" inversion technique was employed in this study to simultaneously invert the seismic and well log data for P-impedance. To validate the inversion accuracy and credibility, I plotted the predicted impedance against the actual impedance calculated from well log data. The result shows that the predicted and actual data are aligned around the 45-degree direction, which indicates their high correlation (figure 15). The inversion accuracy and errors are displayed in (Table 4.1) documenting an acceptable level of accuracy.

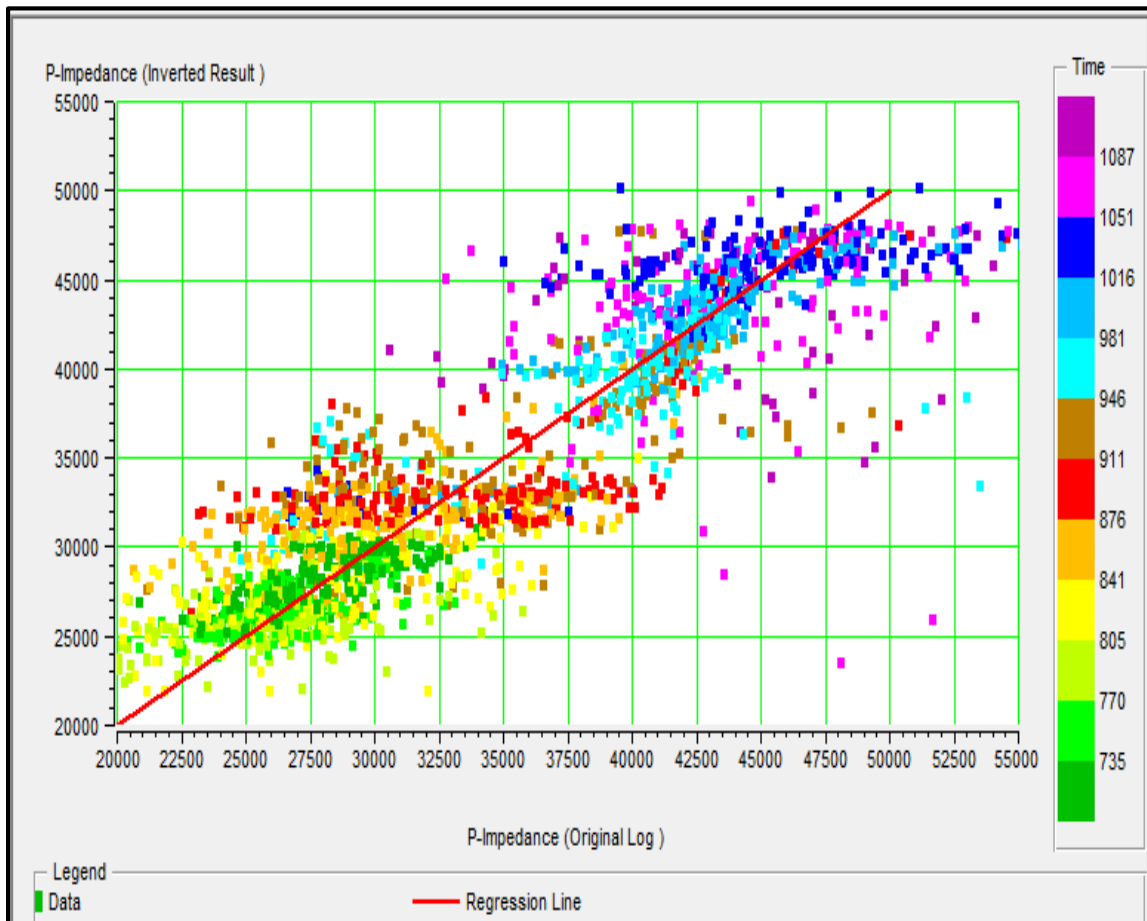


Figure 4. 5: Cross plot between original acoustic impedance calculated from log data (x axis) and inverted acoustic impedance calculated from seismic data being constrained by well logs (y axis), the red is the regression line.

Table 4.1: The correlation coefficients and corresponding estimation errors of inversion result.

Well name	RMS Error Between Original and Inverted Result	Inverted Synthetic Correlation	Synthetic Relative Error
1-10	3888.51	0.99	0.05
10-10	3501.94	0.99	0.06
62-11	4048.51	0.99	0.08
76-10	4533.43	0.99	0.04
17-21	3788.45	0.99	0.47
2-25	4508.21	0.99	0.06
56-10	4871.05	0.99	0.03
25-11	4112.72	0.99	0.03
41-3	4443.42	0.99	0.06
51-10	4424.13	0.99	0.04
52-10	4435.76	0.99	0.04

4.3 Results of Lithology and Porosity Estimation

This study focuses on two target reservoirs in Teapot Basin, namely, Second Wall Creek member of Frontier Formation and Tensleep Formation.

The top of the first target reservoir occurs at depths between 2900-3300ft around 400-441 ms, where its lithology is sand. The top of the second reservoir target occurs at depths between 5500-5900ft (810-840ms) where the lithology is alternating sandstone and dolostone, Darton (1906, 1904). One of the objectives of the study are to distinguish between sandstone, limestone and dolomite constituent fractions of each unit, and to delineate their porosity. From the Schlumberger master chart of neutron porosity and density cross plot, I was able to calculate porosity, and construct a lithology log curve. For the lithology log curve numerical values ranging from 1-3 were assigned, where 1 represents pure sandstone, 2 represents pure limestone, and 3 represents pure dolostone, while the fractional values between 1 to 3 represent mixed lithologies. For example 1.3 indicates a lithology of 70 percent sand and 30 percent limestone; 2.8 represents lithology of 20 percent limestone and 80 percent dolostone, and so on (figures 5.1 and 5.2).

4.3.1 Lithology Identification of Second Wall Creek and Tensleep

After having performed pre-processing, and tying wells to seismic as explained in (chapter 3 section 3.1). I had to decide first which seismic attributes are the most appropriate for predicting the target log (in this case: lithology). First I cross-plotted each attribute versus the lithology log of the reservoir targets, then I calculated the normalized correlation coefficients and ranked them in decreasing order (Tables 4.2, 4.3).

Table 4.2 shows the normalized cross correlation results of different seismic attributes cross-correlated against the well lithology log from Second Wall Creek reservoirs. The attribute with best correlation coefficient is Filter 35/40-45/50, though the correlation seems rather poor, 0.45, with high error percentage around 20%. The weakest correlation was obtained for the attribute Average Frequency which gave a correlation about 0.07, with error of 22%. Table (4.3) contains cross-correlations of different seismic attributes against the lithology log of Tensleep reservoir with normalized correlation coefficients and the corresponding error. The best correlating attribute in this case is Integrated Absolute Amplitude, which gives a correlation coefficient of 0.4 with an error of 32%, the lowest correlation belongs to the from Second Derivative (correlation coefficient -0.05, error about 36%).

From (Tables 4.2, 4.3) we can deduce that none of these attributes can be considered sufficient to be used individually for predicting the lithology log in Second Creek and Tensleep reservoir.

Figure 4.6 shows cross plot between lithology log of nine wells and a single seismic attribute (filter 5/10-15/20 of inverted volume) in the Second Wall Creek reservoir, the red line is regression line. From this figure we can see how widely the two variables are scattered in the graph which explains the low correlation (about 0.46) and high error (about 25%).

Figure 4.7 shows the cross plot between lithology log and another seismic attribute (Dominant Frequency) of Tensleep reservoir, the red line is regression line. While there is a clear positive correlation, the data is scattered in the graph which results in low

correlation (about 0.4) and high error (about 41%). To increase the predictive power of the attributes, I decided to employ combination of a set of attributes rather than single attributes. From the listed attributes in (Tables 4.2, 4.3) a set of attributes were taken simultaneously (by the method of Hampson et al., 2001). I found that using four attributes and applying an eight-point convolutional operator is the best way to handle the differences in frequency between log and seismic data for Second Creek and Tensleep respectively. The appropriate attributes combination were identified using the step-wise regression analysis approach (Hampson et al., 2001). The results are illustrated in (Tables 4.4, and 4.5).

In table (4.4) the first row, for example, shows the best single attribute which is Filter 5/10-15/20 (inversion), the other selected attributes are Cosine instantaneous phase, Filter 25/30-35/40, and Average frequency (inversion result). These four attributes are the best combination of attributes that can be used as input. Although adding more attributes would further reduce the training error, it might cause an increase in validation error. This is very clear in table (4.4) when I added a fifth attribute (filter 35/40-45/50) to the set of 4 attributes above it, which had caused the training error to be reduced from 0.139 to 0.130. At the same time however the validation error increased from 0.180 to 0.190. Finally, only the combination of the first four attributes listed in (table 4.4) with different weights were used to predict the lithology, due to their minimum validation error.

Table 4.5 shows the training and validation errors for combination of up to seven attributes, namely, Integrated Absolute Amplitude, Instantaneous Frequency, Average Frequency (Inversion), Filter 55/60-65/70 (Inversion), Dominant Frequency (Inversion), Filter 25/30-35/40, and Filter 25/30-35/40 (Inversion). For example, the second row is

combination of two, namely the first and second attributes, the third raw is combination of the first, second and third attributes, and so on. The selection criterion for the optimal number of attributes to be used is the behavior of the validation error: we stop adding more attributes when the validation error starts to increase. In the above-discussed case the optimal combination was obtained when I used the first five attributes (table 4.5). Note that, for both reservoir targets the correlation error is slightly improved compared to the case of single attribute

To compute the validation error, in my study I divided the entire input dataset into two groups (Figure 4.8, 4.9): a training dataset (original data in black) and a validation dataset (predicted data, in red).

Figure 4.8 shows the optimal number of attributes to be used to predict the Second Wall Creek reservoir lithology, the horizontal axis indicates the number of attributes employed in the estimation. The vertical axis is the root-mean-square prediction error of attributes. By using a filter operator length of four points, we can see that the optimal number of attributes to be combined are four, and afterward no improvement occurs. (Figure 4.9) illustrates the errors associated with a set of nine attributes in (Tensleep reservoir), the black line is training error of nine attributes when we are using all wells, the red line is validation error of nine attributes when we are excluding one well and re-derive the log of the excluded well. As anticipated, the training error as well as the validation error are decreasing as we add more attributes, however at some point the validation error **is** starts to increase once again when we add more attributes, which is the criterium telling that no more attributes are needed. From (figure 4.8), we can infer it is best to use only a set of

four attributes to avoid a greater validation error, while from (figure 4.9), the optimal number of attributes to be combined with minimum error and high correlation is five.

Figure (4.10) shows the cross plot between original lithology log calculated from density and neutron porosity logs and predicted lithology log estimated from combinations of 4 attributes in Second Wall Creek reservoir. The correlation between the two logs is 0.84 which is considered better than in the case of single attributes in (Figure 4.6), however the data are still scattered.

Figure (4.11) shows the cross plot between original lithology log and predicted lithology log estimated from combinations of five attributes in Tensleep reservoir. The correlation between the two logs is weaker (0.70 with error of 0.32) compared with the case of the Second Wall Creek reservoir, however, it is certainly better than in case of single attributes. The data are still scattered.

Table 4.2: Lithology results of a single seismic attributes estimation, the last two columns contain the estimation and coefficients of correlation (Second Wall Creek).

Target Log	Attribute	Error	Correlation
Lithology	Filter 5/10-15/20 (Inversion)	0.20	0.45
Sqrt-Lithology	Second Derivative	0.20	-0.35
Lithology	Filter 15/20-25/30	0.20	0.33
1/Lithology	Filter 25/30-35/40	0.21	-0.18
1/Lithology	Amplitude Weighted Phase	0.22	-0.18
Lithology	Cosine Instantaneous Phase	0.22	-0.15
(Lithology) ²	Instantaneous Frequency	0.22	0.13
Lithology	Amplitude Envelope	0.22	0.12
Log-Lithology	Apparent Polarity	0.22	0.12
Log-Lithology	Average Frequency	0.22	-0.07

Table 4.3: Single seismic attribute Table with corresponding estimation errors and coefficients of correlation for Tensleep reservoir.

Target Log	Attribute	Error	Correlation
Lithology	Integrated Absolute Amplitude	0.32	-0.40
Lithology	Dominant Frequency	0.33	0.37
1/Lithology	Integrated Amplitude (Inversion)	0.33	-0.34
Log-Lithology	Average Frequency	0.34	0.28
Lithology	Average Frequency	0.34	0.27
Sqrt-Lithology	Filter 15/20-25/30	0.34	-0.24
Sqrt-Lithology	Amplitude Envelope	0.34	-0.22
Lithology	Instantaneous Phase	0.34	0.20
Lithology	Instantaneous Frequency	0.34	0.19
Log-Lithology	Amplitude Weighted Phase	0.34	-0.18
Sqrt-Lithology	Cosine Instantaneous Phase	0.35	-0.15
Lithology	Apparent Polarity	0.35	0.12
Lithology	Second Derivative (Inversion)	0.35	0.06
Lithology	Second Derivative	0.35	-0.05

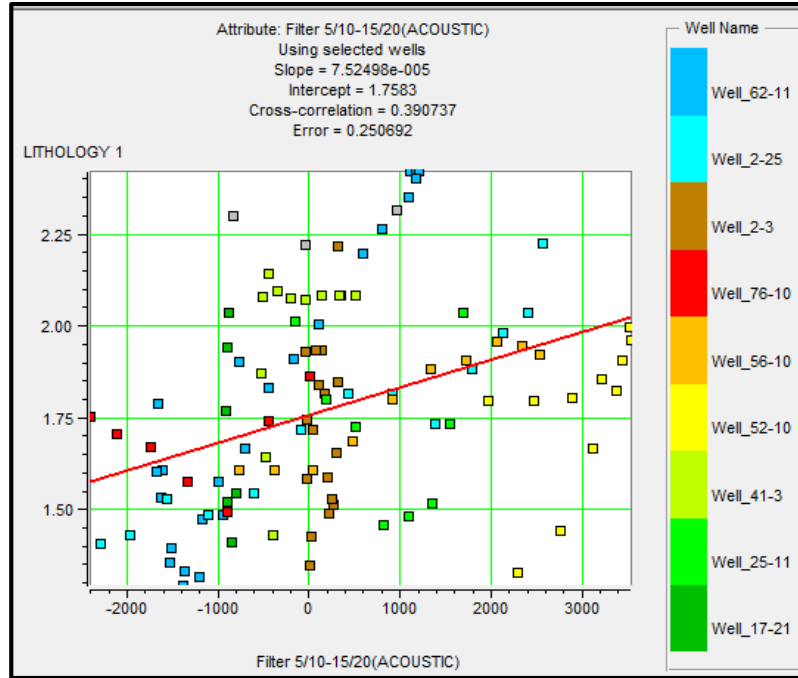


Figure 4.6: Crossplot of actual lithology and Filter 5/10-15/20 attribute (Second Wall Creek).

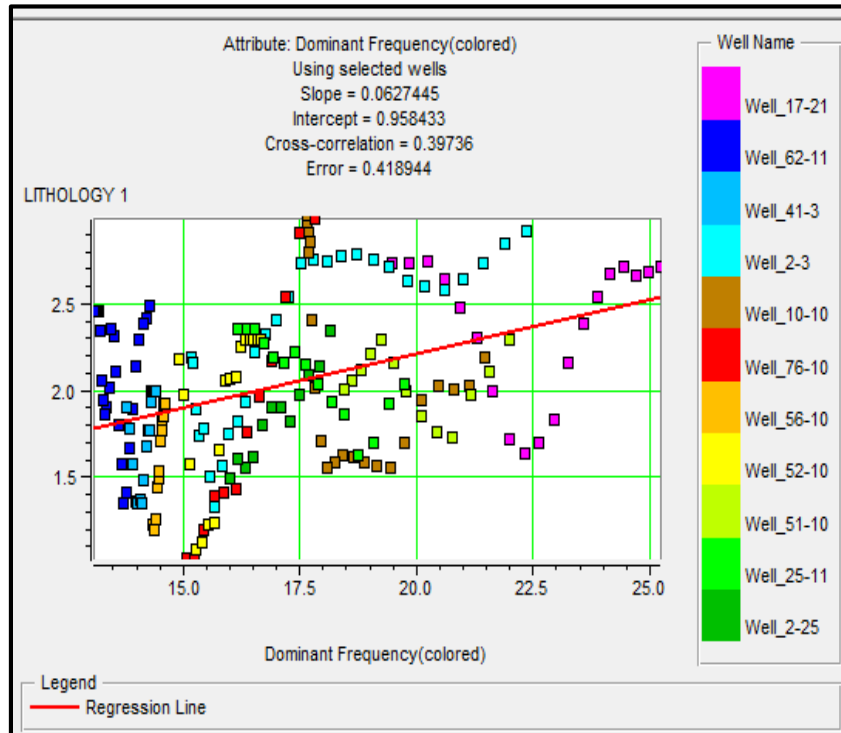


Figure 4.7: Crossplot of original lithology and Dominant Frequency attribute (Tensleep).

Table 4.4: Performance of stepwise regression, implemented for the lithology prediction problem in Second Creek reservoir. Every line illustrates a different attribute transform with increasing number of seismic attributes involved. The set of multi-attributes for each row involves all previous attributes. The error of validation for each transform is illustrated in the final column in the same units as the target log.

Target Log	Attribute	Training Error	Validation Error
Lithology	Filter 35/40-45/50 (Inversion)	0.18	0.20
Lithology	Cosine Instantaneous Phase	0.17	0.20
Lithology	Filter 25/30-35/40	0.15	0.19
Lithology	Average Frequency (Inversion)	0.13	0.18
Lithology	Filter 35/40-45/50	0.13	0.19

Table 4.5: Result of stepwise regression, implemented to the lithology prediction problem in Tensleep reservoirs. Each row reveals a different set of multi-attributes with increasing numbers of attributes. The set of attributes in each row contain all previous attributes. The last column gives the validation error of that transform.

Target Log	Attribute	Training Error	Validation Error
Lithology	Integrated Absolute Amplitude	0.40	0.44
Lithology	Instant Frequency	0.36	0.43
Lithology	Average Frequency (Inversion)	0.35	0.41
Lithology	Filter 55/60-65/70 (Inversion)	0.35	0.40
Lithology	Dominant Frequency (Inversion)	0.32	0.39
Lithology	Filter 25/30-35/40	0.30	0.40
Lithology	Filter 25/30-35/40 (Inversion)	0.27	0.39

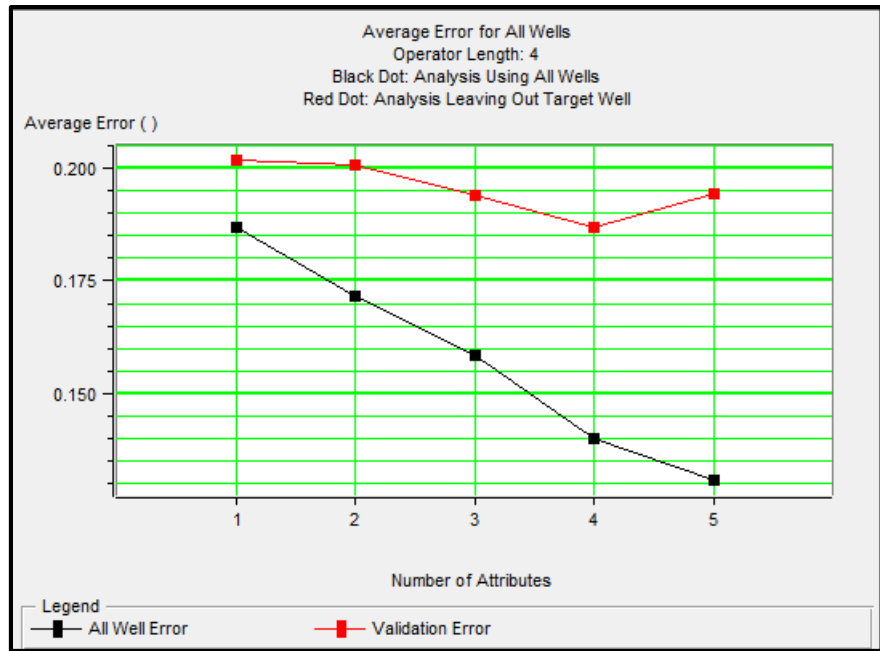


Figure 4.8: Plot of validation error of wells showing the optimal combination of attributes to estimate lithology is four. The black dots show the error using all wells, whereas the red dots illustrate the error once one well is removed. (Second Wall Creek).

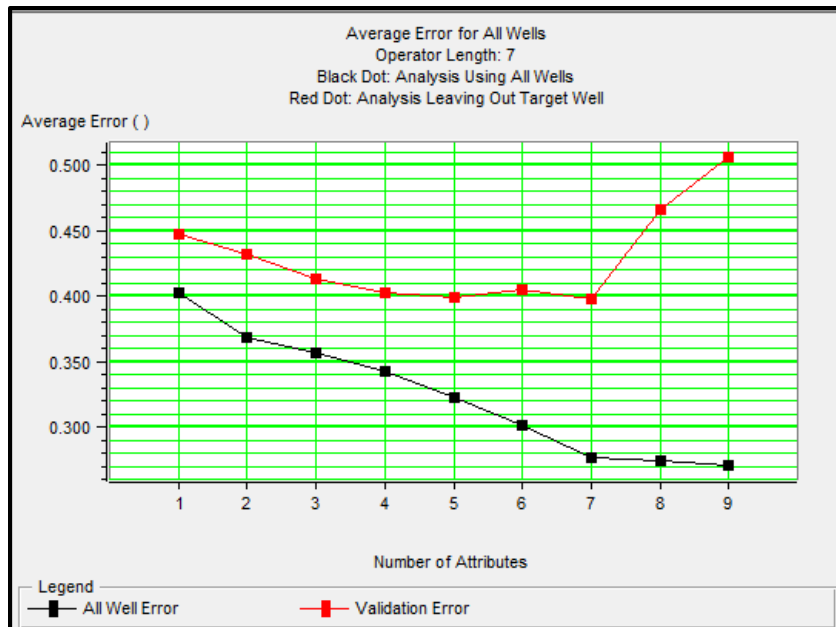


Figure 4.9: Plot of Validation error for all wells showing that the optimal number of attributes to estimate lithology is five. The black dots illustrate the error when we utilizing all wells, whereas the red dot illustrate the error when one well is removed, (Tensleep).

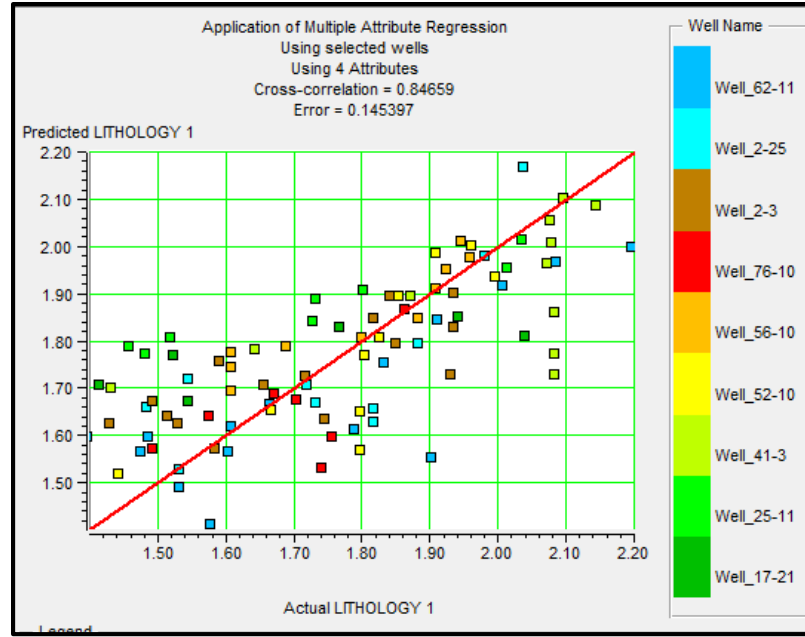


Figure 4.10: Cross validation between original lithology log calculated from density and neutron porosity logs and predicted lithology log estimated by using combinations of 4 different attributes. (Second Wall Creek).

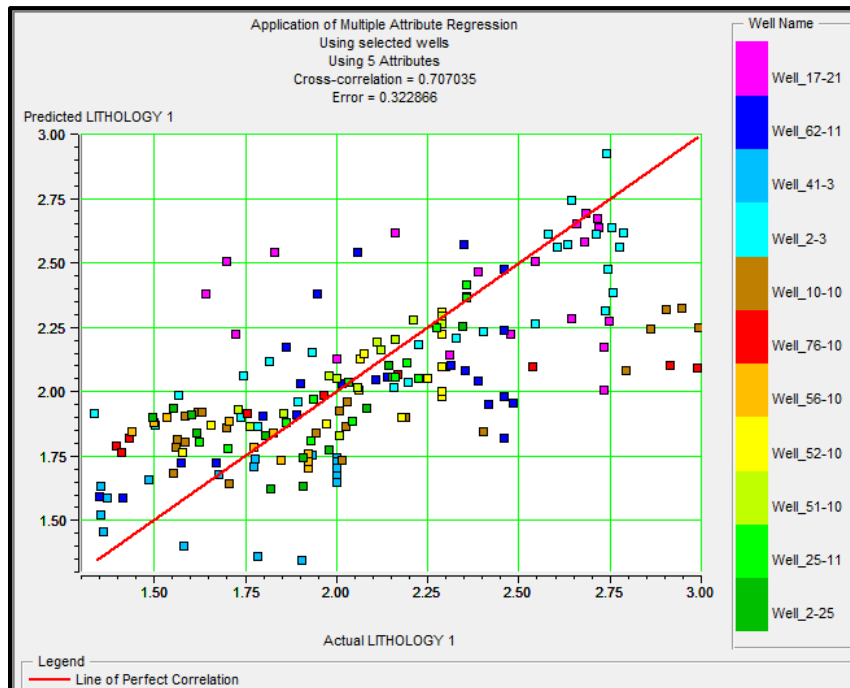


Figure 4.11: Cross plot between original lithology log calculated from density and neutron porosity logs and predicted lithology log estimated from combinations of five attributes. (Tensleep).

4.3.2 Application of Neural Networks

4.3.2.1 Lithology Prediction with an Artificial Neural Network

When an appropriate set of seismic attributes had been identified as illustrated in previous steps, a neural network may be trained to generate pseudo well logs from the cube of seismic attributes. The selection of appropriate neural network is heuristic in nature. Before I found an appropriate network, I investigated and tested four types of networks, and ultimately selected only one to work with. The tested networks differed in the number of hidden layers, the number of neurons in each of those hidden layers, transfer functions of the neurons, training algorithms, and optimization criteria. Among the many networks tested, the most accurate and well-generalizing network was a radial basis function network consisting of input, hidden and output layers with Gaussian transfer functions. All wells were used in the prediction process, the performance of the ANN was analyzed by keeping one well aside as a test case, and training the network on the remaining nine wells. This procedure was performed as many times as number of wells.

Figure (4.12) shows correlation between predicted lithology and actual lithology for Second Creek reservoir. Five attributes were used to train the RBF neural networks with operator length of four points. The correlation coefficient is higher in this case (0.87) than for Multi-attribute Analysis (0.84%), the validation error is less compared with the linear mode, the data is more aligned when checking the fitting (almost 45 degree).

Figure (4.13) shows the result of training RBF neural networks using five attributes, with operator length of seven points with 11 well data from Tensleep reservoir. The model has

reached high improvement in correlation between predicted and calculated logs compared with the case of multi linear attribute: the normalized correlation coefficient is more than 0.87 with a small training error around 0.14.

In both cases, as expected, due to the non-linear behavior of the targets, the Neural Network performed better due to its non-linearity compared with the linear model. This is clearly seen from the coefficient of normalized correlation, and the less amount of outlier data.

Figure (4.14) shows result of training RBF neural networks with the same configuration as figure (4.13) except excluding one well. Note the improvement in correlation between predicted and calculated logs compared with the case of multi linear attribute. The normalized correlation coefficient is more than 0.90 with small training error of 0.15 in units of the lithology log.

Figure (4.15) shows results of using RBF neural networks, with the same number of attributes and parameters as in figure (4.14), after excluding two wells with high error contribution. Note the improvement in correlation between predicted and calculated logs (0.92 with error of 0.14).

The improvement in prediction when I excluded three wells were attributed to two reasons: either high error of these well data or non-perfect well to seismic tie, because the locations of the wells are not far from each other.

Figures (4.16, 4.17) show validation errors of Second Wall Creek and Tensleep reservoirs, respectively. The lower curve (black line) is training error when all wells were used in the analysis, while the upper curve (red line) is validation error when some

specific well was excluded. The differences between training and validation errors in cases of both reservoirs are relatively small.

Figure (4.18) shows the application of the learning output of RBF neural networks to target zone (blue line, Second Wall Creek) of wells using the same number of attributes and parameters as in figure (4.13), Note the good match between actual log (black) and predicted log (red). Figure (4.19) shows application of learning output of RBF neural networks to the target zone (Tensleep reservoirs) using the same number of attributes and parameters as in figure (4.14), Note the excellent match between actual log (black) and predicted log (red).

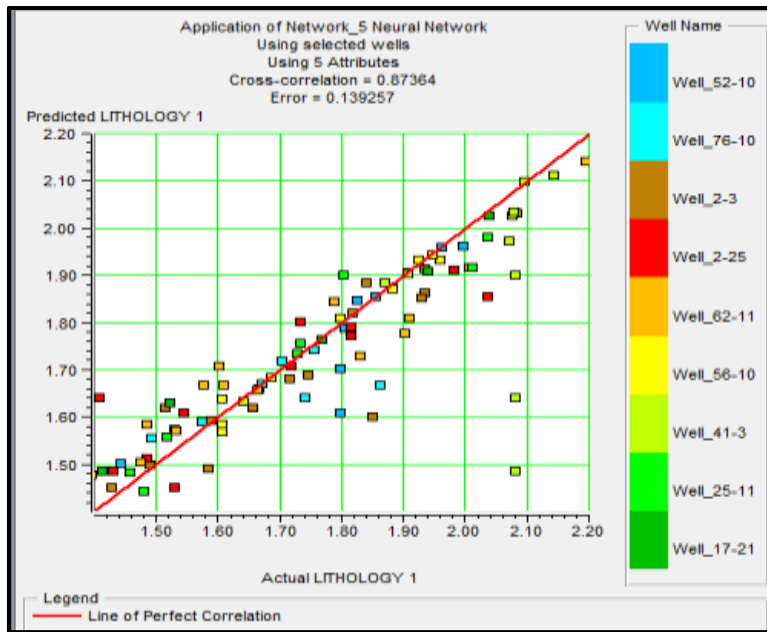


Figure 4.12: Result of using RBF neural networks with the same attributes as in the figure (4-10). Note the improvement in correlation and error between predicted and calculated logs compared with the case of multi linear regression (Second Wall Creek).

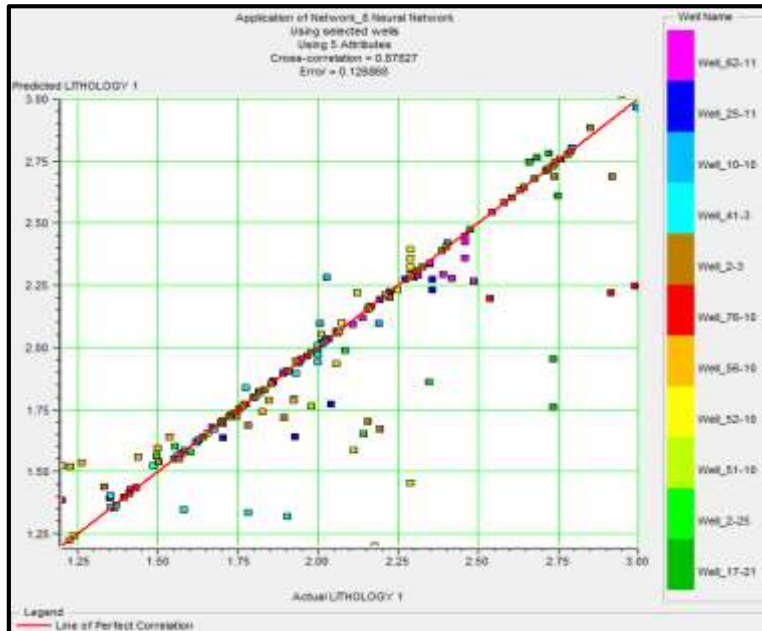


Figure 4.13: Result of using RBF neural networks with the same attributes as in the (figure 4.11). Note the improvement in correlation and error between predicted and calculated logs compared with the case of multi linear regression. (Tensleep).

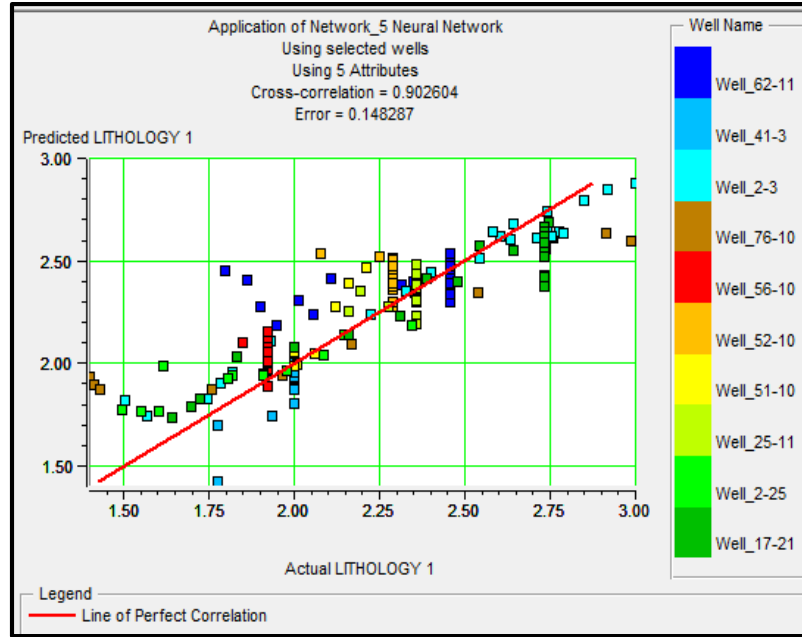


Figure 4.14: Result of using RBF neural networks with the same configuration parameters as in (Figure 4.13). However, one well has been excluded. Note the improvement in correlation and error between predicted and calculated logs compared with the case of six attributes. (Tensleep).

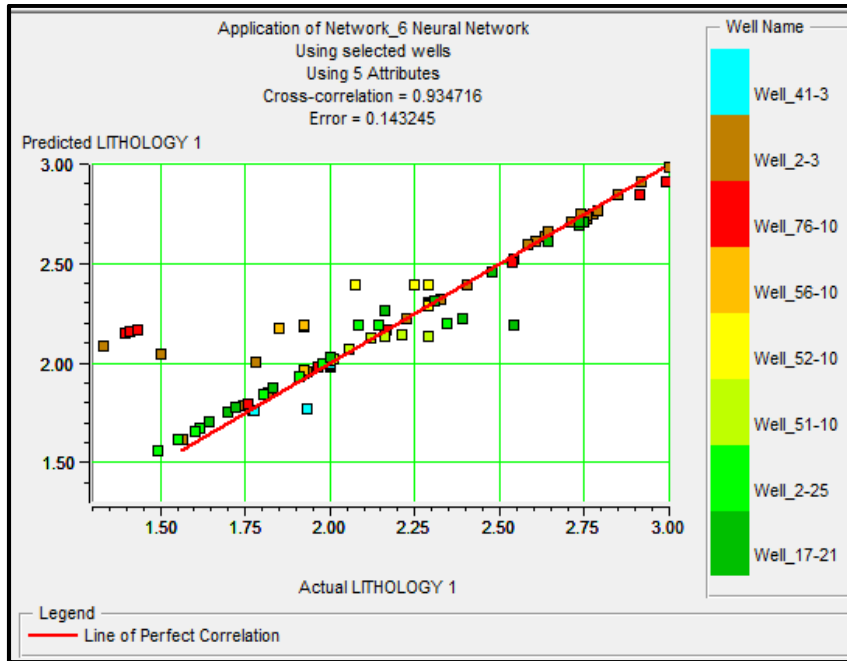


Figure 4.15: Result of using RBFNN's, with the same combination of attributes and parameters as (Figure 4.13), after excluding two wells with high error contribution. Note the improvement in correlation and error between predicted and calculated logs. (Tensleep).

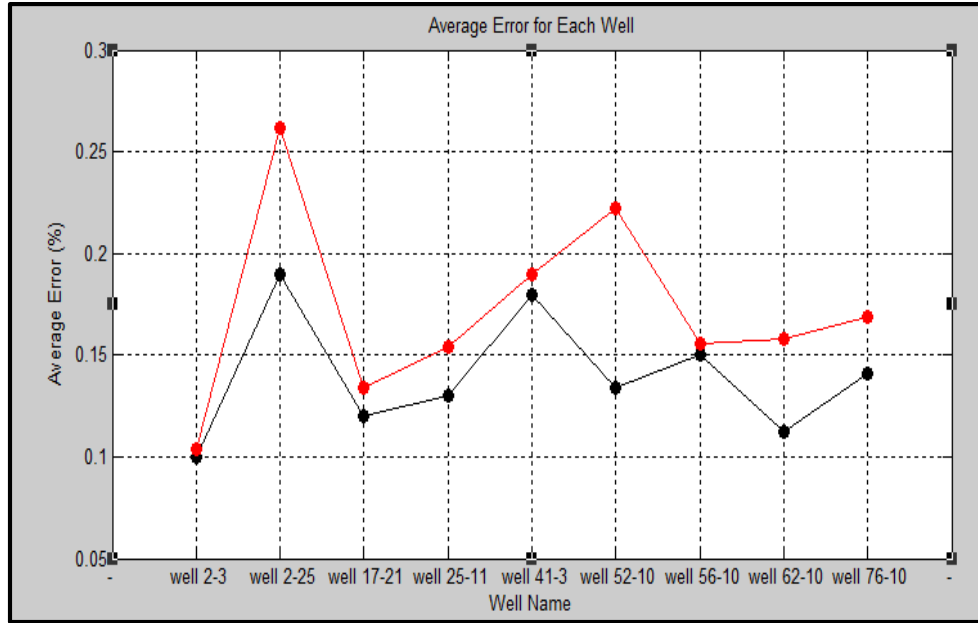


Figure 4.16: The estimation errors for each of the 9 wells (Second Wall Creek). The black line illustrates the estimation error when a particular well is utilized in the prediction. The red line illustrates the validation error when the specified well is not employed in the prediction.

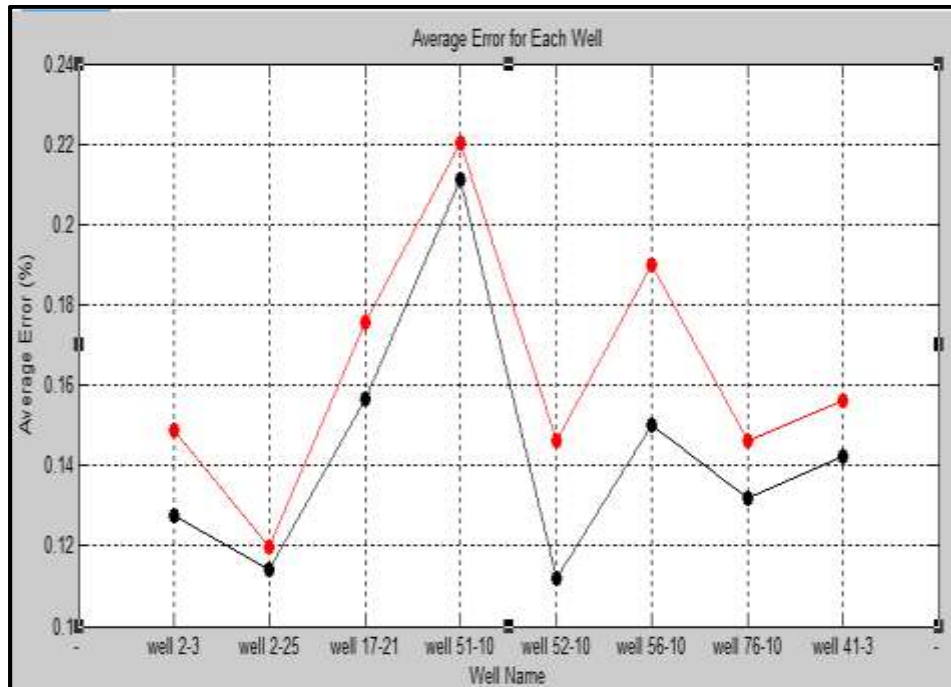


Figure 4.17: The estimation for each of the 8 wells (Tensleep reservoir). The black line illustrates the error of estimation when a particular well is employed in prediction. The red line illustrates the error of validation that well when is not employed in the prediction.

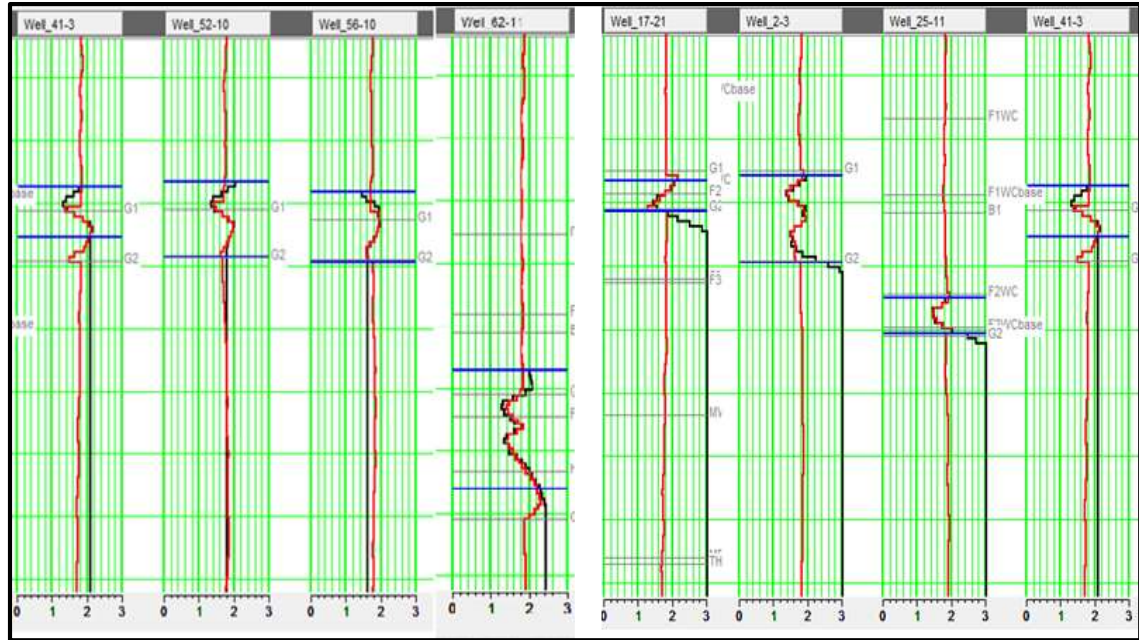


Figure 4.18: Applying the RBFNN's utilizing set of four attributes (Second Wall Creek). The original lithology and the predicted log is shown in black and red respectively.

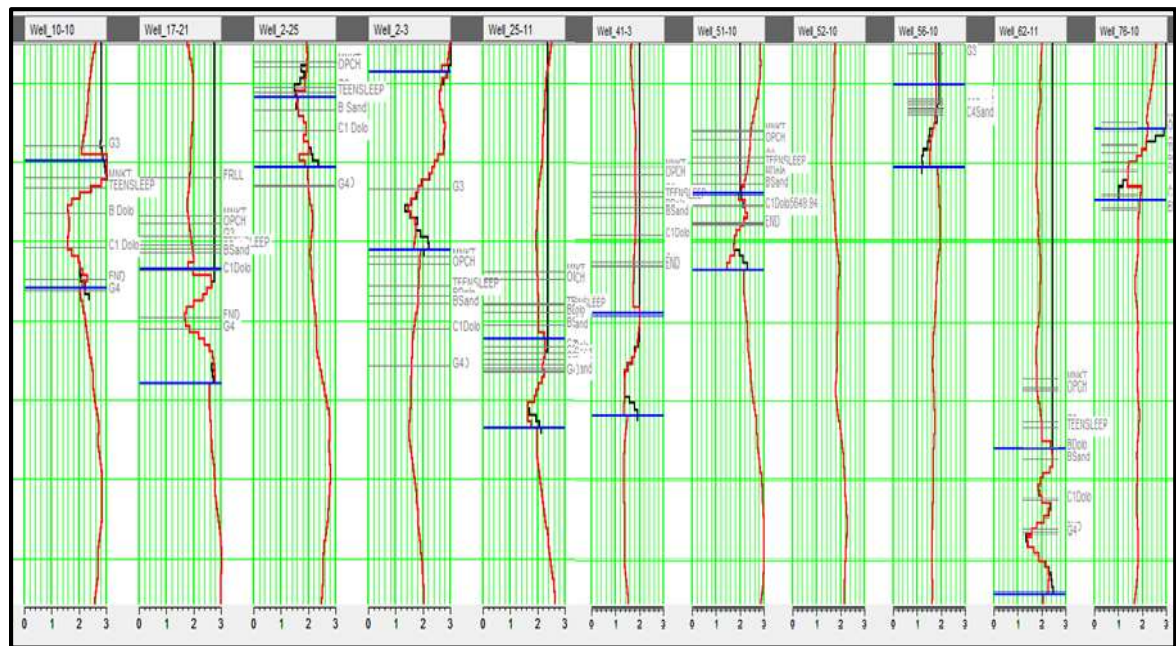


Figure 4.19: Applying the RBFNN's utilizing set of six attributes (Tensleep). The original lithology and the predicted log is shown in black and red respectively.

4.3.3 Corrected Neutron Porosity Result

To predict porosity I applied the same procedures as to predict lithology. To examine which seismic set of attributes is most appropriate to estimate porosity, I cross-plotted the different attributes versus porosity. During this step I calculated the correlation coefficients for all the attributes (Tables 4.6 and 4.7).

Table (4.6) shows the most appropriate single attributes, which can be correlated with the porosity log of Second Wall Creek reservoir. The correlation coefficients for the attributes are ranked in decreasing order.

Table (4.7) shows result of the most appropriate single attributes, which can be correlated with the porosity log of the Tensleep reservoir. Also the attributes were ranked in decreasing order of their correlation with target porosity.

Figure (4.20) shows cross-plot of the most appropriate nonlinear target attribute (which has turned out to be the square root of well log porosity, Second Wall Creek) against Amplitude Weighted Cosine Phase. Although this is the best-correlating attribute for porosity, it only gives a normalized cross correlation of 0.48, and a small error, however, it is considered not having high confidence level. Figure (4.21) shows the cross-plot of well log porosity (Tensleep) against Instantaneous Frequency. The normalized cross correlation is very small (0.30).

Table (4.8) shows the improvement during stepwise regression, implemented to the porosity prediction problem in Second Creek reservoir. The combination of attributes are Amplitude Weighted Phase (Inversion), Instantaneous Phase, Apparent Polarity,

Quadrature Trace (Inversion), Derivative Instantaneous Amplitude. From this Table we see that combination of four attributes is sufficient to predict the porosity, due to the decreasing in validation error up to this number of attributes, and no more, which is the criterium of selecting the optimal number of attributes to be combined.

Table (4.9) shows the performance of multi attribute selection, applied to the porosity prediction problem in Tensleep reservoir. From the Table we can see the best combination of five attributes are Time, Average Frequency, Filter 25/30-35/40, Integrated Absolute Amplitude, Second Derivative, while adding more attributes could only introduce more error. This is clearly seen from the increased validation error when we add another attribute (Filter 55/60-65/70) to the previous attributes.

Figures (4.22, and 4.23) show the optimal number of attribute set to be used to predict porosity in both reservoirs (Second Wall Creek and Tensleep). The black curve indicates the prediction error using all wells in training, whereas the red curve shows the validation error when a well is re-moved and the transform is re-derived. From both figures we see that the validation error first is decreasing when we add more attributes till it reaches some point when it starts to increase with additional attributes. From these two figures the optimal number of attributes to be used to predict porosity in Second Wall Creek and Tensleep reservoirs are four and five, respectively.

Figures (4.24, and 4.25) show a cross-plot of predicted porosity against actual porosity, for the case when a combination of 4, and 5 attributes with various operator lengths were used to derive the transform. A good cross correlation between the predicted and actual porosity was achieved using all proposed attributes together to derive a multi-regression,

the normalized correlations in these cases are 0.63 and 0.85 for Second Wall Creek and Tensleep, respectively.

Table 4.6: Results of porosity prediction employing a single seismic attribute, with estimation errors and coefficients of correlation (Second Wall Creek).

Target Log	Attribute	Error	Correlation
Sqrt-Porosity	Amplitude Weighted Phase (Inversion)	0.03	-0.48
Porosity	Cosine Instantaneous Phase	0.03	-0.43
Porosity	Quadrature Trace	0.03	-0.33
Porosity	Amplitude Weighted Frequency	0.03	-0.32
(Porosity) ²	Instantaneous Frequency	0.03	-0.30
Log-Porosity	Average Frequency	0.03	0.28
Porosity	Instantaneous Phase	0.03	-0.27
Porosity	Amplitude Envelope	0.03	0.22
Porosity	Apparent Polarity	0.03	-0.21

Table 4.7: Results of porosity prediction employing a single seismic attribute, with estimation errors and coefficients of correlation (Tensleep reservoir).

Target Log	Attribute	Error	Correlation
Porosity	Instantaneous Frequency	0.034	0.30
Porosity	Filter 15/20-25/30	0.035	-0.24
Porosity	Amplitude Weighted Phase	0.035	0.20
Porosity	Instantaneous Phase	0.035	0.18
Porosity	Cosine Instantaneous Phase	0.035	0.16
Porosity	Average Frequency	0.035	0.12
Porosity	Second Derivative (Inversion)	0.035	-0.10
Porosity	Amplitude Envelope	0.036	-0.10
Porosity	Apparent Polarity	0.036	0.09
Porosity	Integrated Amplitude (Inversion)	0.036	-0.05
Porosity	Instantaneous Frequency	0.03450	0.30

Table 4.8: Performance of stepwise regression, implemented for the porosity prediction problem in Second Creek reservoir. Each row shows a different attribute transform. The multi attribute transform for every row involves all previous attributes. The final column illustrated corresponding validations.

Target Log	Attribute	Training Error	Validation Error
Porosity	Amplitude Weighted Phase (Inversion)	0.034	0.036
Porosity	Instantaneous Phase	0.033	0.035
Porosity	Apparent Polarity	0.032	0.035
Porosity	Quadrature Trace (Inversion)	0.030	0.033
Porosity	Derivative Instantaneous Amplitude	0.030	0.034

Table 4.9: Performance of stepwise regression, implemented for porosity prediction problem in Tensleep reservoirs. Each row reveals a different attribute transform. The attribute transform for every row involves all previous ones above it. The final column illustrated error of estimation for that conversion.

Target Log	Attribute	Training Error	Validation Error
Porosity	Average Frequency	0.023	0.0272
Porosity	Average Frequency(Inversion)	0.021	0.0240
Porosity	Filter 5/10-15/20	0.018	0.0247
Porosity	Filter 15/20-25/30 (inversion)	0.017	0.0240
Porosity	Filter 25/30-35/40	0.015	0.0240
Porosity	Integrate	0.014	0.0241

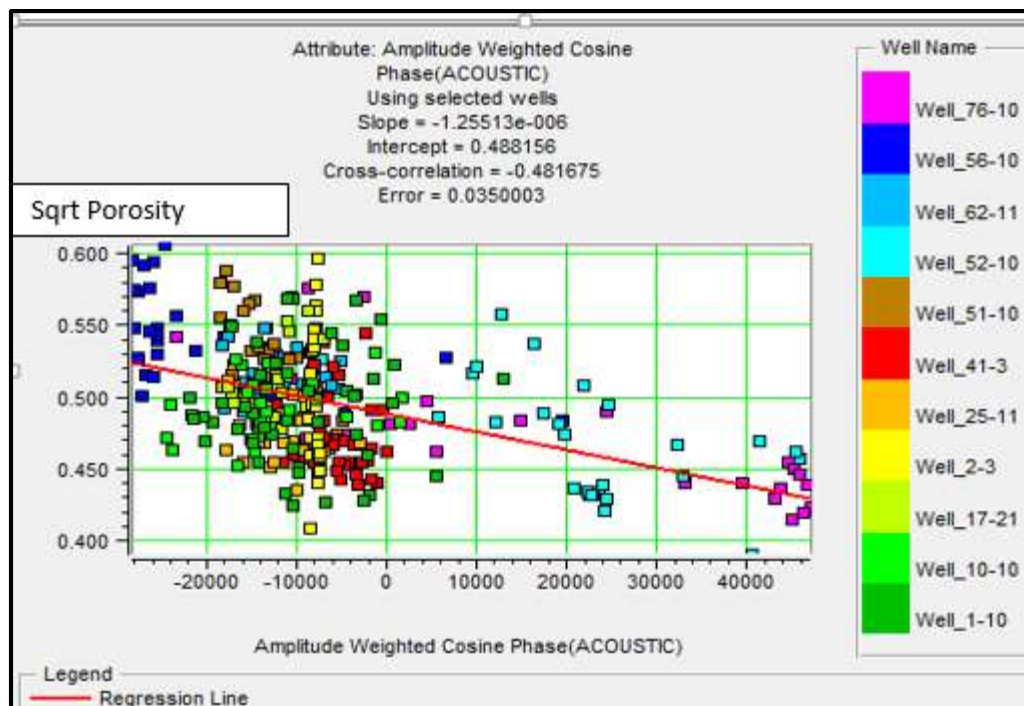


Figure 4.20: Cross plot of a single attribute (Amplitude Weighted Cosine Phase) against square root of porosity (Second Wall Creek).

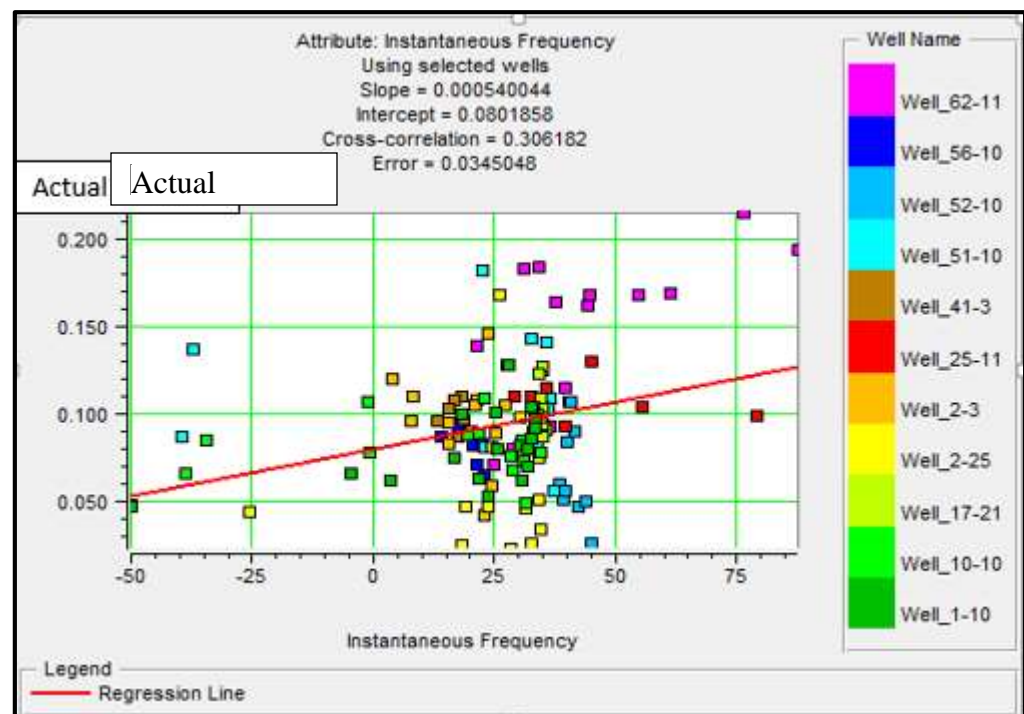


Figure 4.21: Crossplot of a single attribute Instantaneous Frequency against actual porosity (Tensleep).

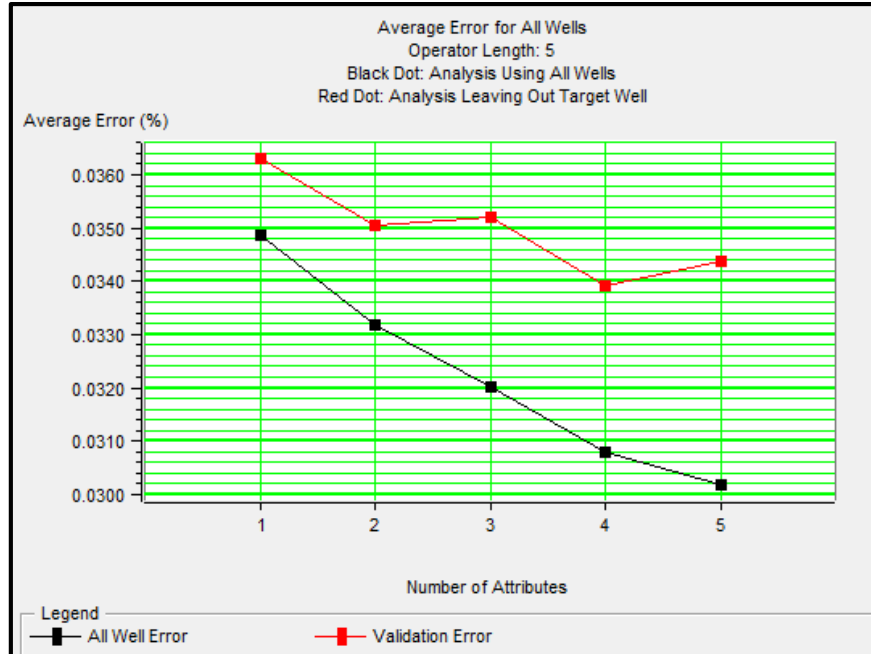


Figure 4.22: Validation for all wells showing that the optimal set of attributes to estimate porosity is five. The red and black dots illustrate the error when one well is removed and error using all wells (Second Wall Creek).

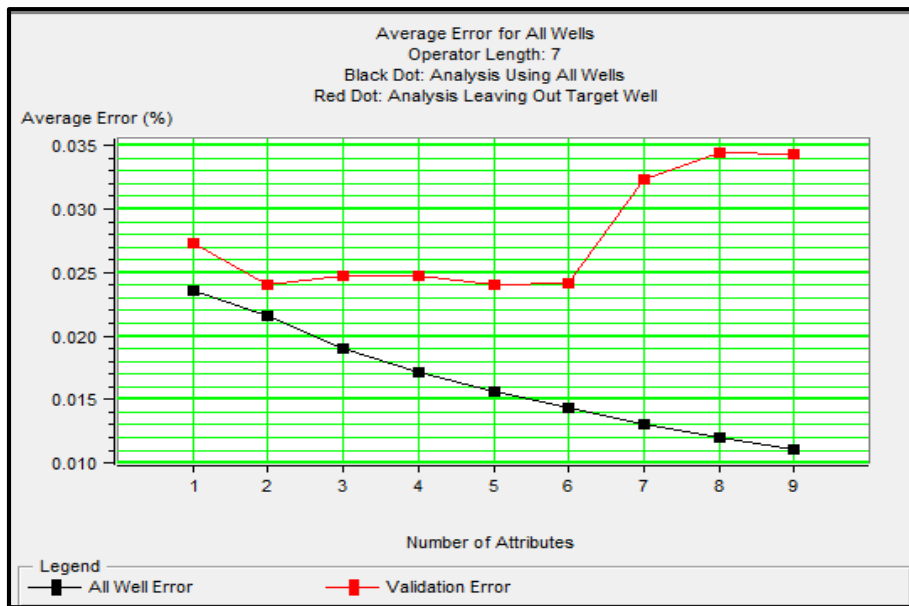


Figure 4.23: Validation for all wells showing that the optimal set of attributes to estimate porosity is five. The red and black dots illustrate the error when one well is removed and error using all wells (Tensleep).

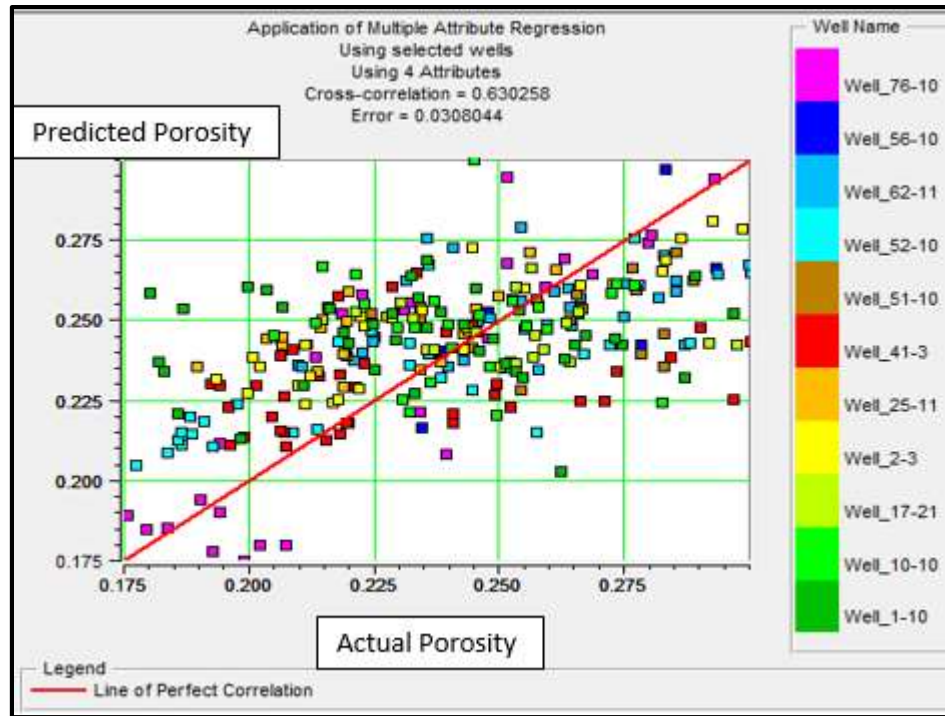


Figure 4.24: Crossplot of original porosity logs against estimated porosity logs in Second Wall Creek.

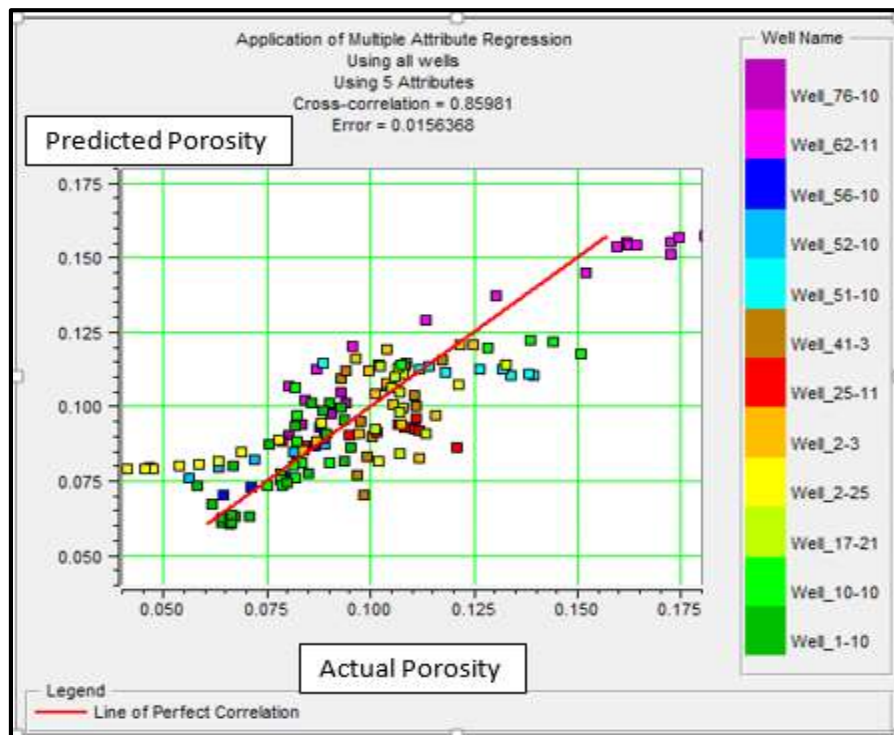


Figure 4.25: Crossplot of original porosity logs against estimated porosity logs in Tensleep reservoir.

4.3.4 Corrected Porosity Prediction with Artificial Neural Network

Having identified the appropriate combination of seismic attributes to estimate porosity by step-wise regression as illustrated in previous steps, a neural network was applied with the same configuration parameters as obtained from step-wise regression.

The performance of the RBF neural network was analyzed by keeping one well aside as a test case, and training the network on the remaining wells. This procedure was repeated, till all wells were tested.

Figure (4.26) shows cross plot of actual measured porosity versus porosity predicted by the RBF neural network for the 11 wells in the study of Second Wall Creek reservoir. Four attributes were used to predict the target. Note the high correlation 0.83 with small error around 2%.

Figure (4.27) illustrates the cross plot of measured porosity versus porosity predicted by the RBF neural network for the 12 wells in the study of Tensleep reservoir. Five attributes were used to predict the target porosity. Note the high correlation, larger than 0.92, with small error around 1%.

Figure (4.28) presents the error analysis of RBF in Second Wall Creek reservoir. A set of 11 wells were used to evaluate the performance. The dots are training errors when using all wells, the red dots are validation error when I excluded one well and re-derived by RBF prediction the log of the excluded well

Figure (4.29) shows the same as Figure (4.28) for the data from Tensleep reservoir. For both reservoirs, the tests demonstrate that the network generalizes well, and has

impressive predictive powers. This is clear when comparing the two curves of predicted and validation error, where only a single well 62-11 in the Tensleep reservoir shows big validation error, which does not match the learning rule. This could be attributed to non-accurate well-to-seismic tie or more heterogeneous local geology near the anomalous well.

Figures (4.30, and 4.31) show results of applying the neural network training result to Second Wall Creek and Tensleep, respectively. The black line is actual porosity log, the red line is predicted porosity. Note the good correlation between them.

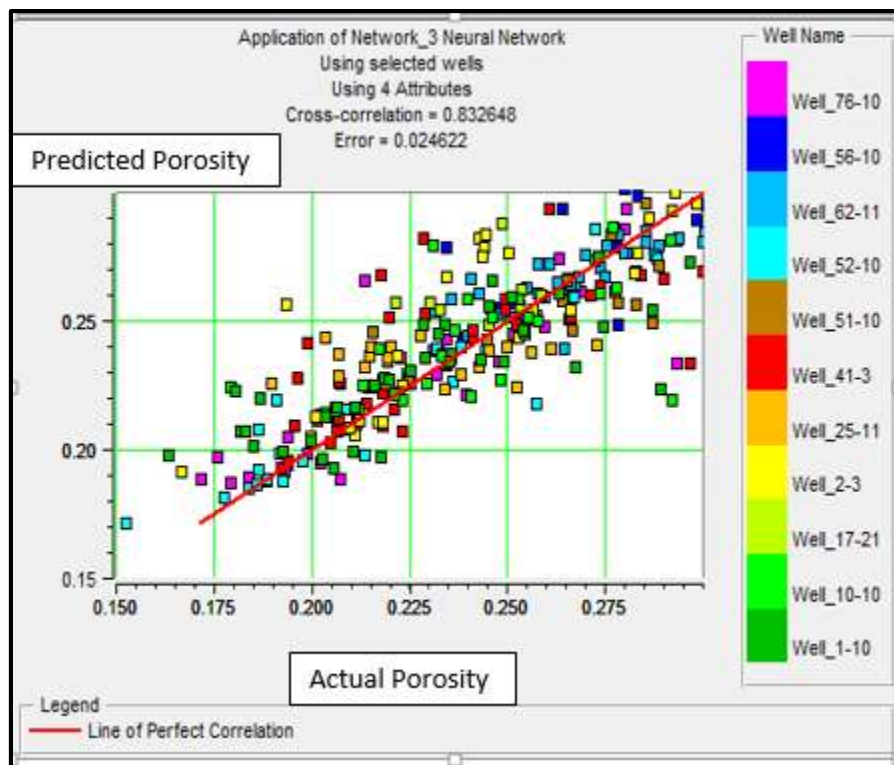


Figure 4.26: Crossplot of estimated porosity versus original porosity. (Second Wall Creek reservoir).

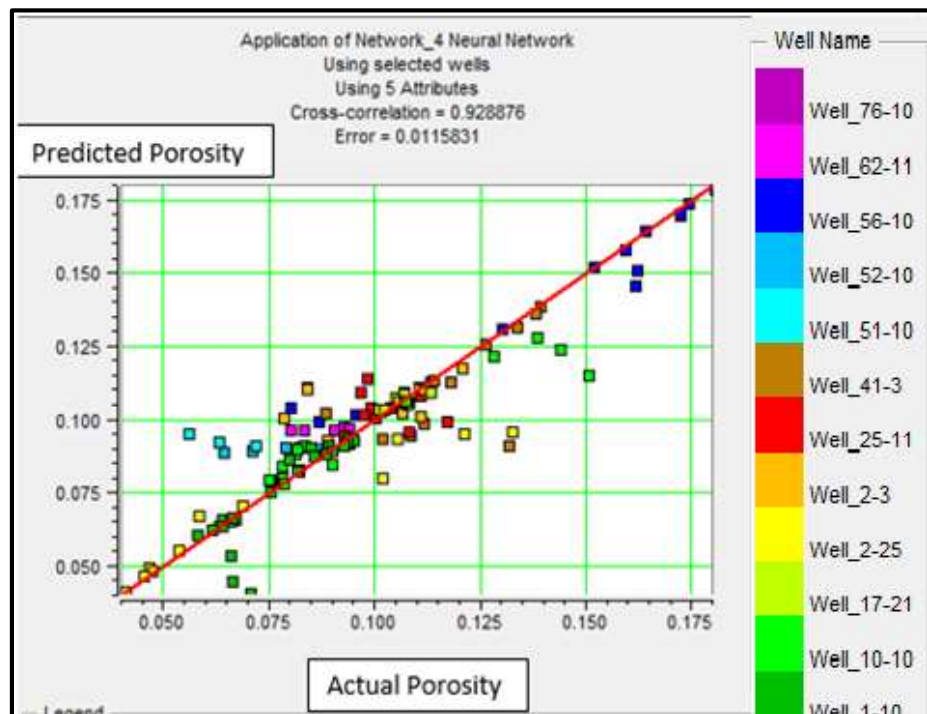


Figure 4.27: Crossplot of estimated porosity against original porosity (Tensleep reservoir).

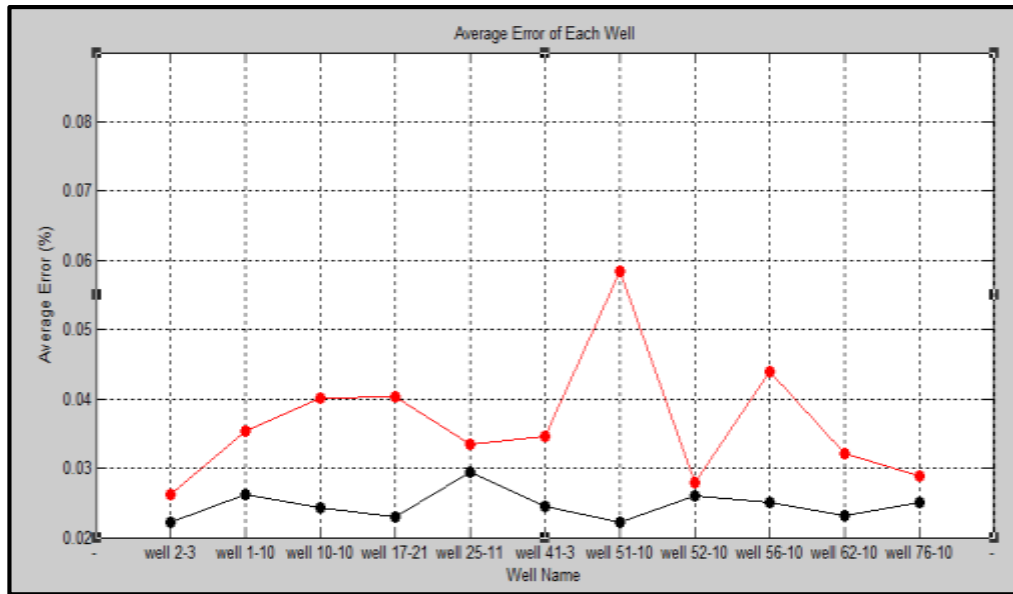


Figure 4.28: Errors of the RBF Neural Network results (Second Wall Creek) using four attributes. The black and red line are Error of the actual and the estimated porosity log.

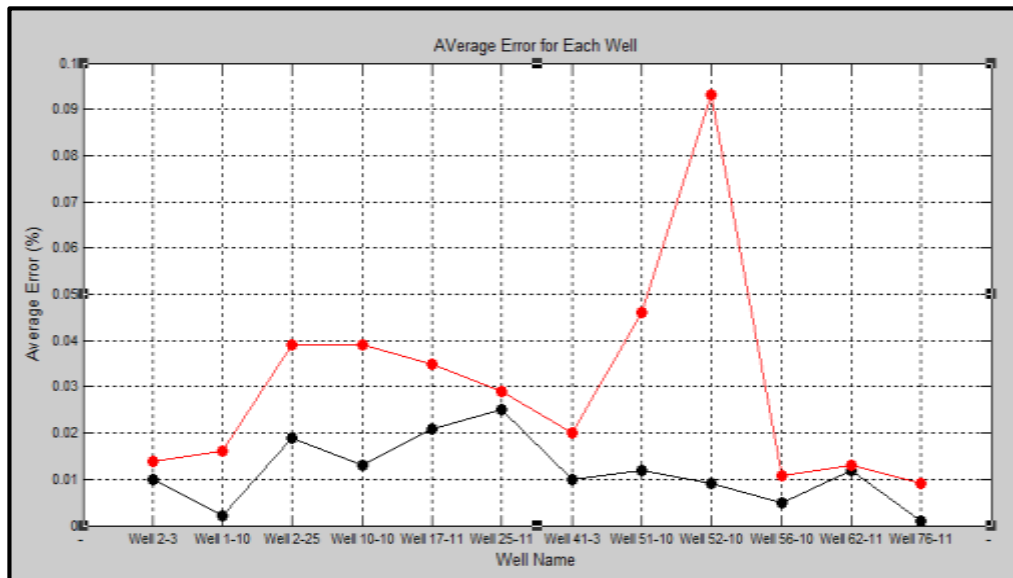


Figure 4.29: Errors of the RBF Neural Network results (Tensleep) using four attributes. The black and red line are Error of the actual and the estimated porosity log.

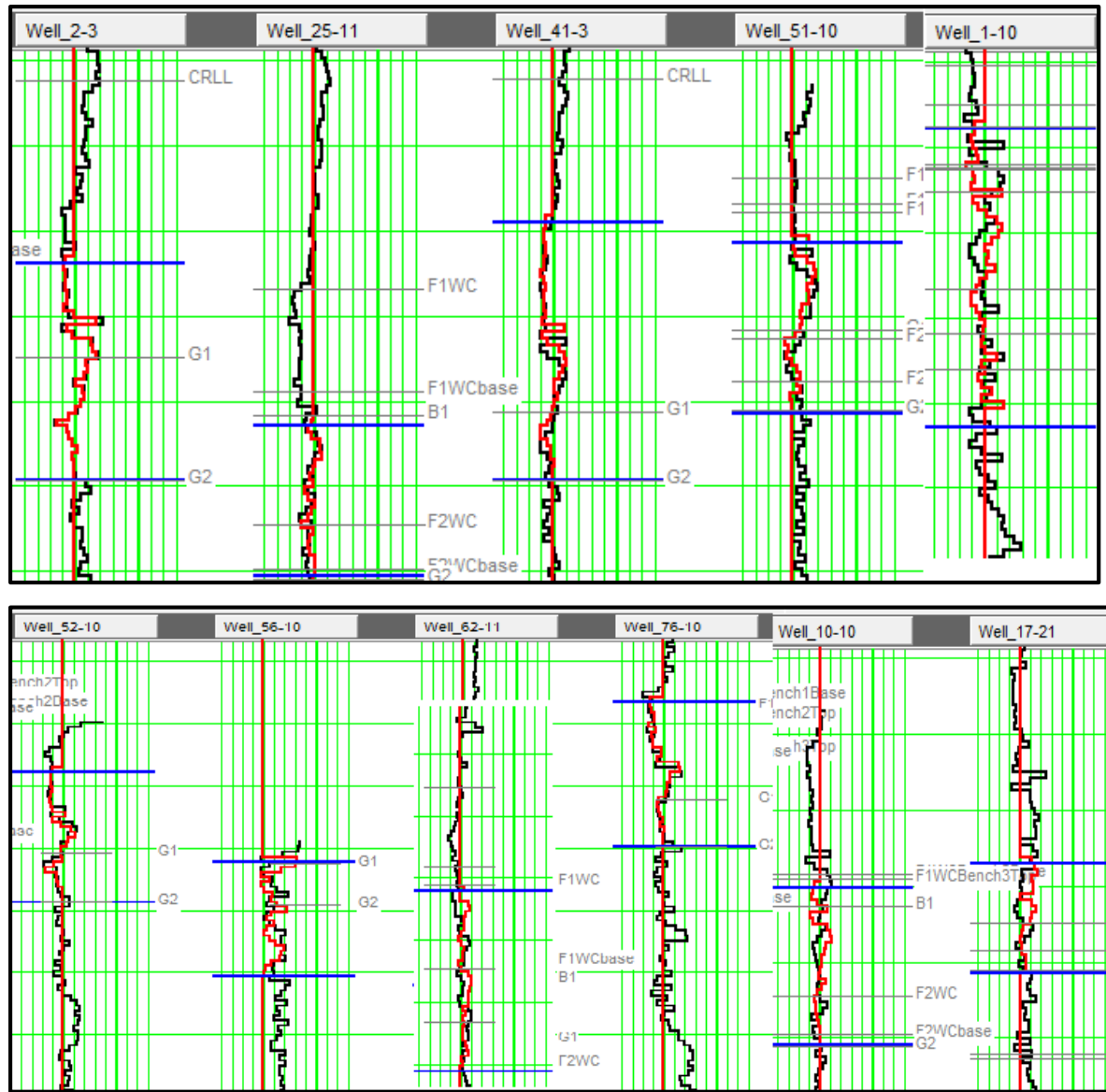


Figure 4.29: RBF results using 4 attributes (Second Wall Creek reservoir). The actual porosity log in black; the estimated log in red.

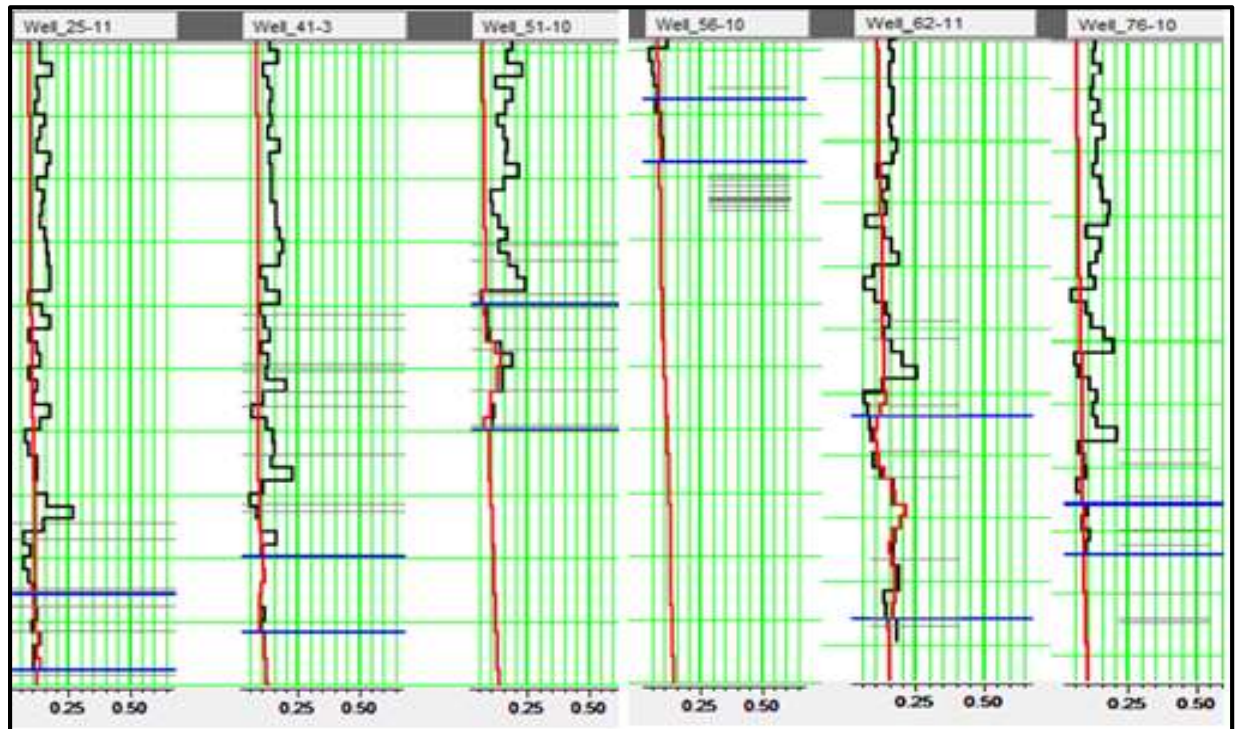
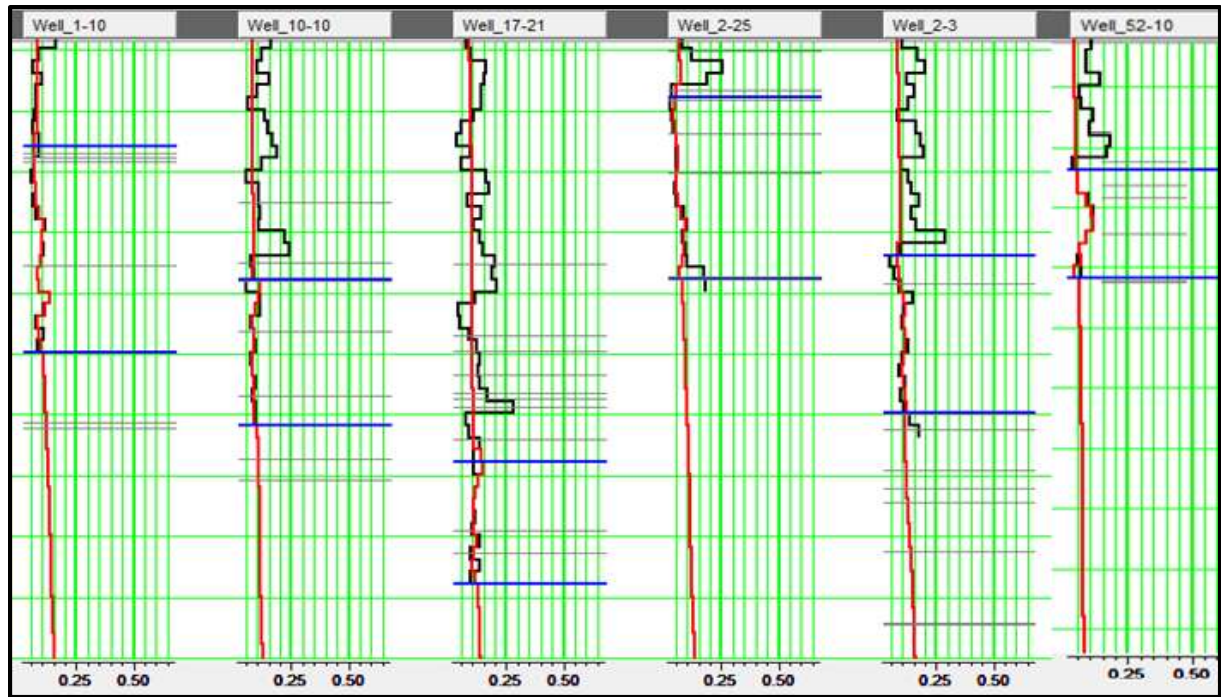


Figure 4.30: RBF results using 5 attributes (Tensleep). The actual porosity log in black; the estimated log in red.

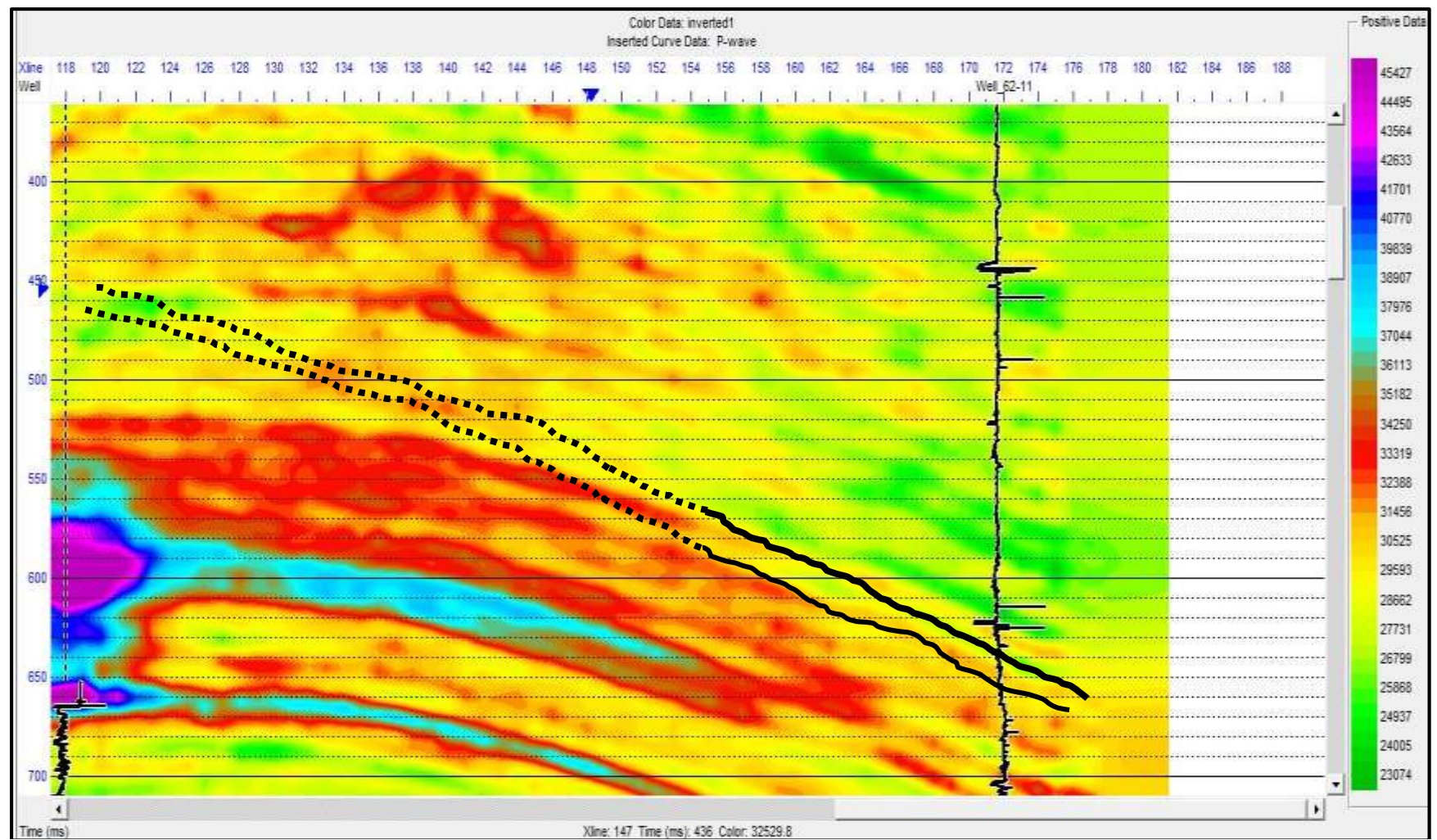
4.4 Section Results

I was satisfied with the training results and the technique was found robust according to the sensitivity tests. As a final step I decided to apply the learning outputs of fractional lithology and porosity from the RBF neural networks training to the zones of interest (Second Wall Creek and Tensleep reservoirs) in the 3D seismic volume. I selected only one inline for each reservoir to evaluate and compare the capabilities of three different models (namely acoustic impedance inversion, porosity and fractional lithology model results), to resolve questions of reservoir heterogeneity and extension.

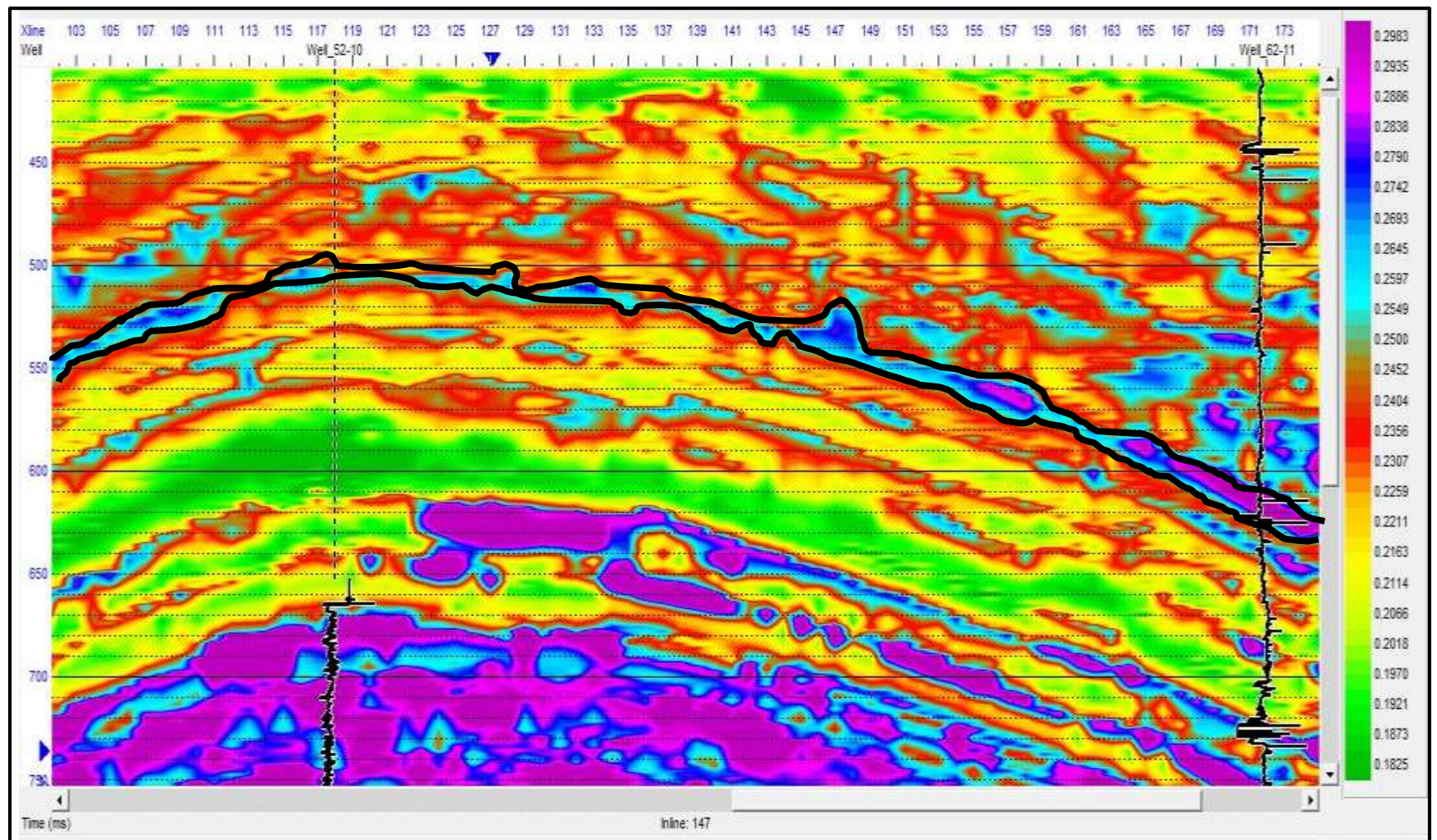
Figures (4-32 a, b, c) show Inline 147 from the 3D seismic survey, with log from well 62-11 superimposed at cross-line 71. The Figure illustrates (a) inverted seismic impedance (b) the RBFN result for porosity prediction and (c) the RBFN result for lithology. The target feature in this inline sections, which is the Second Wall Creek reservoir, is highlighted by black line. Notice in Figure (4-32 a) that even though impedance was inverted by using a sophisticated algorithm such as colored inversion, still the target is not perfectly illuminated, and we cannot trace it to define its extension. Also, the frequency content of this result is too low. However in Figure (4-32 b) the frequency content is much richer in high frequencies than in Figure (4-32 a), so more details can be seen. The key element to observe is the Second Wall Creek reservoir, highlighted by black line. A comparison with our previous result reveals that we obtain much better results with predicted porosity log than with impedance log, Figure (4-32 c) shows the lithology of the same feature, this result is in line with the porosity result obtained in figure (4-32 b), that the high porosity values coincide with low lithology values (low

lithology values represent sand with small amount of lime) which is typical lithology of the reservoir recorded at the well.

Figures (4-33 a, b) show Inline 305 from the 3D seismic survey, illustrating (a) inverted impedance, and (b) the RBFN result for lithology. The target feature in this inline sections is the Tensleep reservoir, it is highlighted by black line between (1063-1200 ms). In Figure (4-33 a) shows inverted impedance, notice that even though the impedance had been inverted by the powerful colored inversion algorithm, still the target has not been completely resolved, especially the thin layer. Also, the frequency content is too low. However, in Figure (4-33 b) the frequency content of the target is much higher than in Figure (4-33 a), much more details have become visible. The key element to observe is the number of the layers that were successfully resolved in the reservoir by using this new approach of fractional lithology.

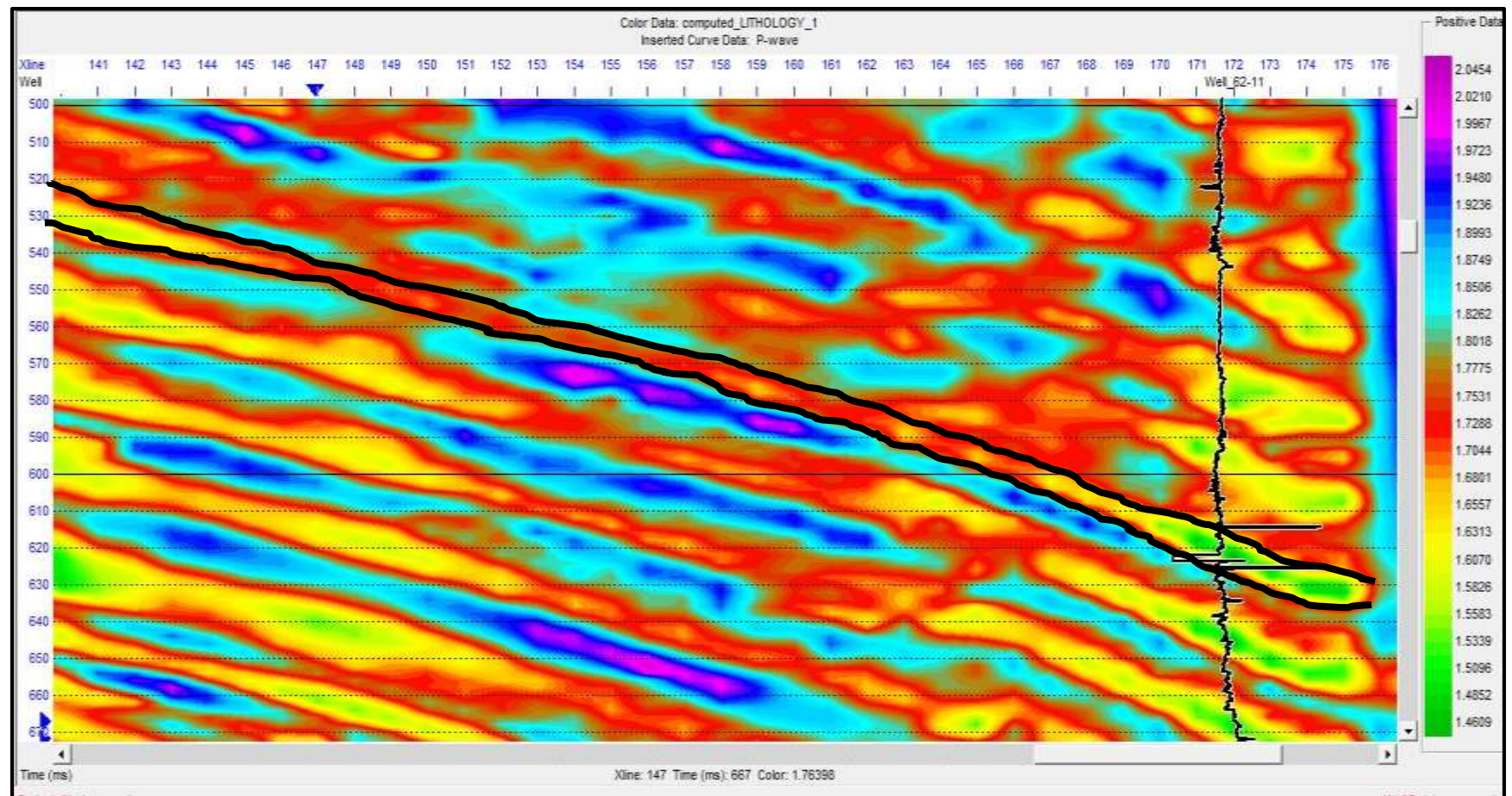


Porosity



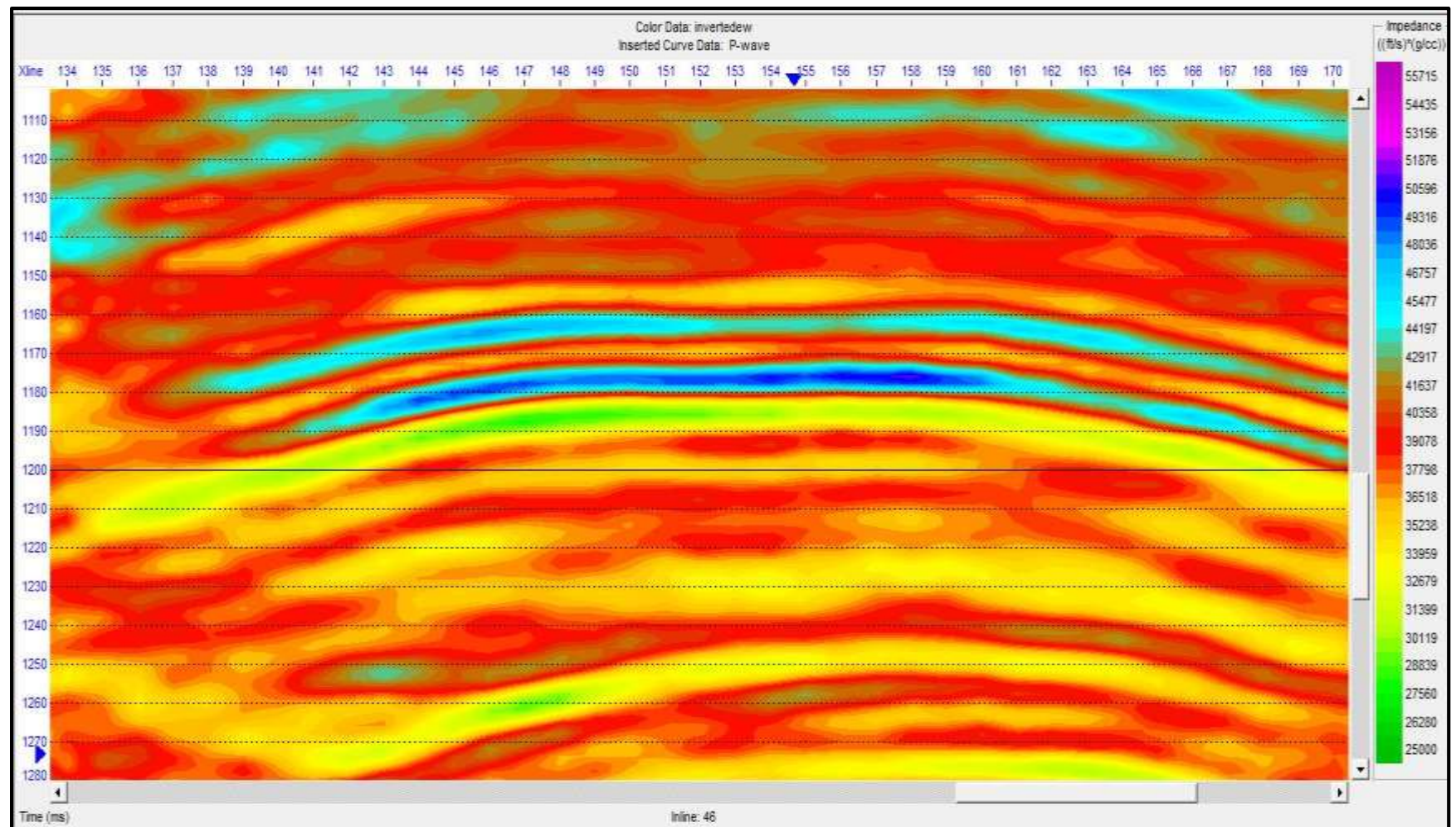
(b)

Fractional Lithology composition



(c)

Figure 4. 31: Inline 147 from the 3D volume, with well 62-11 superimposed at crossline 172, showing (a) inverted impedance, (b) porosity predicted by the RBF algorithm, and (c) the lithology derived by the RBF algorithm.



(a)

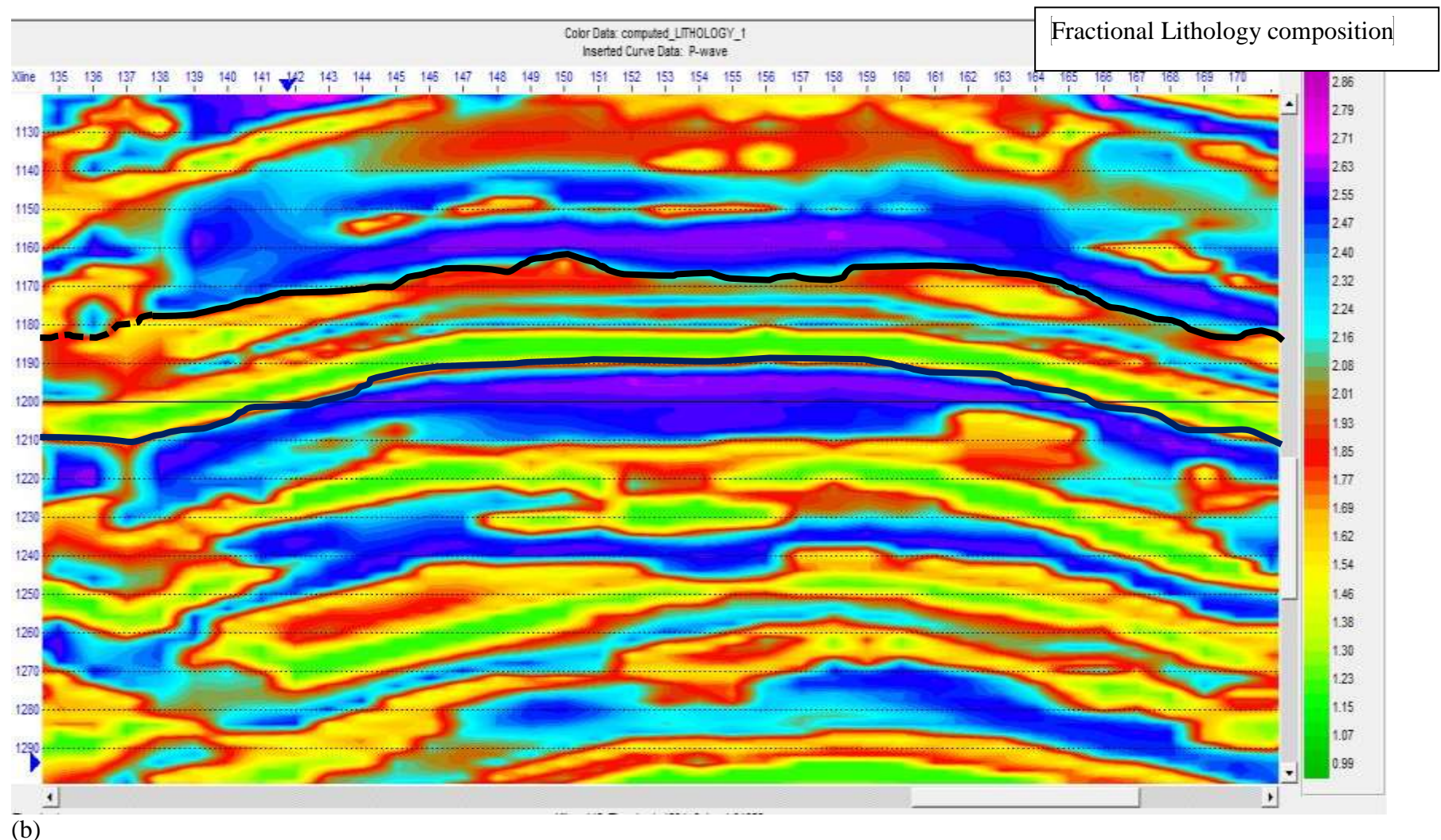


Figure (4.33) Inline 46 from the 3D seismic survey, illustrating (a) inverted impedance, (b) RBF prediction of lithology.

CHAPTER 5

CONCLUSION AND RECOMMENDATION

In this study I have introduced and demonstrated a new approach of lithology prediction based on the digital approximation of the Schlumberger neutron porosity and density master curves. Firstly, I described how to estimate the lithology fraction of three rocks types namely sandstone, limestone, and dolomite and to correct the porosity, then I illustrated how the corrected porosity log and the constructed lithology log should be integrated with seismic attributes to predict porosity and lithology over entire 3D seismic volume. In both prediction cases, there were an improvement in predictive power as we move from simple crossplotting (i.e. single attribute regression) to multivariate linear regression. A further significant improvement was achieved when using artificial intelligence, namely to RBF method. This gradual improvement is vividly observable on the training data and is also demonstrated by the validation data. The correlation coefficients for porosity and lithology are good. For lithology the trend and dispersion of data prediction are more convincing than for porosity. The results indicate that the Radial Basis Function NN is a powerful technique which is suitable to predict fractional lithology and porosity from seismic attributes and to solve complicated problems intractable by conventional methods. The implemented strategy is a robust tool for reducing the costs of well logging and coring. As a follow up of this study I would expect further improvements in cases if there is available core data to validate the result of the predicted fractional lithology

REFERENCES

- [1] Adekanle, A., and Enikanselu, P. A., "Porosity Prediction from Seismic Inversion Properties over 'XLD'Field, Niger Delta, " Am. J. Sci. Ind. Res, vol. 4, no. 1, pp. 31-35, doi: 10.5251/ajcir, 2013
- [2] AlBinHassan, N. M., and Wang, Y., "Porosity Prediction Using the Group Method of Data Handling," Geophysics, vol.76, no.5, pp. O15-O22, 2011
- [3] Anna, L. O., "Geologic assessment of undiscovered oil and gas in the Powder River Basin Province, Wyoming and Montana" USGS Digital Data Series DDS-69-U, 2009
- [4] Avseth, P., Mukerji, T., Jørstad, A., Mavko, G., and Veggeland, T., "Seismic reservoir mapping from 3-D AVO in a North Sea turbidite system," Geophysics, vol.66, no.4, pp. 1157-1176, 2001
- [5] Bhattacharya, J. P., and Willis, B. J., "Lowstand deltas in the Frontier Formation, Powder River Basin, Wyoming: implications for sequence stratigraphic models," *AAPG bulletin*, vol.85, no.2, pp. 261-294, 2001
- [6] Bosch, M., Barton, P, Singh, S., and Trinks, I., "Inversion of traveltimes data under a statistical model for seismic velocities and layer interfaces," Geophysics, vol.70, no.4, pp. R33-R43, 2005
- [7] Bosch, M., Barton, P., Singh, S. C., and Trinks, I., "Seismic inversion for reservoir properties combining statistical rock physics and geostatistics: A review," Geophysics, vol.75, no.5, pp. 75A165-75A176, 2010
- [8] Broomhead, D. S., and Lowe, D., "Multivariable functional interpolation and adaptive networks," Complex Systems, vol.2 pp. 321–355, 1988.

- [9] Busch, M., Fortney, G., and Berry, N., "Determination of lithology from well logs by statistical analysis," *SPE formation evaluation*, vol.2, no.4, pp. 412-418, 1987
- [10] Cantrell, D. L., Swart, P. K., Handford, R. C., Kendall, C. G., and Westphal, H., "Geology and production significance of dolomite, Arab-D reservoir, Ghawar field, Saudi Arabia," *Geearabia-Manama*, vol.6, pp. 45-60, 2001
- [11] Chaki, S., Verma, A. K., Routray, A., Mohanty, W. K., and Jenamani, M., "Well tops guided prediction of reservoir properties using modular neural network concept: A case study from western onshore," India. *Journal of Petroleum Science and Engineering*, vol.123, pp. 155-163, 2014
- [12] Cuddy, S. J., "Litho-facies and permeability prediction from electrical logs using fuzzy logic," *SPE Reservoir Evaluation & Engineering*, vol. 3, no. 4, pp. 319-324, 2000
- [13] Dennen, K., Burns, W., Burruss, R., and Kendra Hatcher, K., "Geochemical Analyses of Oils and Gases, Naval Petroleum Reserve No. 3, Teapot Dome Field, Natrona County, Wyoming," US Geological Survey, 2005
- [14] Derek, H., Johns, R., and Pasternack, E., "Comparative study of aback propagation neural network and statistical pattern recognition techniques in identifying sandstone litho-facies," Proceedings 1990 Conference on Artificial Intelligence in Petroleum Exploration and Production. Texas A and M University, College Station, TX, pp. 41–49, 1990
- [15] Draper, N. R., Smith, H., and Pownell, E., "Applied Regression Analysis, " John Wiley & Sons, Inc, 1966

- [16] Fung, C. C., Wong, K. W., and Eren, H., "Modular artificial neural network for prediction of petrophysical properties from well log data," *IEEE Transactions on Instrumentation and Measurement*, vol.46, no.6, pp. 1295–1299, 1997
- [17] Hamada, G. M., and Elshafei, M. A., "Neural Network Prediction of Porosity and Permeability of Heterogeneous Gas Sand Reservoirs," In *SPE Saudi Arabia Section Technical Symposium*. Society of Petroleum Engineers, 2009.
- [18] Hampson, D. P., Schuelke, J. S., and Quirein, J. A., "Use of multiattribute transforms to predict log properties from seismic data," *Geophysics*, vol.66, no.1, pp. 220-236, 2001
- [19] Helle, H. B., Bhatt, A., and Ursin, B., "Porosity and permeability prediction from wireline logs using artificial neural networks: a North Sea case study," *Geophysical Prospecting*, vol.49, no.4, pp. 217–228, 2002
- [20] Iloghalu, E., "Application of neural networks technique in lithofacies classifications used for 3-D reservoir geological modeling and exploration studies," *AAPG Annual Meeting Abstract*, 2003
- [21] Iturrarán-Viveros, U., and Spurlin, J. H, "The Gamma test applied to select seismic attributes to estimate effective porosity," In *2005 SEG Annual Meeting*. Society of Exploration Geophysicists
- [22] Kirschbaum, M. A., and Roberts, L. N., "Stratigraphic framework of the Cretaceous Mowry Shale, Frontier Formation and adjacent units, southwestern Wyoming Province, Wyoming, Colorado, and Utah," *US Geological Surveydigital data series DDS*, vol.69, 2005

- [23] Kumar, D., Sugianto, H., Li, S., Patel, H., and Land, S., "Using relative seismic impedance to predict porosity in the Eagle Ford shale," SEG Technical Program Expanded Abstracts, pp. 2688-2692. doi: 10.1190/segam2014-0473.1, 2014
- [24] Lancaster, S., and Whitcombe, D., "Fast-track ‘coloured’ inversion," SEG Technical Program Expanded Abstracts, pp. 1572-1575, doi: 10.1190/1.1815711, 2000
- [25] Li, Y., and Anderson-Sprecher, R., "Facies identification from well logs: A comparison of discriminant analysis and naïve Bayes classifier," *Journal of Petroleum Science and Engineering*, vol.53, no.3, pp. 149-157, 2007
- [26] Hagan, M. T., Demuth, H. B., and Beale, M. H., "Neural network design," Boston: Pws Pub, pp. 2-14, 1996
- [27] Merewether, E.A., Cobban, W.A., and Cavanaugh, E.T., "Frontier Formation and equivalent rocks in eastern Wyoming" *The Mountain Geologist*, v.6, no.3, p. 67–102, 1979
- [28] Merewether, E.A., Cobban, W.A., and Spencer, CW., "The Upper Cretaceous Frontier Formation in the Kaycee-Tisdale Mountain area, Johnson County, Wyoming, in Laudon," *The Mountain Geologist*, p. 33–44. 1976
- [29] Moody, J., and Darken, C. J., "Fast learning in networks of locally-tuned processing units," *Neural computation*, vol.1, no.2, pp. 281-294, 1989
- [30] Na’imi, S. R., Shadizadeh, S. R., Riahi, M. A., and Mirzakhalian, M., "Estimation of reservoir porosity and water saturation based on seismic attributes using support vector regression approach," *Journal of Applied Geophysics*, vol.107, pp. 93-101, 2014

- [31] Nikravesh, M., and Aminzadeh, F., "Mining and fusion of petroleum data with fuzzy logic and neural network agents," *Journal of Petroleum Science and Engineering*, vol. 29, no.3, pp. 221-238, 2001
- [32] Nikravesh, M., and Hassibi, M., "Intelligent reservoir characterization (IRESC)," In :Proceedings of IEEE International Conference on Industrial Informatics Banff, Alberta, Issue, 21–24, pp369–373, 2003
- [33] Nikravesh, M., Novak, B., and Aminzadeh, F., "Data mining and fusion with integrated neuro- fuzzy agents: rock properties and seismic attenuation. In: Proceeding of JCIS 1998," The Fourth Joint Conference on Information Sciences, North Carolina, and USA characterization trends, *Journal of Petroleum Science and Engineering*, vol.31, pp. 67–79, 1998
- [34] Phan, S., and Sen, K., "Porosity estimation from seismic data at Dickman Field, Kansas for carbon sequestration," In 2010 SEG Annual Meeting No.1, pp. 2299-2303, 2010
- [35] Rogers, S.J., J.H. Fang, C.L. Karr, and D.A. Stanley, "Determination of lithology from well logs using a neural network," *AAPG Bulletin*, vol.76, pp. 731-739, 1992
- [36] Russell, B. H., Hampson, D. P., and Lines, L. R., "Application of the radial basis function neural network to the prediction of log properties from seismic attributes," *Society of Exploration Geophysics*, vol.34, no.1/2, pp. 15-23, 2003
- [37] Saggaf, M. M., and Nebrija, L., "A fuzzy logic approach for the estimation of facies from wire-line logs," *AAPG bulletin*, vol.87, no.7, pp. 1223-1240, 2003

- [38] Sakurai, S., and Melvin, J., "Facies discrimination and permeability estimation from well logs for the Endicott field," in SPWLA 29th Annual Logging Symposium. Society of Petrophysicists and Well-Log Analysts, San Antonio, Texas 1988
- [39] Santoso, D., Alam, S., Hendraya, L., Alfian, Sulistiyono., and Munadi, S., "Estimation of limestone reservoir porosity by seismic attribute and AVO analysis," Exploration Geophysics, vol.26, no.2/3, pp. 437-443, 1995
- [40] Schultz, P. S., Ronen, S., Hattori, M., and Corbett, C., "Seismic guided estimation of log properties, parts 2," The Leading Edge, vol.13, pp674–678, 1994
- [41] Schultz, P. S., Ronen, S., Hattori, M., and Corbett, C., "Seismic-guided estimation of log properties (part 1: A data-driven interpretation methodology)," The Leading Edge, vol. 13, no. 5, pp. 305-310, 1994
- [42] Siripitayananon, P., Chen, H. C., and Hart, B. S., "A new technique for lithofacies prediction: back-propagation neural network," Proceedings of the 39th Annual ACM-SE Conference, Citeseer, pp. 3-38, 2001
- [43] Smith, L. J., and Maret, J. P., "Sand-shale ratio and sandy reservoir properties estimation from seismic attributes: An integrated study: an integrated study," Society of Exploration Geophysicists Expanded Abstracts, no.1, pp. 108–110, 1995
- [44] Taji, K., Miyake, T., and Tamura, H., "On Error Backpropagation Algorithm Using Absolute Error Function," 1999 IEEE International Conference on Systems, Man, and Cybernetics, IEEE SMC '99 Conference Proceedings, Vol. 5, pp. 401-406, 1999
- [45] Taner, M. T., Koehler, F., and Sheriff, R. E., "Complex Seismic Trace Analysis," Society of Exploration Geophysicists, vol.44, no.6, pp. 1041-1063, 1979

- [46] Tang, H., White, C., Zeng, X., Gani, M., and Bhattacharya, J., "Comparison of multivariate statistical algorithms for wireline log facies classification," AAPG Annual Meeting Abstract, vol. 88, p. 13, 2004
- [47] Todorov, T. I., "Integration of 3C-3D seismic data and well logs for rock property estimation," University of Calgary, 2000
- [48] Walls, J. D., Taner, M. T., Guidish, T., Taylor, G., Dumas, D., and Derzhi, N., "North Sea reservoir characterization using rock physics, seismic attributes, and neural networks; a case history," In Proceedings of 69th Society of Exploration Geophysicists (SEG) Annual International Meeting, Houston, TX, pp. 1572-1575, 1999
- [49] White, R. and Simm, R., "Tutorial: Good practice in well ties," First Break, 21, pp. 75–83. 2003
- [50] White, R. E., and Hu, T. "How accurate can a well tie be?" *The Leading Edge*, vol.17, no.8, pp. 1065-1071, 1998
- [51] Wolff, M., and Pelissier-Combescure, J., "FACIOLOG: automatic electrofacies determination," In *Society of Professional well log analysts annual logging symposium*, pp. 6-9, 1982
- [52] Wong, P. M., Jian, F. X., and Taggart, I. J., "A critical comparison of neural networks and discriminant analysis in lithofacies, porosity and permeability predictions," Journal of Petroleum Geology, vol.18, no.2, pp. 191-206, 1995

Appendix

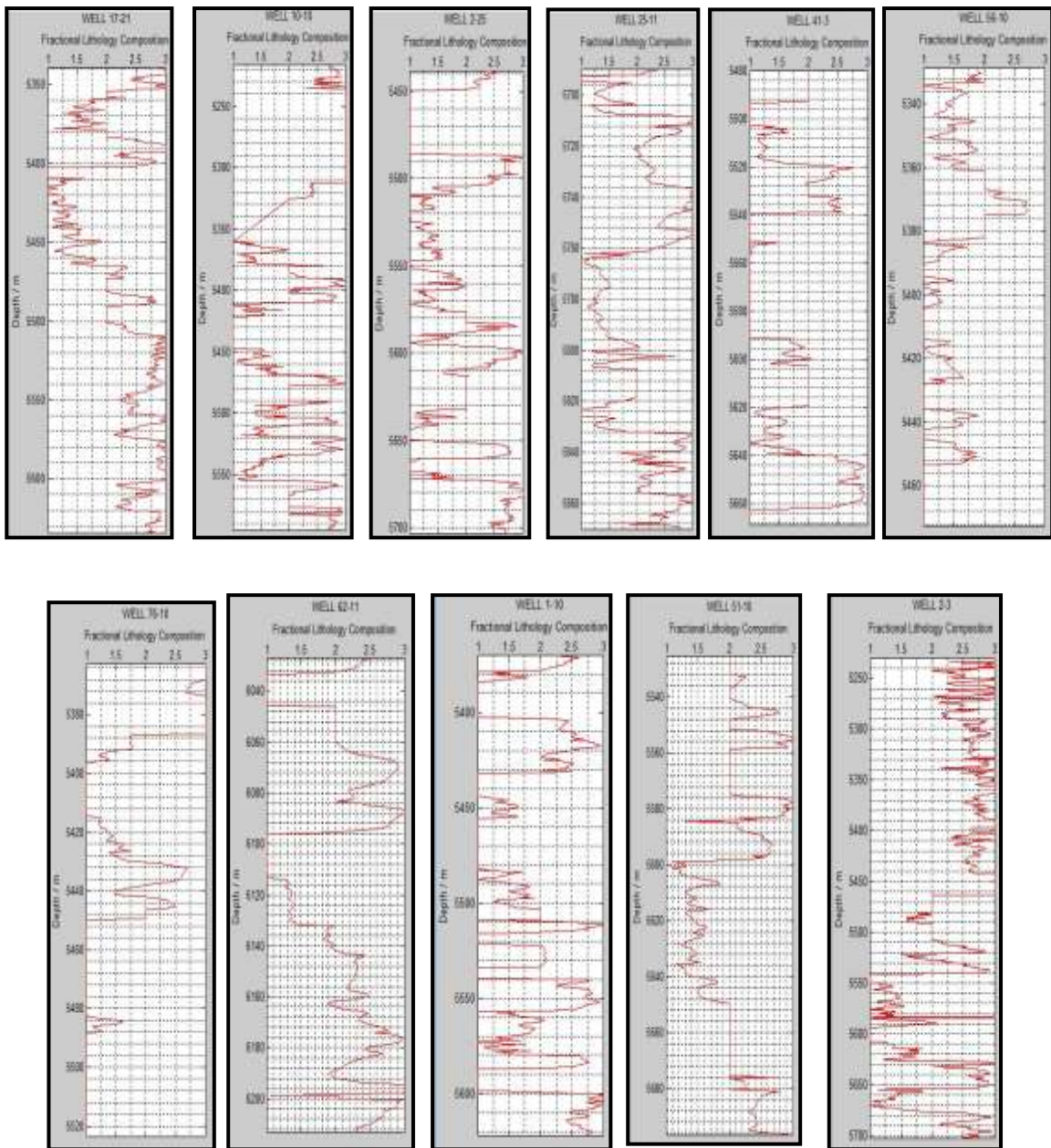


Figure 5.1: Fractional lithology log of 11 wells from Tensleep reservoir, the horizontal scale of 1, 2 and 3 is corresponding to sand, lime and dolo stone numerical codes, respectively. Note that the all three types of rocks actually occur in the graph.

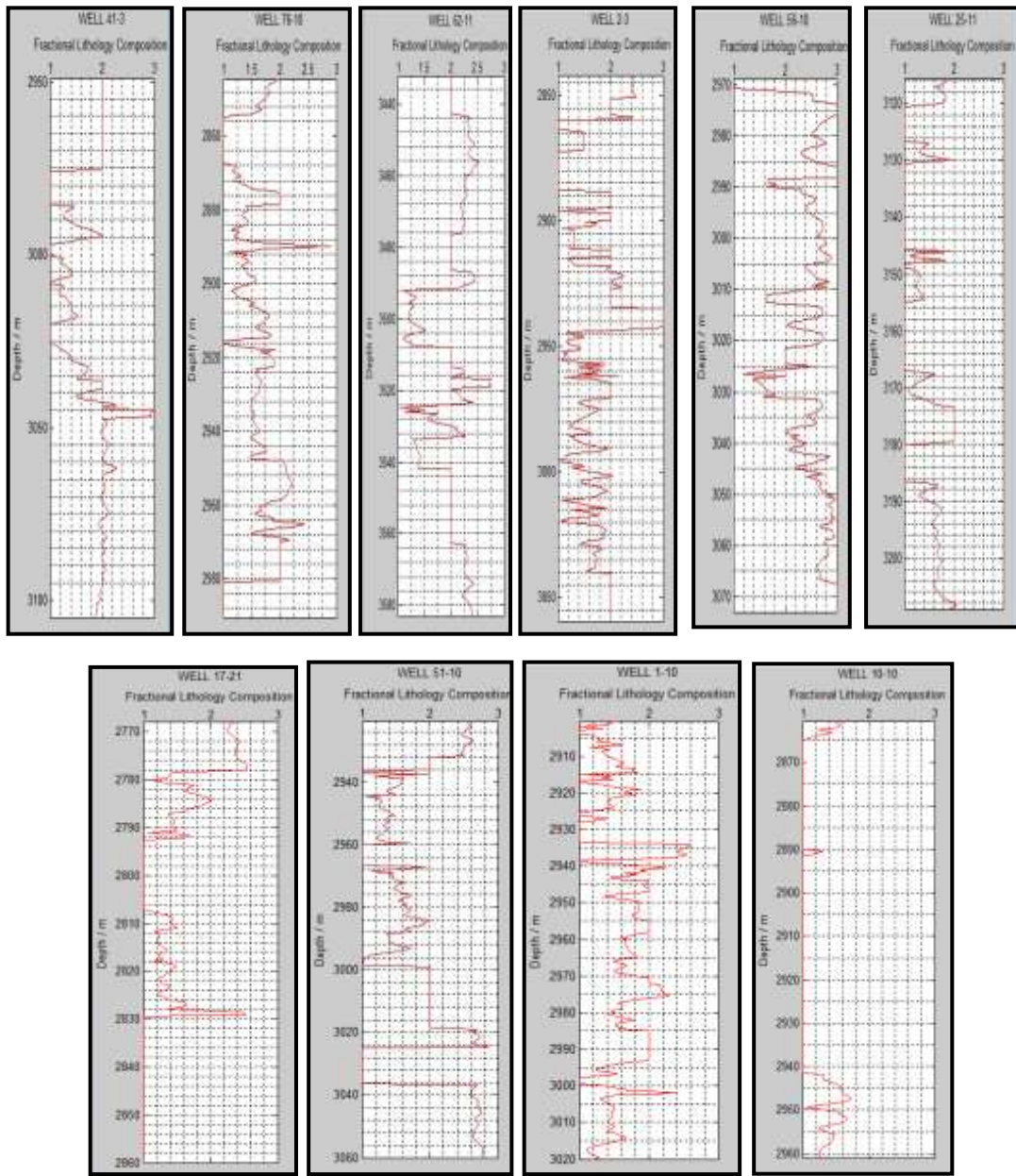


Figure 5.2: Fractional lithology log of 10 wells form Second Wall Creek reservoir, the horizontal scale of 1, 2 and 3 is corresponding to sand, lime and dolomite numerical codes, respectively. Note that the dominate rock types in all wells is sandstone.

Table 5.1: Processing workflow (Courtesy of EXCEL Geophysical Services Inc).

<u>PROCESSING SEQUENCE</u>
FORMAT CONVERSION – SEGD IEEE to Internal
GEOMETRY APPLICATION
RECORD AND TRACE EDITS
REFRACTION STATIC DERIVATION
Green Mountain Delay Time Method - Single Layer Case - $V_o = 4000'/s$
Statics computed to 6500' datum @ 9000'/s
AMPLITUDE RECOVERY
$1/(time*vel^2)$ spherical divergence correction $t^{1.4}$ Gain Correction
SURFACE CONSISTENT AMPLITUDE SCALING
MINIMUM PHASE CONVERSION
Filter derived from correlated sweep
SURFACE CONSISTENT MINIMUM PHASE SPIKING DECONVOLUTION
140 msec Operator - 0.1% Prewhitening
SPECTRAL BALANCING
6/10 – 90/100 Hz 8 gates
STATIC TO PROCESSING DATUM
CDP SORT
VELOCITY ANALYSIS
SURFACE CONSISTENT RESIDUAL STATIC
VELOCITY ANALYSIS
SURFACE CONSISTENT RESIDUAL STATIC
NORMAL MOVEOUT CORRECTION
TRACE EQUALIZATION
1000 msec AGC

FIRST BREAK MUTE

STATICS TO FINAL FLAT DATUM

Datum = 6500 ft - Replacement Velocity = 9000 ft/sec

DIP MOVEOUT CORRECTION

INVERSE NORMAL MOVEOUT CORRECTION

VELOCITY ANALYSIS

NORMAL MOVEOUT CORRECTION

MUTE ANALYSYS

CMP STACK

SEGY OUTPUT OF THE UNFILTERED FINAL STACK

BANDPASS FILTER

STOLT 3D TIME MIGRATION

100% of the RMS stacking velocities

SEGY OUTPUT OF THE UNFILTERED POST STACK TIME MIGRATION

FX PREDICTIVE FILTER

BANDPASS FILTER

TRACE SCALING

1000 ms windows, 50% overlap

SEGY OUTPUT OF THE FX FILTERED MIGRATION

FX PREDICTIVE FILTER

BANDPASS FILTER

TRACE SCALING

1000ms windows, 50% overlap

SEGY OUTPUT OF THE FX FILTERED DMO STACK

Vitae

Name : Abuzar

Mamun Ali faud

Nationality : Sudanese

Date of Birth : 18/08/1984

Email :

abuzarfuaad@yahoo.com

Address :

Present Address: Earth Sciences Department, King Fahd University of Petroleum and Minerals, P.O. Box 8610, Dhahran 31261, Saudi Arabia,
g201201680@kfupm.edu.sa

Permanent Address: Square 22, Ombada-Wad Esaa , Khartoum/Sudan, G.S.M
NO: +24915635084

Academic Background : My education background, as for many people in my area, stems from formal education school. Below, I summarize how this area have shaped and changed my attitude and thinking.

- BSc in GEOLOGY (FIRST CLASS) 2004-2008
AL-NELAIN UNIVERSITY, KHARTOUM, SUDAN
BSc PROJECT
TEXTURE AND MICROSTRUCTURE OF THE OLD GRANITOIDE ROCK (SABALOKA IGNEOUS COMPLEX)